Université de Montréal

Mechanism of N-Type Inactivation in Shaker Potassium Channels

par Roshan Pandey

Département de Biochimie
Faculté de Médecine

Thèse présentée
en vue de l'obtention du grade de Philosophiae Doctor (PhD)
en biochimie
option Cellular Dynamics of Molecular Complexes

Aout, 2021

UNIVERSITÉ DE MONTRÉAL

Faculté de Médecine

Cette thèse intitulée:

Mechanism of N-Type Inactivation in Shaker Potassium Channels

Présenté par

Roshan Pandey

A été évaluée par un jury composé des personnes suivantes

Stephen Michnick

Président-rapporteur

Rikard Blunck

Directeur de recherche

Jurgen Sygusch

Codirecteur

Roberto Araya

Membre du jury

Thomas Claydon

Examinateur externe

Michele Brochu

Représentant de la doyenne

Résumé

Hyperexcitabilité est l'un des changements les plus importants observés dans de nombreuses maladies neuro-dégénératives telles que la sclérose latérale amyotrophique (SLA) et la maladie d'Alzheimer. De nombreuses recherches études se sont concentrées sur la réduction de l'hyperexcitabilité, soit en inactivant les canaux sodiques ce qui va réduire la génération de potentiels d'action, soit en prolongeant l'ouverture des canaux potassiques ce qui va qui ramener la membrane à son état de repos et réduire l'activité des neurones. Ainsi, pour cibler l'hyperexcitabilité, il faut tout d'abord comprendre les différents aspects de la fonction des canaux ioniques au niveau.

Les objectifs des travaux présentés dans cette thèse consistent à déterminer le mécanisme d'inactivation dans les canaux potassiques Shaker. Les canaux Shaker Kv s'inactivent rapidement pour culminer le potentiel d'action et maintenir l'homéostasie des cellules excitables. L'inactivation de type N est causée par les 46 premiers acides aminés situés de l'extrémité N-terminale du canal, encore appelé, peptide d'inactivation (IP). De nombreuses études mutationnelles ont caractérisé l'inactivation de type N au niveau fonctionnel, cependant, la position de l'IP à l'état de repos et leur transition lors de l'inactivation est encore débattue. L'objectif de la première étude consiste à évaluer le mouvement des IP pendant leur inactivation à l'aide de la fluorométrie en voltage imposé. En insérant un acide aminé non naturel, la 3-[(6-acétyl-2-naphtalényl) amino]-L-alanine (Anap), qui est sensible aux changements d'environnement, nous avons identifié séparément les mouvements de la boule et de la chaîne. Nos données suggèrent que l'inactivation de type N se produit dans un mouvement biphasique en libérant d'abord le IP, ce qui va bloquer le pore du côté cytoplasmique. Pour affiner davantage la position de repos des IP, nous avons utilisé le transfert d'énergie de résonance à base de lanthanide et le métal de transition FRET. Nous proposons que le IP se situe dans la fenêtre formée par le canal et le domaine T1, interagissant avec les résidus acides-aminés du domaine T1.

Dans notre deuxième étude, nous avons montré que le ralentissement de l'inactivation de type N observé dans la première étude est causée par une expression élevée des canaux Shaker. En effet, l'extrémité C-terminale du canal interagit avec les protéines d'échafaudage associées à

la membrane pour la formation d'amas. Nous avons aussi montré qu'en tronquant les quatre derniers résidus C-terminaux impliqués dans la formation des amas, nous empêchons également le ralentissement de la cinétique d'inactivation dans les canaux Shaker. Nous avons également démontré que l'inactivation lente de type N n'est pas affectée par l'accumulation des cations potassiques [K+] externe ou toute diaphonie entre les sous-unités voisines. Cette étude élucide non seulement la cause du ralentissement de l'inactivation, mais montre également que les canaux modifient leur comportement en fonction des conditions d'expression. Les résultats trouvés au niveau moléculaire ne peuvent donc pas toujours être extrapolés au niveau cellulaire.

Mots-clés: Canaux KV, acides aminés non-naturels, Anap, fluorimétrie en voltage impose, tmFRET, LRET

Abstract

Hyperexcitability of neurons is a major symptom observed in many degenerative diseases such as ALS and Alzheimer's disease. A lot of research is focused on reducing hyperexcitability, either by inactivating sodium channels that will reduce the generation of action potentials, or by prolonging the opening of potassium channels which will help to bring the membrane back to resting state and thus, reduce firing frequency of neurons. At the molecular level, it is important to understand different aspects of ion channel function to target hyperexcitability.

The aim of this thesis was to investigate in two projects the inactivation mechanism in Shaker potassium channels. Shaker Kv channels inactivate rapidly to culminate the action potential and maintain the homeostasis of excitable cells. The so-called N-type inactivation is caused by the first 46 amino acids of the N-terminus of the channel, known as the inactivation peptide (IP). Numerous mutational studies have characterized N-type inactivation functionally, however, the position of the IP in the resting state and its transition during inactivation is still debated. The aim of the first project was to track the movement of IP during inactivation using voltage clamp fluorometry. By inserting an unnatural amino acid, 3-[(6-acetyl-2-naphthalenyl) amino]-L-alanine (Anap), which is sensitive to changes in environment, we identified the movements of ball and chain separately. Our data suggests that N-type inactivation occurs in a biphasic movement by first releasing the IP, which then blocks the pore from the cytoplasmic side. To further narrow down the resting position of the inactivation peptide, we used Lanthanide-based Resonance Energy transfer and transition metal FRET. We propose that the inactivation peptide is located in the window formed by the channel and the T1 domain, interacting with the acidic residues of the T1 domain.

In a follow-up study, we explored the reason underlying slow inactivation kinetics observed during the study of N-type inactivation in the first project. High expression of Shaker channels results in slowing of the N-type inactivation. The C-terminus of the channel interacts with membrane associated scaffold proteins for cluster formation. In this study, we have shown that by truncating the last four C-terminal residues involved in cluster formation, and hence preventing channel clustering, we also prevent slowing of the inactivation kinetics in Shaker

channels. We also showed that slow N-type inactivation is not affected by accumulation of external [K^+] or any crosstalk between the neighboring subunits. The second project not only elucidates the cause of the inactivation slow-down but illustrates that the channels alter their behavior dependent on the expression conditions. Results found on the molecular level can thus not always be extrapolated to the cellular level.

Keywords: Kv channels, unnatural amino acids, Anap, voltage clamp fluorometry, lanthanide resonance energy transfer, transition metal Forster resonance energy transfer

Table of contents

List of figures

List of abbreviations

4-AP 4-aminopyridine
aaRS aminoacyl tRNA synthethase
Anap 3-(6-acetylnaphthalen-2-ylamino)-2-aminopropanoic acid
BCN bicyclononynes
COVC cut-open oocyte voltage clamp
E. coli Escherichia coli
GV conductance-voltage relationship
FRET f rster resonance energy transfer
fUAA fluorescent unnatural amino acid
IP inactivation particle
KV voltage-gated potassium channel
LRET lanthanide resonance energy transfer
NaV voltage-gated sodium channel
pAnap plasmid encoding for Anap-synthetase and tRNA
QV charge-voltage relationship
QY quantum yield
S4-S5L S 4 -S5 linker
TCO trans-cyclooctene
TEA tetraethylammonium
TEVC two electrode voltage clamp
TMR tetramethylrhodamine
TMRM tetramethylrhodamine maleimide
TTX tetradotoxin
UAA unnatural amino acid
VCF voltage clamp fluorometry
VS voltage sensor
WT wild type
X. laevis Xenopus laevis

Acknowledgements

I would like to thank my supervisors, Rikard Blunck and Jurgen Sygusch for giving me this opportunity to come to Canada and pursue PhD in their lab. They have always been a pillar of support throughout my PhD.

I also want to acknowledge all my colleagues who made my stay in the university a memorable experience.

Finally, I want to thank my family, especially my wife, for being a huge support during this time.

Chapter 1

1 Introduction

Ions play a pivotal role in the physiology of electrical conduction in excitable cells. They are responsible for maintaining the resting membrane potential as well as conduction of an electrical impulse. Bernstein provided the earliest idea of membrane potential resulting from ion concentration gradient in 1902. He postulated that the membrane is permeable to potassium ions, whose concentration is 50 times more inside the cell. During excitation, the membrane becomes permeable to all ions, which brings the potential to zero, and with this mechanism, excitation travels along the cell as a self-propagating wave [1]. Later on, Kenneth Cole's laboratory measured the resting membrane potential to be around -60 mV (Vm) by inserting electrodes in a giant squid axon. They also showed that the membrane potential goes beyond 0 mV during an action potential, as postulated by Julius Bernstein. By inserting a thin wire in the axon, they created an isopotential surface in the longitudinal section of the axon, which laid the foundation of the voltage-clamp method used today [2, 3].

The experiments performed by Hodgkin and Huxley (HH model) showed a great deal of insight into the movements of ions across the cellular membrane. The outer side of the membrane contained a high concentration of Na+, whereas the cytosol contained a higher concentration of K+ ions. The overshoot during an action potential was caused by an increase in Na+ permeability of the membrane, resulting in an overshoot of the membrane potential almost to the equilibrium potential of Na+. The different phases of the membrane current were explained as the movement of different ions across the membrane. The movement of K+ ions was low at resting potential, which increased at the end phase of an action potential. Conduction of Na+ ions was zero at resting Vm and increased significantly during the rising phase of the action potential. Another component was leak conduction, which predominantly conducted K+ ions and served to maintain the resting membrane potential [4-8].

Holdgkin and Huxley described that passage of ions through the membrane was performed by conducting units specific for each set of ions, which opened and closed in response to the change in membrane potential [9-12]. Their model successfully described the ionic basis of electrical

excitability in cells. The HH model also showed that Na+ and K+ flux across the cell is the basis of excitation and generation of action potentials. The change in membrane potential governs the permeability of the cell membrane for the conduction of these ions. These findings also gave rise to new questions like how these ions are transported across the membrane, what is the basis of selectivity for one ion over the other.

Following the initial kinetic model by Hodgkin and Huxley, many theories were put forward to explain the movement of charge across the membrane. These included permeation across a homogenous membrane, binding and migration along charged sites, passage on carriers, and flow through pores. The discovery of valinomycin, a K+ selective carrier, gave an idea that membrane proteins are involved in transporting ions across the membranes. Later on, the use of tetrodotoxin (TTX) and quaternary ammonium ion (TEA) to block Na+ and K+ specific currents, respectively [13, 14], further validated the presence of membrane-embedded proteins regulating the flow of ions. In the 1970s, with improvements in cloning and protein purification techniques, the Na+ channel was isolated from electric eel by exploiting the binding affinity of these channels to TTX toxin [15, 16]. The most significant breakthrough came in 1984 when the Na+ channel was cloned from the cDNA [17], revealing a complete amino acid sequence.

In the last couple of decades, ion channel research has come a long way. The crystal structure of the bacterial potassium channel, Kcsa, given by Mackinnon and his group [18], was a significant achievement in delineating the detailed structure of the channel. With the advancement of biophysical techniques such as crystallography and cryo-EM, structures are solved in rapid succession, showing the commonalities in the architecture and the differences. Both give a deep insight into the working mechanism of ion channels.

1.1 Potassium channels

Julius Bernstein first showed the role of K+ channels in cellular excitability. It was later confirmed by Hodgkin and Huxley when they showed the movement of K+ ions during the action potential. However, it was only in 1987 that the first K+ channels were identified in Drosophila [19]. K+ channels are one of the largest ion channel families. They are found in all cell types, including neurons, muscles, and other tissues. Their primary role is to maintain potassium homeostasis in the cells, thus controlling the excitability in neurons and other cell types. Apart

from their role in maintaining electrical balance in the cells, they are also found in the epithelial tissues involved in the transport of salt and water [20].

K+ channels can be structurally categorized into three groups (Fig 1.1): the inward rectifier (Kir) family, which assembles as homotetramers and contain two transmembrane helices that form the pore domain; K2P family, which assembles as dimers and contains four transmembrane helices and two pores; and the voltage-gated potassium channels which contain six transmembrane helices with single pore domain and assembles as homo- and heterotetramers. The K+ channel families are further diversified by the interaction of their principle transmembrane domain with auxiliary subunits to gain functional specialization in various tissues.

Kir and K2P channels differ from Kv channels in possessing two and four transmembrane helices, respectively. Kir channels conduct potassium into the cell, a behavior anomalous to other families of the K+ channels. The inward rectification is caused due to blockage of the pore by divalent ions and polyamines [21, 22]. K2P channels are different from other K+ channels as they contain two pore-forming regions. Like Kir channels, they are also responsible for maintaining resting state potential and control action potential height and duration [23, 24]. They contain four transmembrane domains which come together as a dimer to form a single pore channel [25, 26].

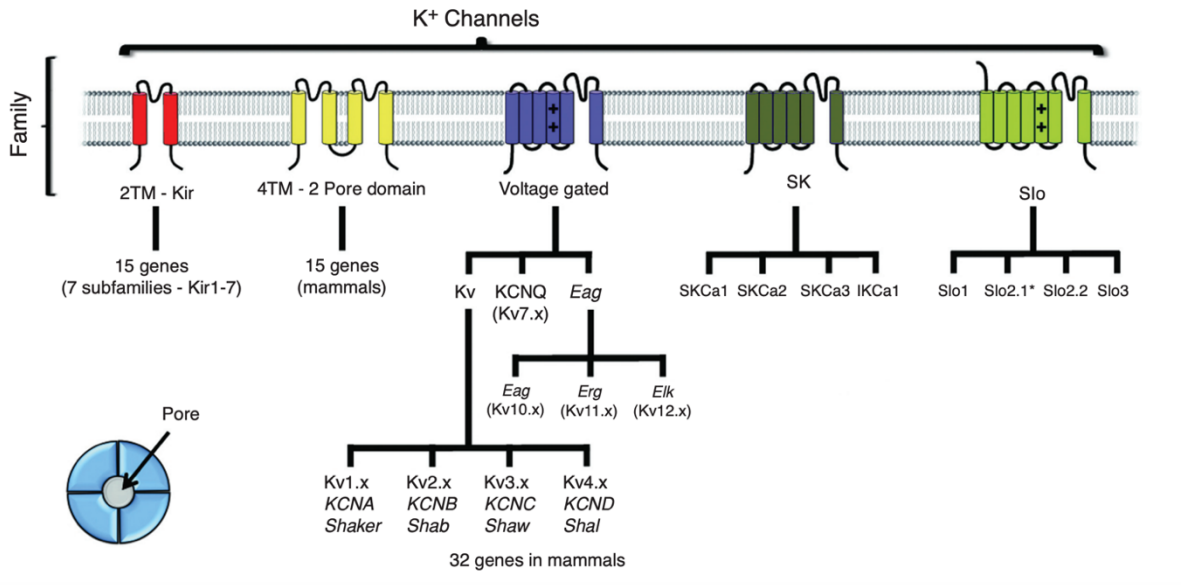

Figure 1.1 Kv Channel family Tree

Structural classification of Potassium channel family (Gonzalez et al, Comprehensive Physiology 2012).

1.1.1 Voltage-dependent K^+ Channels (Kv Channels)

Kv channels are composed of 40 genes of K+ channels divided into ten families: KCNA (Kv1), KCNB (Kv2), KCNC (Kv3), KCND (Kv4), KCNF (Kv5), KCNG (Kv6), KCNQ (Kv7), KCNV (Kv8), KCNS (Kv9), KCNH [Kv10, Kv11, Kv12, including ether-a-go-go related gene (EAG, ERG)] [27]. The multiplicity of Kv channels is further diversified by forming heterotetramers among different family members or with accessory subunits [27]. On activation, these channels produce either inactivating current (A-type) or non-inactivating current (delayed rectifiers). Non-inactivating currents help in repolarization and shaping the action potential. On the other hand, inactivating currents lead to early termination of repolarization, thus making the neuron ready to fire another action potential [28].

Kv1 channels are homologous to Shaker channels from Drosophila. Kv1 channels were first identified by Hodgkin and Huxley in their experiment on giant squid axon. As they opened after sodium channels and did not show any inactivation in the time scale of measurements, they were called delayed rectifiers. Later on, other members of this family were also identified. All members of this family show non-inactivating current except Kv1.4 [29]. However, they show inactivation when coexpressed with Kvß subunits.

Kv2 channels are homologous to Shab in Drosophila. Kv2.1 and 2.2 are majorly found in CNS neurons, especially in GABAnergic neurons [30, 31]. Kv2.1 can form heterotetramers with Kv5, Kv6, Kv8, and Kv9 subunits [27]. Chronic hypertension has been shown to decrease the expression levels of Kv2 channels [32].

Kv3 channels are counterparts of Drosophila Shaw channels. Kv3.3 and Kv3.4 show A-type inactivating currents, whereas Kv3.1 and Kv3.2 behave as delayed rectifiers. They are found in the cerebellum, skeletal muscle, arterial smooth muscle, and germ cells. They are essential for high firing frequency in auditory neurons and GABAnergic neurons [33, 34]. Kv3.1 knockout mice show impaired motor skills and reduced muscle contraction force [35]. Kv3.4, together with MiRP2, forms low voltage activating channels in the skeletal muscles. Mutations in MiRP2 have been associated with periodic paralysis [36].

Kv4 channels produce Ito currents in heart muscles and ISA in somatic neurons. They are mainly found in the brain, heart, lung, liver, kidney, testis, thyroid gland, pancreas, and pulmonary artery [37, 38]. Kv4 channels coexpress with KChiP subunits, which increases their surface expression and modulates their gating kinetics [39]. They are mainly responsible for repolarizing cardiac action potential and preventing backpropagation of action potential in hippocampus neurons. Seizure activity has been shown to reduce Kv4.2 expression in the hippocampus, whereas Kv4.3 mRNA expression levels are decreased in patients with paroxysmal atrial fibrillation [40, 41].

Kv7.1 is found in the heart, rectum, kidney, ears, pancreas, lung, and placenta. They are involved in the repolarization of the cardiac action potential. They coassemble with KCNE1 to form cardiac IKs channels. They are also involved in recycling potassium in the basolateral membrane of intestinal cells and the inner ear. Loss of function in Kv7.1 gene is associated with congenital long QT syndrome and polymorphic ventricular arrhythmias [42]. Kv7.2 and 7.3 channels are distributed in the brain, sympathetic ganglia, heart, lung, breast, eye, germ cell, placenta, small intestine [43]. They determine the subthreshold excitability of neurons and also coassemble to form M currents in the brain [44]. Knocking out the Kv7.2 gene in mice causes benign familial neonatal convulsions with myokymia [45].

Kv5, Kv6, Kv8, and Kv9 channels coexpress with Kv2 and modify their kinetics and expression level.

Kv10 channels, also known as eag channels, derived their name from a drosophila mutant ether-a-go-go, which shows enhanced neurotransmitter release at the neuromuscular junction. It is closely related to Kv11 (herg) and Kv12 (elk) channels [46] [47]. Kv10.1 is mainly found in the brain, placenta, myoblast, and some tumor cell type, while Kv10.2 is exclusively found in CNS.

HERG channels (ether-a-go-go-related gene) are found in the heart, brain, kidney, lung, liver, ovary, pancreas, testis, small intestine, tonsil, uterus, and microglia. They form cardiac Ikr channels in the heart. C-type inactivation observed in these channels shows much faster kinetics (1-3ms) than other K+ channels and modulates its conductance properties. They are responsible for ending the plateau phase of cardiac action potential [48].

Kv12 channels are mainly expressed in the nervous system and show activating and deactivating currents. Kv12.2 knockout mice show persistent neuronal excitability, spontaneous seizures, and increased sensitivity to convulsants [49].

Since this thesis was based on Kv1 channels, they will be described in more detail below.

Kv1 channels are majorly expressed in muscles, the heart, and the brain. Kv1.1 and 1.2 are highly expressed in the hippocampus, cerebellum, cerebral cortex, and thalamus. Kv1.1 is also found to be expressed in the heart, retina, and skeletal muscles, whereas Kv1.2 is found in the spinal cord, heart, smooth muscle cells [41, 50]. Malfunction in Kv1.1 has been associated with episodic ataxia type 1 and myokymia [51]. Kv1.3 channels are found in the brain, as well as islets, spleen, lymph nodes, thymus, fibroblasts, B and T lymphocytes, tonsils, and macrophages. Due to their extensive expression in immunological tissues, it has been studied as a potential therapeutic target for immunosuppressants [52]. Kv1.5 is found in the aorta, kidney, colon, stomach, smooth muscle, hippocampus, cortex, pituitary, and pulmonary artery. Kv1 channels can also coassemble with other members of the family to form heterotetramers due to the presence of the tetramerization domain on the cytoplasmic side of the channel [53, 54]. Kv1.x channels are also known to bind to scaffold proteins like PSD95, SAP97, or dlg [55]. These scaffold proteins are responsible for the surface expression of Kv1.x channels as well as their clustering.

1.1.2 Kv channel structure

KcsA was the first crystal structure of a potassium channel and was solved by the Mackinnon group [18]. It showed, in great detail, the selectivity filter present in the pore, which is

almost identical to the selectivity filter of the eukaryotic Kv channels. Later on, the first mammalian Kv chimera channel structure was crystallized from Rattus norvegicus by the same group [56], followed by crystallization of a full-length channel in the presence of lipids [57]. Kv channels assemble as tetramers, with each monomer comprising six transmembrane helices. When viewed from the extracellular side, Kv channels show 4-fold symmetry with the pore at the center surrounded by four voltage sensor domains [18, 58] (Fig 1.2). Helices S1-S4 form the voltage sensor domain (VSD), which senses the membrane potential to open the channel. Helices S5-S6 of all four monomers form a single central ion-conducting pore. The C- and N-termini of the channel are located on the cytoplasmic side. The S4 helix is lined by highly conserved positively charged residues, responsible for sensing the change in membrane potential. The movement of these charged residues towards the extracellular side of the membrane can be detected as small transient currents known as gating currents. Hence, these charges are called gating charges. During depolarization, the movement of these gating charges opens the channels leading to channel activation.

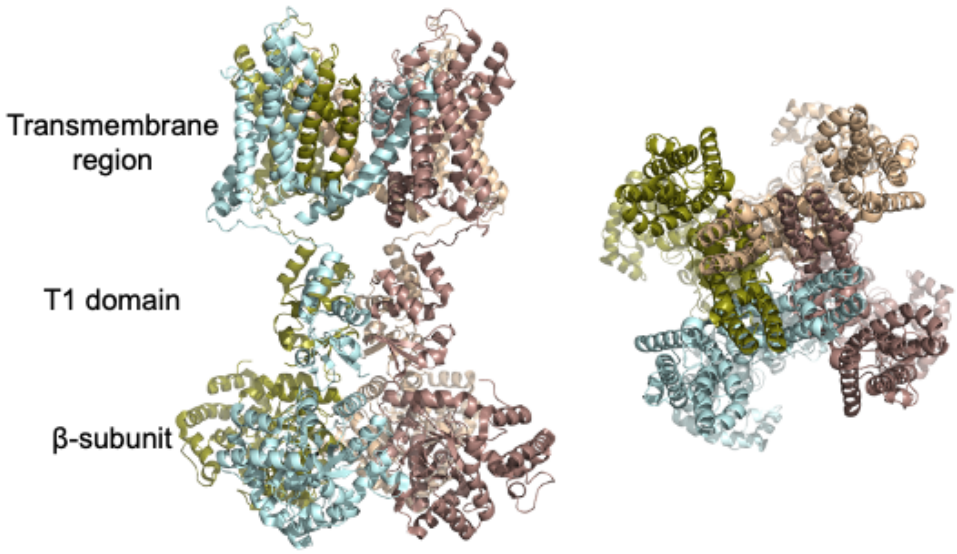

Figure 1.2: Crystal structure of Kv1.2/2.1 Chimera

Side view and top view of the Kv1.2/2.1 crystal structure where each color represents a monomer. (PDB ID: 2R9R)

1.2 Channel Activation

The S4 helix contains positively charged residues, five arginines (R1 to R4, R6), and one lysine (K5), responsible for sensing the change in membrane potential. These residues are present at every third position in the S4 helix and are surrounded by negatively charged amino acids from helices S1-S3. The distribution of positive and negative charges forms a network that interacts to stabilize each other. The positive charges move along this network towards the extracellular side during membrane depolarization. The surrounding negative charges are divided into two groups: the external negative cluster, which consists of E183 (S1Helix) and E226 (S2 Helix), and an internal negative cluster consisting of E154 (T1-S1 linker), E236 (S2 Helix), and D259 (S3a Helix). The two clusters are separated by a phenylalanine residue 233 in the center of the S2 helix, which is conserved in all Kv channels (except KvAP). This separation is known as the phenylalanine gap or charge transfer center [59, 60]. In the crystal structure of the Kv1.2/2.1 chimera, which shows the channel conformation in the open state, residues R3 and R4 form hydrogen bonds with the external negative cluster, whereas K5 and R6 interact with the internal negative cluster.

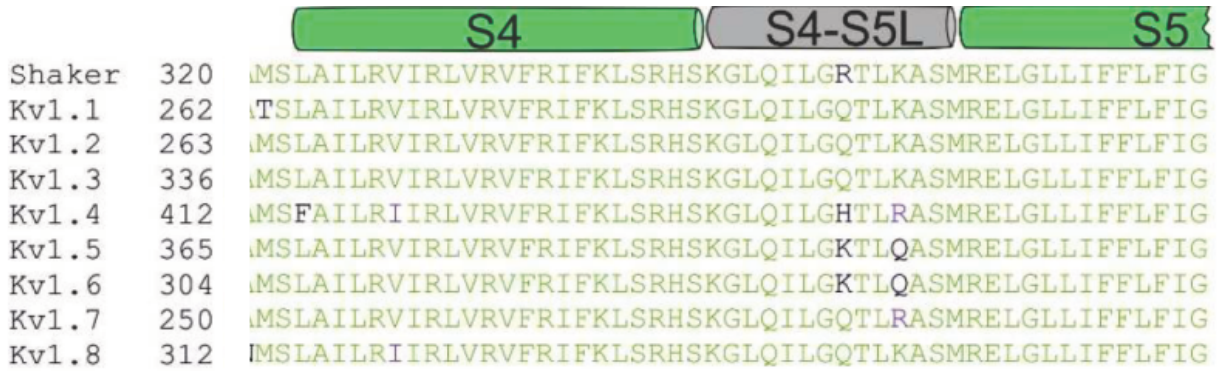

Figure 1.3: Amino acid sequence alignment of Kv channels

Amino acid sequence alignment of Shaker and the human KV1 subfamily with locations of secondary structures. Green residues are identical and blue residues indicate similarity. The C- and N-termini have been omitted for space-saving purposes. Alignment is generated using T-coffee (http://tcoffee.crg.cat/apps/tcoffee/index.html) with input sequence IDs: Shaker-P08510, Kv1.1-Q09470, Kv1.2-P16389, Kv1.3-P22001, Kv1.4-P22459, Kv1.5-P22460, Kv1.6-P17658, Kv1.7-Q96RP8, Kv1.8-Q16322.

During channel activation, it has been proposed that the external negative cluster electrostatically attracts R3 and R4 to move towards the extracellular surface. The bottom half of the S4 helix below R3 adopts a 3-10 conformation, allowing the S4 helix to extend by 5Å [57].

Overall, there is an upward translation and tilt of the S4 associated with the charge movement [61]. The voltage sensor of all four subunits is activated before the final pore opening. The activated VSDs transfer their energy through the S4-S5 linker for pore opening and ion conduction in a process known as electro-mechanical coupling [62].

1.3 Channel Inactivation

The conduction of ions through the pore is controlled from the extracellular side by the selectivity filter, which preferentially allows K+ ions to pass through the pore. The ion conduction is blocked by a helix bundle crossing formed by the S6 helix from the cytoplasmic side. These two gates prevent the flow of potassium ions during the resting state of the channel. However, another scenario can prevent the passage of ions through the pore, known as channel inactivation. Inactivation refers to the blockage of K+ ion flow from the cytoplasmic side. The channels undergo inactivation from an open state, primarily by either N-type or C-type inactivation (refer to below) (Fig 1.4).

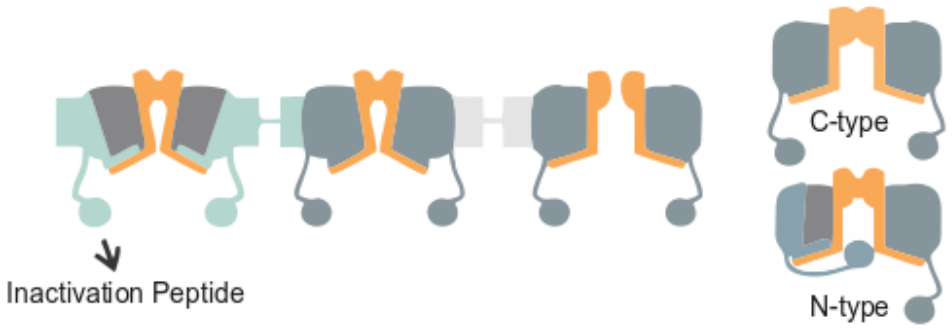

Figure 1.4: Inactivation in Kv channels

Two types of inactivation observed in Kv channels: C-type and N-type.

1.3.1 N-type Inactivation

N-type is a fast inactivation mechanism observed within few milliseconds of Kv channel opening. Such fast inactivation mechanism is essential for modulating duration and pattern of action potential in excitable cells. The N-terminal of any of the four subunits diffuses from the cytoplasmic side to block the channel, hence N-type inactivation. The role of the N-terminus inactivation peptide in fast inactivation was identified in 1990 by the Aldrich group after the

introduction of molecular cloning. By introducing mutations in the N-terminus of Shaker channels, they showed that the inactivation could be removed, thus identifying that the N-terminal of the channel is responsible for the fast inactivation mechanism seen in Shaker channels [63].

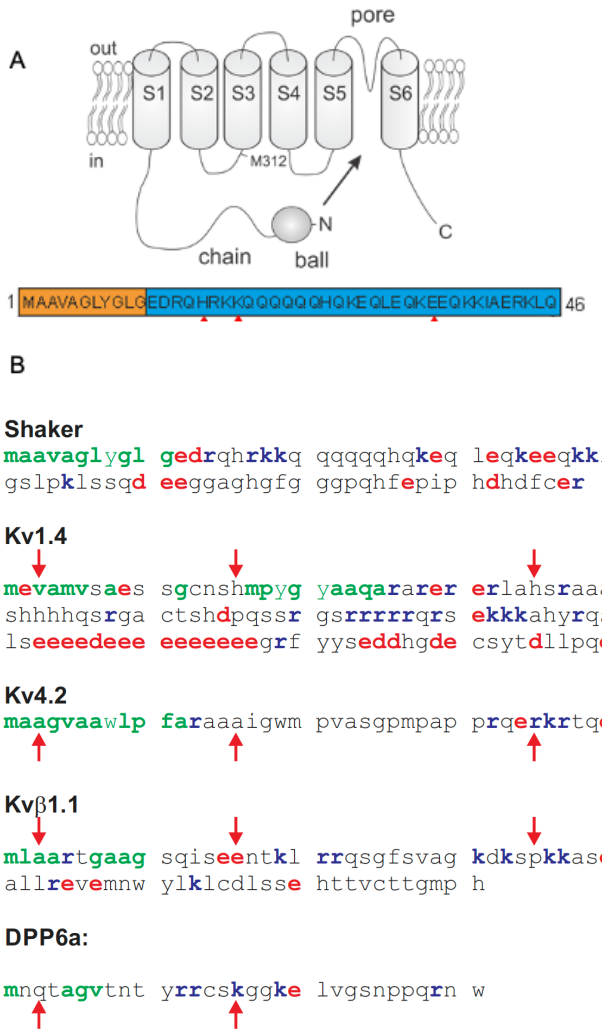

Fig 1.5: N-terminal ball and chain in Kv channels

A) Cartoon representation of the transmembrane helices showing N-terminal ball and chain. The sequence of the ball and chain is also shown with the hydrophobic tip highlighted in orange and the chain region highlighted in blue. **B)** Comparison of inactivation peptide sequence in different Kv channels.

The N-terminal part of the channel responsible for blocking the pore is the Inactivation Particle (IP). IP is formed by the first 46 amino acids and has been suggested to have a ball and chain type of structure (Fig 1.5). The ball part consists of hydrophobic residues that enters the pore and interacts with the pore lining residues through hydrophobic interactions [64] (Fig 1.6). Since pore opening is a requirement for the N-type inactivation, various pore blockers, such as TEA, have been shown to interfere with the binding of IP from the cytoplasmic site [65] as they compete for the same binding site. The chain part consists of various charged residues with an overall positive charge. During channel inactivation, interaction of these positively charged residues with the acidic residues of the T1-S1 linker has been suggested to stabilize the IP. Removal of charge from the chain region has been shown to affect inactivation kinetics [63, 66, 67]. The IP is said to block the channel from the cytoplasmic side by entering through the window between the T1 domain and the channel. However, how it enters through the window and where it is located in the resting state is still unknown.

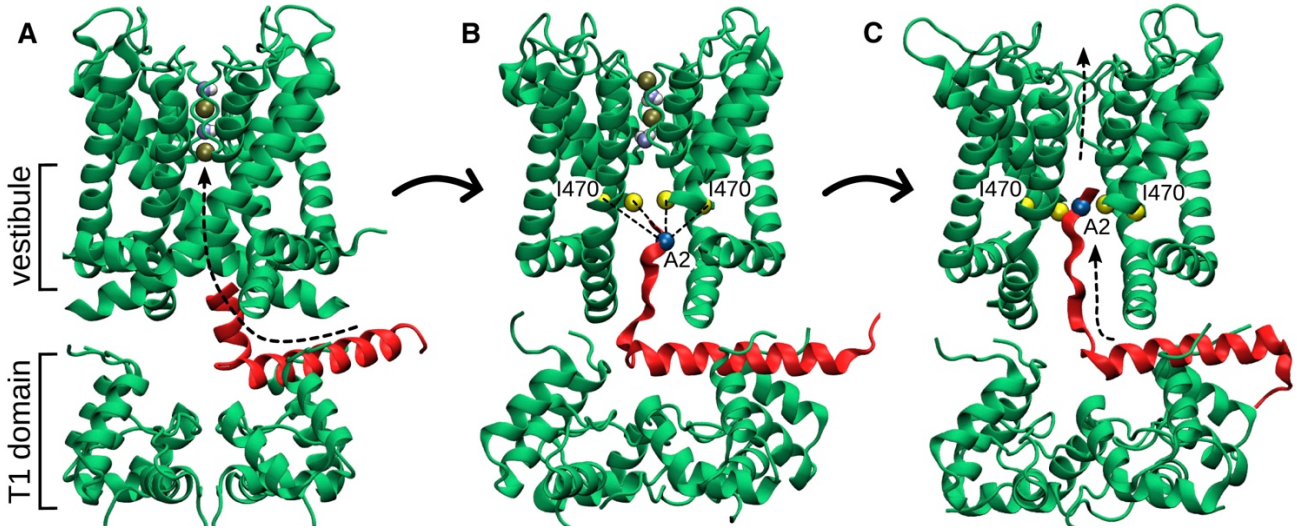

Figure 1.6: Simulation model for N-type inactivation

Entry of IP (red) into the pore determined by molecular simulations (Holmgren *et al* 2017). IP enters as an *α*-helix into the pore, where it unfolds to interact with the residues lining the inner pore.

N-type inactivation is also seen in mammalian Kv channels like Kv1.4, Kv3.4, and Kv4.2 channels. Coexpression of Kv1.x channels with β-subunit imparts fast inactivation to the otherwise non-inactivating channels [29]. Apart from β-subunits, DPP6 auxiliary subunits have been shown to modulate Kv4.x channels kinetics [68]. Comparison of fast inactivation in different Kv channels

shows that the general ball and chain type of architecture is consistent in all of them, comprising of a hydrophobic tip and a charged chain region (Fig 1.5B). However, there are some differences in the sequence of the inactivation peptides that influences the secondary structure of the peptide, and hence, inactivation kinetics. NMR structure of Kv 1.4 IP shows a flexible N-terminal with a helix capped with β-turn motif, whereas Kv 3.4 lacks any typical secondary structure and just forms a compact folding [69]. These structural differences are implicated in the functional properties as well: a Kv 3.4 derived inactivation peptide completely blocks non inactivating Kv1.1 currents, whereas a peptide from Kv1.4 only partially inactivates it, even at 10-fold higher concentration. Such differences in inactivation kinetics may be attributed to the different electrostatic interaction of these IPs to the receptor site formed by the internal mouth of the pore.

1.3.2 C-type inactivation

C-type inactivation regulates the flow of ions through the selectivity filter. In contrast to N-type inactivation, the C-type inactivation results from a conformational change in the selectivity filter on the extracellular side of the pore, which renders the pore nonconducting. A study based on molecular simulations reported that the presence of trapped water molecules in the backbone of the selectivity filter is responsible for keeping the selectivity filter in a deformed, non-conductive state[70] [71] [72]. The formation of hydrogen bonds with the protein backbone increases the residing time of these water molecules, responsible for delayed recovery from this type of inactivation.

C-type inactivation is inhibited by high extracellular K+ as well as TEA applied externally. The inhibition of C-type inactivation in such conditions has been suggested through a foot in the door type of mechanism in which the presence of ions in their binding site in the selectivity filter prevents conformational changes responsible for slow inactivation [73]. Furthermore, C-type inactivated Kv channels become permeable to Na+ ions in the absence of K+ ions, suggesting that the structural changes involved in the process are only local and leads to widening of the selectivity filter, thus allowing hydrated Na+ ions to pass through [74]. Yellen *et al* 1994 [75] showed that the mutation T449C results in stabilization of C-type inactivation. Liu *et al* also showed through mutated cysteine accessibility studies that the modification of residues 448-450 in Shaker are

accelerated after C-type inactivation [76]. These studies point out that a structural rearrangement in the selectivity filter is a plausible cause of C-type inactivation observed in Kv channels.

Inactivation of channels is an important phenomenon to maintain cellular excitability. Inactivation of sodium channels prevents prolonged depolarization, and that of potassium channels prevents the cells from entering the hyperpolarized state. A delay in the culmination of sodium current or accelerated inactivation of potassium channels can lead to sustained depolarization, resulting in hyperexcitability. Hyperexcitability is one of the most common features of many neurological and cardiac disorders [77 , 78]. A better understanding of these inactivation mechanisms is pertinent in understanding these channelopathies and finding a cure for them.

1.4 Clustering of Kv channels

Density of ion channels plays an important role in regulating neuronal excitability. Clustering of Nav channels at nodes of ranvier is crucial for driving saltatory conduction. Similarly, glutamergic receptors are concentrated at post synaptic density to drive the action potential forward. Generations of action potential from excitatory and inhibitory postsynaptic potentials is governed by the cluster of Kv and Nav channels present at the axon initial segment. Thus, channel clustering is an important physiological phenomenon which requires tight regulation to maintain precise distribution of channels and receptors. MAGUKs (membrane-associated guanylate kinases) are one such group of scaffold proteins that regulates the trafficking, maintenance and recycling of receptors and channels in the membrane. Several members of this group (PSD-93, PSD-95, SAP97) play important role in trafficking and clustering of Kv channels [79]. Apart from Kv channels, these channels also control clustering of AMPA and NMDA receptors at synapse [80]. These proteins contain three PSD-95/discs large/Zona occludens-1 (PDZ) domains alongwith a src-homology-3 (SH3) domain and an inactive guanylate kinase (GK) domain. Shaker channels have been shown to interact with the PDZ domain through their C-terminal motifs [81] and removal of this motif results in diffused expression pattern and lower current density [82]. MAGUKs also help in stabilization of channels in the membrane by controlling recycling of channels from the membrane.

1.5 Thesis Objective

K+ channels are the most diverse group of ion channels. Many K+ channels have been the main focus of pharmacological research due to their crucial role in different physiological aspects. Kv1.3 channels have been shown to counterbalance the effect of incoming Ca2+ ions in T-cells, thus controlling the signaling pathway activated by Ca2+ ions for cytokine secretion and cell proliferation. Therefore, the role of Kv1.3 blockers as immunosuppressants is being investigated actively [83]. Kv4.3 channels have been the target for antiarrhythmic drugs by blocking the Ito in the heart. Kv7 channels are responsible for modulating synaptic plasticity and neuronal excitability in the brain. Activators of Kv7 currents, known as m-currents, are being explored to enhance the neuronal K+ conductance [84].

One of the major functions of the K+ channel is the repolarization of excitable cells, which thus controls the firing frequency and generation of action potentials. Any impairment in the K+ channel function can either extend or decrease the repolarization, directly affecting cellular excitability. Lower cellular excitability can lead to depression disorders, whereas hyperexcitability can cause seizures, pain, and anxiety-related disorders. Therefore, the modulation of K+ conductance, which is majorly controlled by N-type inactivation of the channel, is an important step that governs cellular excitability.

The N-type inactivation has been extensively characterized after the Aldrich group first identified it. However, these studies were restricted to functional data. With the recent advancement in the fluorescence techniques that allow following intracellular movement, we can finally aim to identify the resting position and path of the IP, the N-terminal part of the channel responsible for inactivation. Recent advances in cryo-EM microscopy made it possible to obtain structures of ion channels that were difficult to crystallize. However, the flexible nature of the IP still makes it challenging to identify high-resolution structures.

In order to identify the position of the IP and to get more dynamic information about its movements to inactivate the channel, we decided to do LRET and tmFRET experiments. Since the IP was present on the cytoplasmic side, to label the desired positions and achieve more specific labeling, we genetically incorporate an unnatural amino acid (UAA) through orthogonal

tRNA/synthetase pair [85]. This technique offers the advantage of incorporating an unnatural amino acid with desired properties at a site that is inaccessible to conventional reagents and fluorophores. The objective of this thesis was to delineate the inactivation pathway of IP by using various techniques based on the genetic incorporation of UAA.

By performing VCF using a fluorescent UAA, we would track the path followed by IP from resting state to inactivation. The IP is known to block the channel from the cytoplasmic side. However, the detailed view of how it reaches the pore and interacts with the pore is still elusive. Simultaneous measurement of current and fluorescence changes will allow us to get a broader picture. To identify where the IP resides in the resting state, we would perform Lanthanide Resonance Energy Transfer (LRET). By incorporating a UAA with an azide group, we can use the click chemistry to bind a fluorophore from the cytoplasmic side [86]. Click chemistry would provide a fast, more specific labeling of the fluorophore to determine the resting state position of IP.

To perform a fluorescence-based experiment in Xenopus oocytes, higher expression levels of the channels are required to obtain maximum signal. One phenomenon that is consistently seen at the higher expression of the Shaker channel is slowed inactivation kinetics. Previous studies have tried to explain this slow inactivation as a result of mixed N-type and C-type inactivation [87] or a phenomenon observed at higher K+ concentration near the membrane [88, 89]. A dig into the literature revealed that clustering of channels via C-terminus and slower N-type inactivation via the N-terminus share structural characteristics [90]. The goal of the second paper is to identify the relation between channel clustering and slow inactivation kinetics. One of the mechanisms for channel clustering is the interaction of the C-terminal with scaffold proteins like PSD-95 [55]. Therefore, by removing the residues at C-terminal that interact with PSD-95, we aim to see if clustering can be prevented, and in turn, faster inactivation kinetics can be restored in Shaker channels at higher expression levels.

1.6 References

1. Bernstein, J., *Untersuchungen zur Thermodynamik der bioelektrischen Strome.* Pflfigers Arch. ges. Physiol., 1902. **92: 521-562**.
2. Cole, K.S., *Dynamic Electrical Characteristics of the Squid Axon Membrane.* Archives Des Sciences Physiologiques, 1949. **3**(2): p. 253-258.
3. Marmont, G., *Studies on the Axon Membrane .1. A New Method.* Journal of Cellular and Comparative Physiology, 1949. **34**(3): p. 351-382.
4. Hodgkin, A.L. and A.F. Huxley, *A quantitative description of membrane current and its application to conduction and excitation in nerve.* J Physiol, 1952. **117**(4): p. 500-44.
5. Hodgkin, A.L. and A.F. Huxley, *The dual effect of membrane potential on sodium conductance in the giant axon of Loligo.* J Physiol, 1952. **116**(4): p. 497-506.
6. Hodgkin, A.L. and A.F. Huxley, *The components of membrane conductance in the giant axon of Loligo.* J Physiol, 1952. **116**(4): p. 473-96.
7. Hodgkin, A.L. and A.F. Huxley, *Currents carried by sodium and potassium ions through the membrane of the giant axon of Loligo.* J Physiol, 1952. **116**(4): p. 449-72.
8. Hodgkin, A.L. and A.F. Huxley, *Movement of sodium and potassium ions during nervous activity.* Cold Spring Harb Symp Quant Biol, 1952. **17**: p. 43-52.
9. Haeuser, B.F. and A.L. Hodgkin, *The after effects of impulses in giant nerve fibres.* J Physiol, 1955. **129**(3): p. 51-2P.
10. Hodgkin, A.L. and R.D. Keynes, *The potassium permeability of a giant nerve fibre.* J Physiol, 1955. **128**(1): p. 61-88.
11. Hodgkin, A.L. and R.D. Keynes, *Active transport of cations in giant axons from Sepia and Loligo.* J Physiol, 1955. **128**(1): p. 28-60.
12. Hodgkin, A.L. and W.A. Rushton, *The electrical constants of a crustacean nerve fibre.* Proc R Soc Med, 1946. **134**(873): p. 444-79.
13. Narahashi, T., J.W. Moore, and W.R. Scott, *Tetrodotoxin Blockage of Sodium Conductance Increase in Lobster Giant Axons.* J Gen Physiol, 1964. **47**: p. 965-74.
14. Armstrong, C.M., *Inactivation of the potassium conductance and related phenomena caused by quaternary ammonium ion injection in squid axons.* J Gen Physiol, 1969. **54**(5): p. 553-75.
15. Agnew, W.S., et al., *Purification of the tetrodotoxin-binding component associated with the voltage-sensitive sodium channel from Electrophorus electricus electroplax membranes.* Proc Natl Acad Sci U S A, 1978. **75**(6): p. 2606-10.
16. Miller, J.A., W.S. Agnew, and S.R. Levinson, *Principal glycopeptide of the tetrodotoxin/saxitoxin binding protein from Electrophorus electricus: isolation and partial chemical and physical characterization.* Biochemistry, 1983. **22**(2): p. 462-70.
17. Noda, M., et al., *Primary structure of Electrophorus electricus sodium channel deduced from cDNA sequence.* Nature, 1984. **312**(5990): p. 121-7.
18. Doyle, D.A., et al., *The structure of the potassium channel: molecular basis of K+ conduction and selectivity.* Science, 1998. **280**(5360): p. 69-77.
19. Tempel, B.L., et al., *Sequence of a probable potassium channel component encoded at Shaker locus of Drosophila.* Science, 1987. **237**(4816): p. 770-5.
20. Hille, B., *Ion channels of excitable membranes*. 2001: Sinauer Associates, Inc.

21. Lopatin, A.N., E.N. Makhina, and C.G. Nichols, *Potassium Channel Block by Cytoplasmic Polyamines as the Mechanism of Intrinsic Rectification.* Nature, 1994. **372**(6504): p. 366-369.
22. Matsuda, H., A. Saigusa, and H. Irisawa, *Ohmic conductance through the inwardly rectifying K channel and blocking by internal Mg2+.* Nature, 1987. **325**(7000): p. 156-9.
23. Ilan, N. and S.A. Goldstein, *Kcnko: single, cloned potassium leak channels are multi-ion pores.* Biophys J, 2001. **80**(1): p. 241-53.
24. Plant, L.D., S. Rajan, and S.A. Goldstein, *K2P channels and their protein partners.* Curr Opin Neurobiol, 2005. **15**(3): p. 326-33.
25. Martinac, B., *Mechanosensitive ion channels: molecules of mechanotransduction.* J Cell Sci, 2004. **117**(Pt 12): p. 2449-60.
26. Lesage, F. and M. Lazdunski, *Molecular and functional properties of two-pore-domain potassium channels.* Am J Physiol Renal Physiol, 2000. **279**(5): p. F793-801.
27. Gutman, G.A., et al., *International Union of Pharmacology. LIII. Nomenclature and molecular relationships of voltage-gated potassium channels.* Pharmacol Rev, 2005. **57**(4): p. 473-508.
28. Patel, S.P. and D.L. Campbell, *Transient outward potassium current, 'Ito', phenotypes in the mammalian left ventricle: underlying molecular, cellular and biophysical mechanisms.* J Physiol, 2005. **569**(Pt 1): p. 7-39.
29. Heinemann, S.H., et al., *Functional characterization of Kv channel beta-subunits from rat brain.* J Physiol, 1996. **493 (Pt 3)**: p. 625-33.
30. Hermanstyne, T.O., et al., *Immunolocalization of the Voltage-Gated Potassium Channel Kv2.2 in GABAergic Neurons in the Basal Forebrain of Rats and Mice.* Journal of Comparative Neurology, 2010. **518**(21): p. 4298-4310.
31. Mohapatra, D.P., K.S. Park, and J.S. Trimmer, *Dynamic regulation of the voltage-gated Kv2.1 potassium channel by multisite phosphorylation.* Biochem Soc Trans, 2007. **35**(Pt 5): p. 1064-8.
32. Archer, S.L., et al., *Molecular identification of the role of voltage-gated K+ channels, Kv1.5 and Kv2.1, in hypoxic pulmonary vasoconstriction and control of resting membrane potential in rat pulmonary artery myocytes.* J Clin Invest, 1998. **101**(11): p. 2319-30.
33. Erisir, A., et al., *Function of specific K(+) channels in sustained high-frequency firing of fast-spiking neocortical interneurons.* J Neurophysiol, 1999. **82**(5): p. 2476-89.
34. Grissmer, S., et al., *Pharmacological characterization of five cloned voltage-gated K+ channels, types Kv1.1, 1.2, 1.3, 1.5, and 3.1, stably expressed in mammalian cell lines.* Mol Pharmacol, 1994. **45**(6): p. 1227-34.
35. Ho, C.S., R.W. Grange, and R.H. Joho, *Pleiotropic effects of a disrupted K+ channel gene: reduced body weight, impaired motor skill and muscle contraction, but no seizures.* Proc Natl Acad Sci U S A, 1997. **94**(4): p. 1533-8.
36. Abbott, G.W., et al., *MiRP2 forms potassium channels in skeletal muscle with Kv3.4 and is associated with periodic paralysis.* Cell, 2001. **104**(2): p. 217-31.
37. Brahmajothi, M.V., et al., *In situ hybridization reveals extensive diversity of K+ channel mRNA in isolated ferret cardiac myocytes.* Circ Res, 1996. **78**(6): p. 1083-9.
38. Davies, A.R. and R.Z. Kozlowski, *Kv channel subunit expression in rat pulmonary arteries.* Lung, 2001. **179**(3): p. 147-61.

39. Nakamura, T.Y., et al., *Different effects of the Ca(2+)-binding protein, KChIP1, on two Kv4 subfamily members, Kv4.1 and Kv4.2.* FEBS Lett, 2001. **499**(3): p. 205-9.
40. Brundel, B.J., et al., *Alterations in potassium channel gene expression in atria of patients with persistent and paroxysmal atrial fibrillation: differential regulation of protein and mRNA levels for K+ channels.* J Am Coll Cardiol, 2001. **37**(3): p. 926-32.
41. Tsaur, M.L., et al., *Differential expression of K+ channel mRNAs in the rat brain and down-regulation in the hippocampus following seizures.* Neuron, 1992. **8**(6): p. 1055-67.
42. Keating, M.T. and M.C. Sanguinetti, *Molecular and cellular mechanisms of cardiac arrhythmias.* Cell, 2001. **104**(4): p. 569-80.
43. Smith, J.S., et al., *Differential expression of kcnq2 splice variants: implications to m current function during neuronal development.* J Neurosci, 2001. **21**(4): p. 1096-103.
44. Wang, H.S., et al., *KCNQ2 and KCNQ3 potassium channel subunits: molecular correlates of the M-channel.* Science, 1998. **282**(5395): p. 1890-3.
45. Biervert, C., et al., *A potassium channel mutation in neonatal human epilepsy.* Science, 1998. **279**(5349): p. 403-6.
46. Elkins, T., B. Ganetzky, and C.F. Wu, *A Drosophila mutation that eliminates a calcium-dependent potassium current.* Proc Natl Acad Sci U S A, 1986. **83**(21): p. 8415-9.
47. Warmke, J.W. and B. Ganetzky, *A family of potassium channel genes related to eag in Drosophila and mammals.* Proc Natl Acad Sci U S A, 1994. **91**(8): p. 3438-42.
48. Sanguinetti, M.C., et al., *A mechanistic link between an inherited and an acquired cardiac arrhythmia: HERG encodes the IKr potassium channel.* Cell, 1995. **81**(2): p. 299-307.
49. Zhang, X., et al., *Deletion of the potassium channel Kv12.2 causes hippocampal hyperexcitability and epilepsy.* Nat Neurosci, 2010. **13**(9): p. 1056-8.
50. Beckh, S. and O. Pongs, *Members of the RCK potassium channel family are differentially expressed in the rat nervous system.* EMBO J, 1990. **9**(3): p. 777-82.
51. D'Adamo, M.C., et al., *Episodic ataxia type-1 mutations in the hKv1.1 cytoplasmic pore region alter the gating properties of the channel.* EMBO J, 1998. **17**(5): p. 1200-7.
52. Rangaraju, S., et al., *Kv1.3 potassium channels as a therapeutic target in multiple sclerosis.* Expert Opin Ther Targets, 2009. **13**(8): p. 909-24.
53. Kreusch, A., et al., *Crystal structure of the tetramerization domain of the Shaker potassium channel.* Nature, 1998. **392**(6679): p. 945-8.
54. Li, M., Y.N. Jan, and L.Y. Jan, *Specification of subunit assembly by the hydrophilic amino-terminal domain of the Shaker potassium channel.* Science, 1992. **257**(5074): p. 1225-30.
55. Gomperts, S.N., *Clustering membrane proteins: It's all coming together with the PSD-95/SAP90 protein family.* Cell, 1996. **84**(5): p. 659-62.
56. Lee, S.Y., et al., *Structure of the KvAP voltage-dependent K+ channel and its dependence on the lipid membrane.* Proc Natl Acad Sci U S A, 2005. **102**(43): p. 15441-6.
57. Long, S.B., et al., *Atomic structure of a voltage-dependent K+ channel in a lipid membrane-like environment.* Nature, 2007. **450**(7168): p. 376-82.
58. MacKinnon, R., *Determination of the subunit stoichiometry of a voltage-activated potassium channel.* Nature, 1991. **350**(6315): p. 232-5.

59. Chen, X., et al., *Structure of the full-length Shaker potassium channel Kv1.2 by normal-mode-based X-ray crystallographic refinement.* Proc Natl Acad Sci U S A, 2010. **107**(25): p. 11352-7.
60. Tao, X., et al., *A gating charge transfer center in voltage sensors.* Science, 2010. **328**(5974): p. 67-73.
61. Kalstrup, T. and R. Blunck, *Dynamics of internal pore opening in K(V) channels probed by a fluorescent unnatural amino acid.* Proc Natl Acad Sci U S A, 2013. **110**(20): p. 8272-7.
62. Kalstrup, T. and R. Blunck, *S4-S5 linker movement during activation and inactivation in voltage-gated K(+) channels.* Proc Natl Acad Sci U S A, 2018. **115**(29): p. E6751-E6759.
63. Hoshi, T., W.N. Zagotta, and R.W. Aldrich, *Biophysical and molecular mechanisms of Shaker potassium channel inactivation.* Science, 1990. **250**(4980): p. 533-8.
64. Vergara-Jaque, A., et al., *A Structural Model of the Inactivation Gate of Voltage Activated Potassium Channels.* Biophysical Journal, 2017. **112**(3): p. 247a-247a.
65. Choi, K.L., R.W. Aldrich, and G. Yellen, *Tetraethylammonium blockade distinguishes two inactivation mechanisms in voltage-activated K+ channels.* Proc Natl Acad Sci U S A, 1991. **88**(12): p. 5092-5.
66. Fan, Z., et al., *Electrostatic interaction in the NH(2)-terminus accelerates inactivation of the Kv1.4 channel.* Biochim Biophys Acta, 2010. **1798**(11): p. 2076-83.
67. Fan, Z., et al., *Electrostatic interaction between inactivation ball and T1-S1 linker region of Kv1.4 channel.* Biochim Biophys Acta, 2012. **1818**(1): p. 55-63.
68. Wang, H., et al., *Structural basis for modulation of Kv4 K+ channels by auxiliary KChIP subunits.* Nat Neurosci, 2007. **10**(1): p. 32-9.
69. Antz, C., et al., *NMR structure of inactivation gates from mammalian voltage-dependent potassium channels.* Nature, 1997. **385**(6613): p. 272-5.
70. Berneche, S. and B. Roux, *Energetics of ion conduction through the K+ channel.* Nature, 2001. **414**(6859): p. 73-7.
71. Ostmeyer, J., et al., *Recovery from slow inactivation in K+ channels is controlled by water molecules.* Nature, 2013. **501**(7465): p. 121-4.
72. Cordero-Morales, J.F., L.G. Cuello, and E. Perozo, *Voltage-dependent gating at the KcsA selectivity filter.* Nat Struct Mol Biol, 2006. **13**(4): p. 319-22.
73. Rasmusson, R.L., et al., *Inactivation of voltage-gated cardiac K+ channels.* Circ Res, 1998. **82**(7): p. 739-50.
74. Starkus, J.G., et al., *Ion conduction through C-type inactivated Shaker channels.* J Gen Physiol, 1997. **110**(5): p. 539-50.
75. Yellen, G., et al., *An engineered cysteine in the external mouth of a K+ channel allows inactivation to be modulated by metal binding.* Biophys J, 1994. **66**(4): p. 1068-75.
76. Liu, Y., M.E. Jurman, and G. Yellen, *Dynamic rearrangement of the outer mouth of a K+ channel during gating.* Neuron, 1996. **16**(4): p. 859-67.
77. Jarecki, B.W., et al., *Human voltage-gated sodium channel mutations that cause inherited neuronal and muscle channelopathies increase resurgent sodium currents.* J Clin Invest, 2010. **120**(1): p. 369-78.
78. Benatar, M., *Neurological potassium channelopathies.* QJM, 2000. **93**(12): p. 787-97.
79. Won, S., et al., *MAGUKs: multifaceted synaptic organizers.* Curr Opin Neurobiol, 2017. **43**: p. 94-101.

80. Han, K. and E. Kim, *Synaptic adhesion molecules and PSD-95.* Prog Neurobiol, 2008. **84**(3): p. 263-83.
81. Kim, E., et al., *Clustering of Shaker-type K+ channels by interaction with a family of membrane-associated guanylate kinases.* Nature, 1995. **378**(6552): p. 85-8.
82. Zandany, N., et al., *Alternative splicing modulates Kv channel clustering through a molecular ball and chain mechanism.* Nat Commun, 2015. **6**: p. 6488.
83. Koo, G.C., et al., *Blockade of the voltage-gated potassium channel Kv1.3 inhibits immune responses in vivo.* J Immunol, 1997. **158**(11): p. 5120-8.
84. Marrion, N.V., *Control of M-current.* Annu Rev Physiol, 1997. **59**: p. 483-504.
85. Chatterjee, A., et al., *A genetically encoded fluorescent probe in mammalian cells.* J Am Chem Soc, 2013. **135**(34): p. 12540-3.
86. Nikic, I., et al., *Labeling proteins on live mammalian cells using click chemistry.* Nature Protocols, 2015. **10**(5): p. 780-791.
87. Hoshi, T., W.N. Zagotta, and R.W. Aldrich, *Two types of inactivation in Shaker K+ channels: effects of alterations in the carboxy-terminal region.* Neuron, 1991. **7**(4): p. 547-56.
88. Baukrowitz, T. and G. Yellen, *Modulation of K+ current by frequency and external [K+]: a tale of two inactivation mechanisms.* Neuron, 1995. **15**(4): p. 951-60.
89. Starkus, J.G., S.H. Heinemann, and M.D. Rayner, *Voltage dependence of slow inactivation in Shaker potassium channels results from changes in relative K(+) and Na(+) permeabilities.* J Gen Physiol, 2000. **115**(2): p. 107-22.
90. Lewin, L., et al., *Direct Evidence for a Similar Molecular Mechanism Underlying Shaker Kv Channel Fast Inactivation and Clustering.* J Mol Biol, 2019. **431**(3): p. 542-556.

2 Chapter 2

Methodology

2.1 Incorporation of unnatural amino acids

During protein translation, the ribosome synthesizes a polypeptide according to mRNA directions. The genetic code from the mRNA is identified by the anticodon present on the tRNA. The tRNA then incorporates the amino acid associated with it. The 20 canonical amino acids found in higher organisms have specific set of tRNA and aminoacyl tRNA synthetase [1], which is known as orthogonal aaRS/tRNA pair.

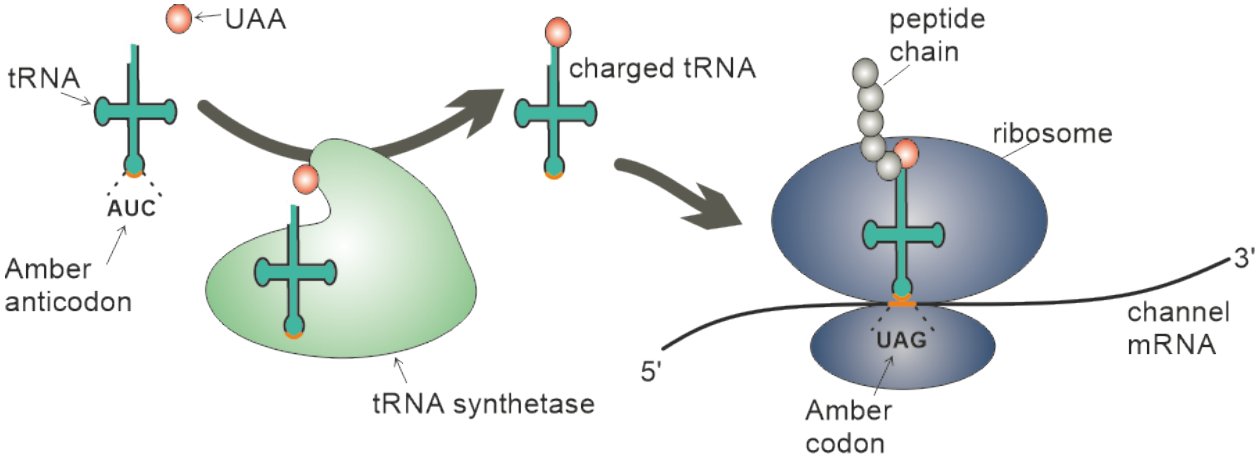

Figure 2.1: Insertion of UAA during protein translation

UAA specific tRNA and tRNA synthetase are expressed in the cells. The tRNA recognizes the UAA and binds to it in order to incorporate it in the translated protein.

However, this basic machinery of protein expression can be modified to incorporate other amino acids with desired functions to further investigate the protein structure and function. Since no tRNA is found to bind to stop codons, stop codons lead to the termination of protein synthesis. By aminoacylating a tRNA reprogrammed to complement one stop codon, this new tRNA can be used

to incorporate non canonical amino acids (or unnatural amino acids, UAA) into a protein. A truncated tRNA can be aminoacylated with UAAs., The incorporation of UAA mostly utilizes the amber stop codon since it is the least utilized in mammalian organisms [2]. These noncanonical amino acids are chosen to alter the physiochemical and biological properties of the amino acid they replace. Many different kinds of UAAs have been synthesized for various structure function analysis. These include spectroscopic probes, metal ion chelators, photo-affinity probes and photocaged amino acids, posttranslational modifications, and amino acids with orthogonal chemical activity for the site-specific modification of proteins. By engineering new heterologous aaRS/tRNA pair, many UAAs have been genetically encoded at desired sites in different bacterial, yeast and mammalian expression systems (Fig 2.1).

2.2 Cut open voltage clamp

Ion channels are most widely studied by overexpressing the desired channels in the oocytes of Xenopus laevis (African frog). The big size of the egg and low endogenously expressed channels makes it a very good model for the electrophysiological studies. In order to study the membrane properties, the two-electrode voltage clamp (TEVC) technique was developed. In this method, as the name suggests, two electrodes are inserted into the cytosol of the oocyte, one for injecting current to maintain the membrane at a desired potential and the other to sense the voltage. By recording the current required to keep the voltage constant, ion channel kinetics can be studied. The TEVC technique was improved to the Cut open voltage clamp (COVC) technique by Bezanilla and Stefani in 1998 [3]. It was designed to reach the desired voltage much faster thus allowing to record faster current dynamics and gating currents compared to TEVC. It has the additional benefit of allowing access to the intracellular milieu of the oocytes, which can be exchanged.

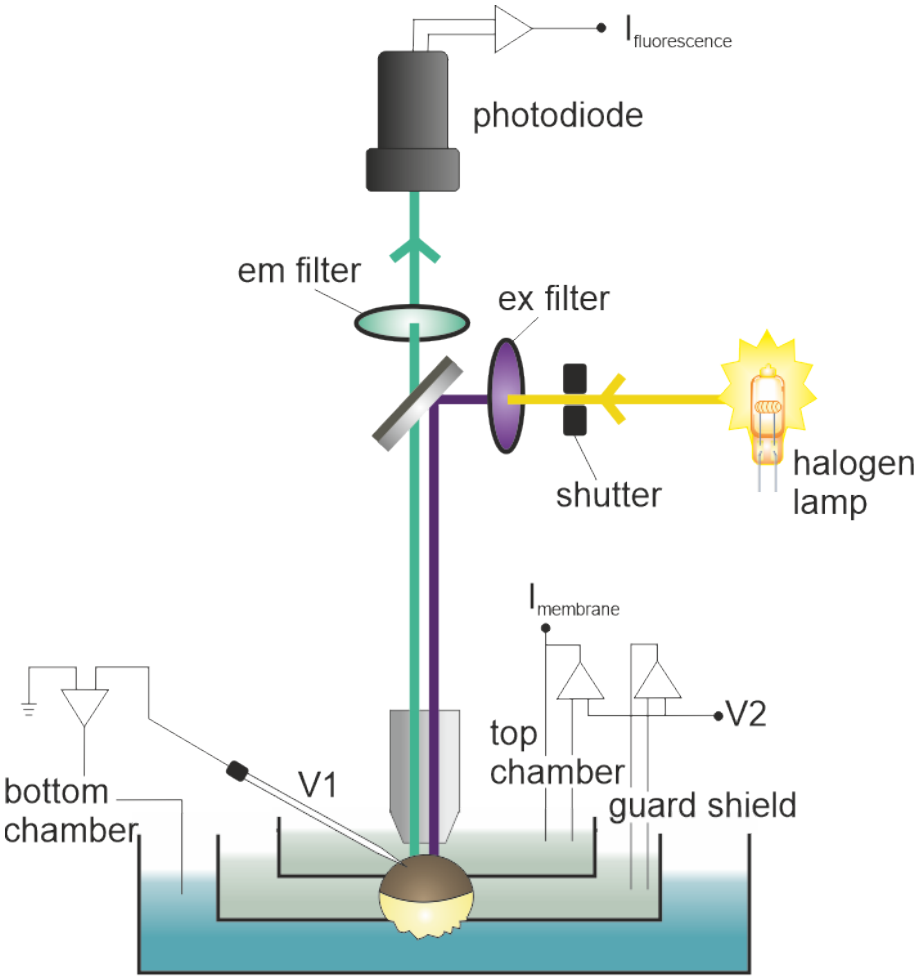

Figure 2.2: Illustration of the COVC and VCF setup

A permeabilized oocyte is mounted on a chamber of three electrically separated compartments. The bottom chamber is clamped to 0 mV (as measured by V1), while the top chamber and guard shield are clamped to the command potential (as measured by V2). V1 senses the voltage under the membrane and current is injected into the oocyte via the bottom chamber. For fluorescence measurements, the excitation light is directed towards the oocyte surface via a dichroic mirror and the emitted light is detected by a photodiode.

The COVC setup consists of 3 compartments (Fig 2.2). The top compartment is named the recording chamber and is used to clamp the oocyte by inserting an electrode (V1). The middle chamber acts as an electronic guard shield to maintain a defined voltage on the oocyte membrane. The bottom compartment is used to permeabilize the oocyte membrane by 0.1% saponin in order to gain access to the cytoplasmic environment and to inject current.

There are 5 bath electrodes to control the 3 compartments, which are connected to the electrical components by agar bridges. Electrodes P1 (top chamber) and GS1 (middle chamber) record the bath potential, and P2 and GS2 inject current to the top and middle chamber, respectively, to maintain P1 and GS1 at command potential. By maintaining the middle chamber at the same potential, guard shield prevents any current leakage between the top and bottom chamber, and any leak between bottom and guard chamber will only affect the guard current (which is ignored). During passive mode or clamp OFF setting, the V1 electrode reads the membrane potential of the oocyte. When the clamp is turned ON, the oocyte interior is held at ground potential through an active feedback loop between the inserted electrode V1 and the current injecting bath electrode I in the bottom chamber. COVC is able to achieve faster clamping speeds due to lower access resistance for intracellular current injection and electrical isolation of recording chamber and guard chambers. The access resistance is considerably reduced by permeabilizing the oocyte membrane in the lower chamber, leading to elimination of the bottom access resistance and more accurate and faster electrical response.

2.3 Voltage Clamp Fluorometry

When light falls on a fluorescent molecule, the electromagnetic radiation can excite the electrons in resonance to a higher electronic energy level (S1). The probability for electron excitation at a specific wavelength is given by the molar extinction coefficient of the fluorophore. After excitation to the higher energy state, the electron loses some energy through vibrational relaxation to come to the ground vibrational energy level of the excited S1 state. When the electron returns to the ground electronic state (S0), the energy released is less than the energy gained in excitation, which leads to emission of a photon of longer wavelength (Fig 2.3). This change in wavelength between the excited and emitted radiation is known as Stokes shift. However, the transition of electrons to the ground state does not always result in release of a photon. The energy can alternatively be dissipated to the surrounding through solution quenching or as heat. The probability that the excited electron will release a photon is known as quantum yield (QY). QY varies from 0.2 to 0.9 for conventional fluorophores.

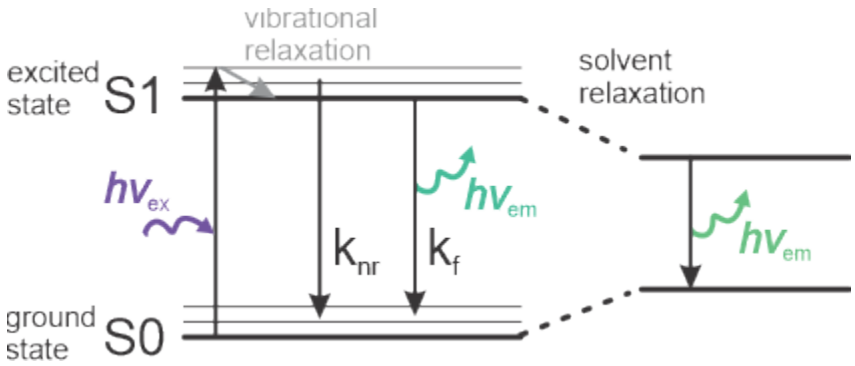

Figure 2.3: Jablonski diagram

Jablonski diagram illustrating excitation of a molecule from the S0 ground state to a vibrational level of the S1 excited state. The molecule returns to ground state either via a non-radiative pathway (k_{nr}) or by emitting a photon [4]. The energy of the emitted photon depends on the solvent hydrophobicity.

Fluorescence measurements are extensively used nowadays to probe structural and conformational changes in proteins. Voltage clamp fluorometry was developed as an improvement over scanning cysteine accessibility mutagenesis by the Isacoff laboratory [5]. In this technique, structural rearrangements in proteins are viewed as changes in fluorescence. A decrease in fluorescence results from exposure to solvent (solvent relaxation) or proximity to a quencher (quenching) during structural transitions. Simultaneous measurement of current/gating charges and recording of fluorescence intensity allows study of channel kinetics in real time. Moreover, the short lifetime of a fluorophore in the excited state (10-9 - 10-12s) allows detection of fast kinetics. Since the fluorophore reports changes in a localized area around its introduction site, it spatially resolves dynamic changes in the protein. VCF has been a pioneering the technique to study conformational changes in ion channels.

2.4 Lanthanide Resonance Energy Transfer (LRET)

LRET is a variant of FRET (Förster Resonance Energy Transfer). FRET can be used to measure distance between two positions separated by 15-100 Å. Two positions are labelled by fluorophores, donor and acceptor with the emission of donor overlapping with the excitation of acceptor fluorophore. When the donor is excited, energy is transferred to the acceptor fluorophore

dependent on their relative distance, allowing to calculate the distance between the donor and acceptor [6].

When the donor is excited, it produces an oscillating electric dipole field that decays with distance. A nearby acceptor with excitation energies corresponding to the frequencies of the electric field produced by the dipole absorbs this energy and gets excited. The probability of acceptor being excited decays with distance as E ∝R-6. The energy transferred can be used to calculate the distance using the following equation:

$$R = R_O \left(\frac{1}{E} - 1\right)^{1/6},$$

where R is the distance between donor and the acceptor, E is the amount of energy transferred and Ro is a constant which depends on the spectral properties of the donor acceptor pair and the orientation of their electric dipoles. It is the distance at which 50% of the energy is transferred.

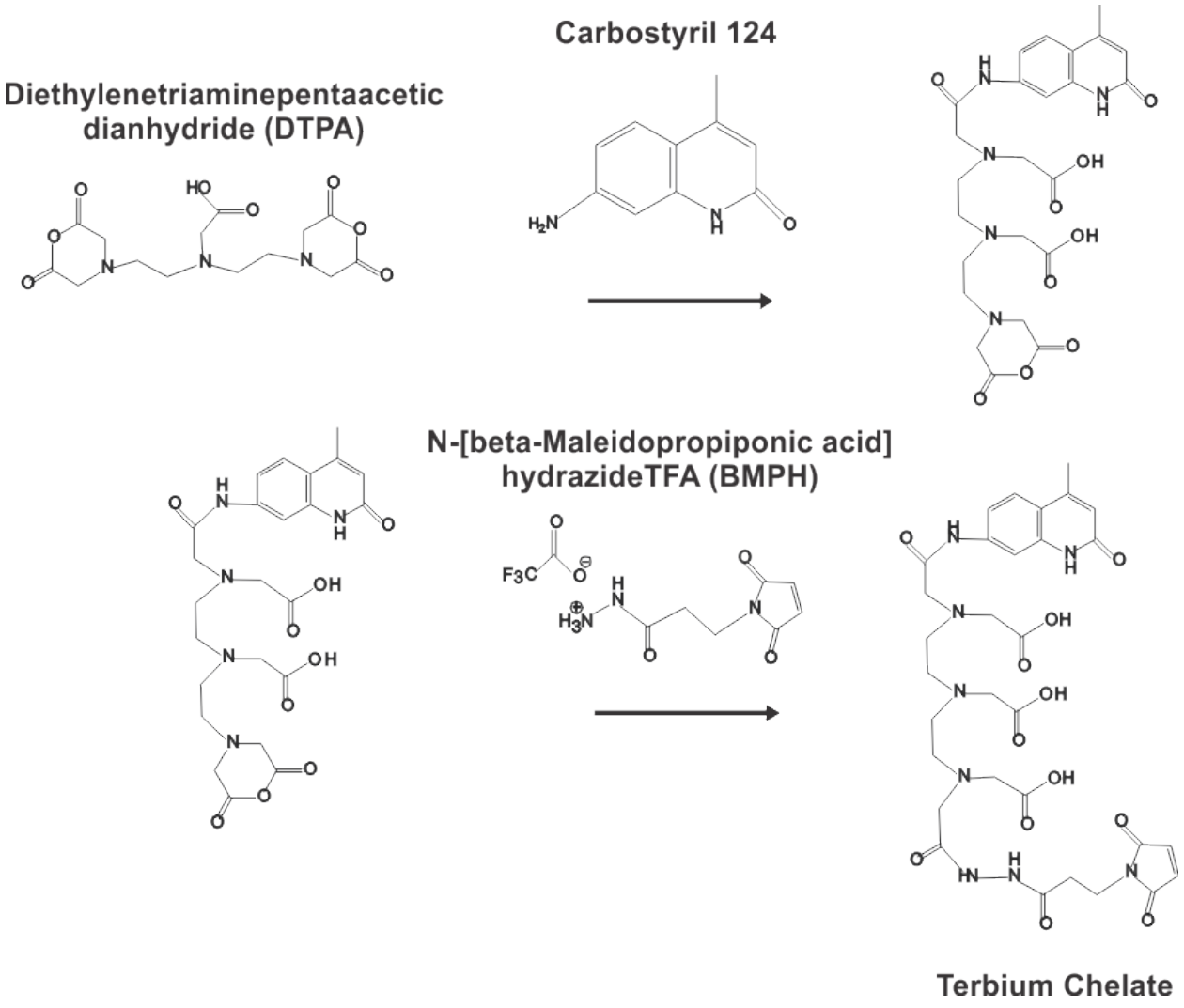

Figure 2.4: Synthesis of terbium chelate

Reaction scheme according to which the terbium chelate used in this thesis was synthesized in the laboratory (modified from [7]).

In the variation LRET, instead of an organic fluorophore, a lanthanide group element (terbium or europium) is used. Due to their low extinction coefficient, they are poor absorbers of photon and hence require an additional antenna molecule that absorbs the light and transfers it to lanthanide atom. The entire complex contains 3 different components (Fig 2.4): an antenna molecule that absorbs the incoming photon and transfer it to the lanthanide atom, a chelate that coordinates the atom and shields it against the quenching effect of the solvent, and a linker molecule (e.g. maleimide) to covalently bind the fluorophore to the desired position in the

fluorophore. The lanthanides show a characteristic emission spectrum (Fig 2.5) and possess very long decay lifetimes (usually milliseconds as compared to nanoseconds for organic fluorophores). These properties greatly enhance accuracy and signal to noise ratio for these measurements.

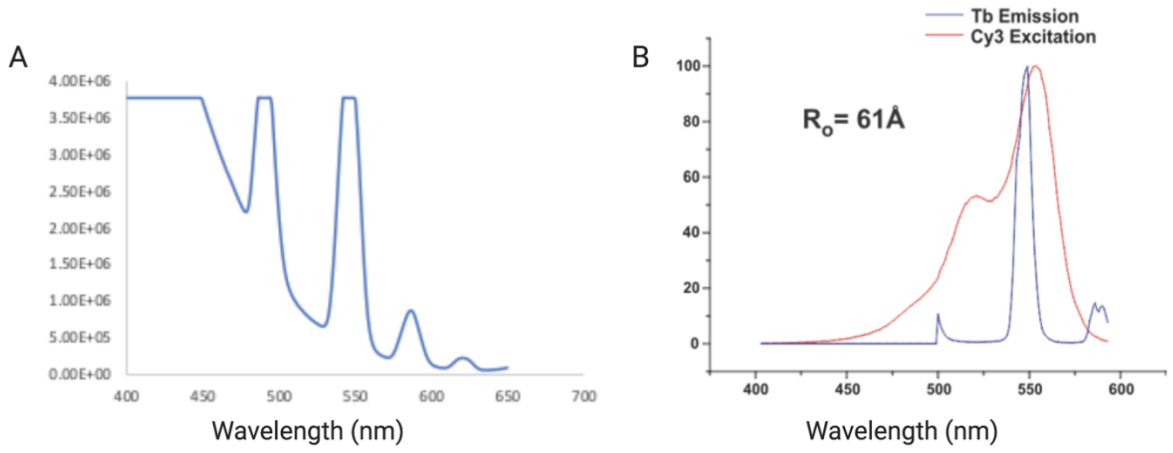

Figure 2.5: Emission spectra of terbium chelate

A) Emission spectra of terbium chelate. B) Spectral overlap of terbium chelate with cy3 fluorophore.

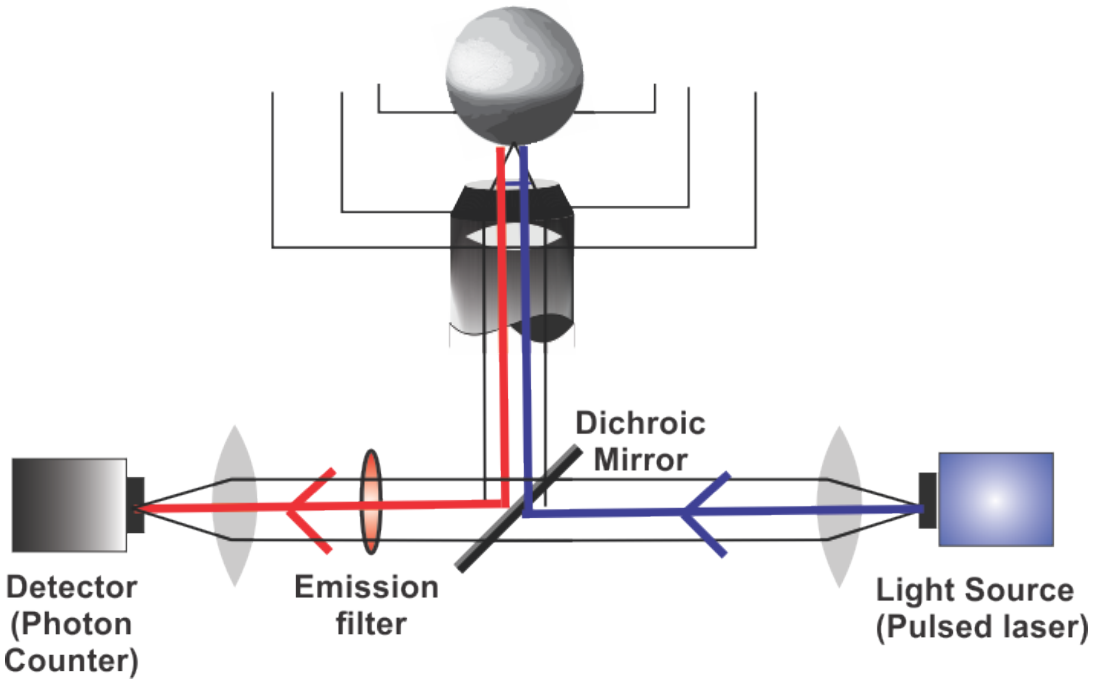

Figure 2.6: LRET setup

The LRET setup consists of an inverted microscope. The oocyte is placed on top of the objective. A pulsed laser (337nm) is used to excite the donor fluorophores and the fluorescent emission from the acceptor is recorded by a photon counter.

2.5 Transition metal FRET (tmFRET)

Ever since their inception, FRET and LRET techniques have been used extensively to study the interaction between two proteins [8]. By measuring the amount of energy transfer, they can be used to estimate distance between the two labelled molecules. However, the average R_0 values for different pairs varies from 30-80 Å thus limiting the shortest distance that can be reliably measured. Also, large fluorophore size and presence of linkers used to attach them to the proteins increase the conformational flexibility of the dye [9, 10]. Thus, it may not accurately translate the dynamics of the protein chain being measured. Additionally, uncertainty in measurement of fluorophore orientation relative to each other further exacerbates the inaccuracy. Lanthanide metal ions used in tmFRET have relatively small RO values (10-20 Å which allows measurement of smaller distances with greater accuracy. Their small size and multiple transition dipoles also reduce the orientation dependence of these measurements.

In tmFRET, a transition metal ion is used to absorb the energy of donor fluorophore. The degree of quenching is a direct measure of the FRET efficiency. Transition metal ions have been shown to absorb light in the visible region[11-15]. The small size of metal ion along with multiple absorption dipoles greatly reduces the orientation dependence between donor and acceptor. This, in turn, helps in more accurate distance determination. Also, each metal binding position can be used for binding different metal ions, thus resulting in a different FRET pair. The Ro values for transition metal ion FRET pair varies from 9 to 16 Å. This allows measurement of close-range distances.

The attachment of metal ions to the protein backbone can be accomplished by site-directedly introducing di-histidine motifs into the protein. Di-histidine motifs bind metal ions with high affinity. The binding affinity of the metal ion to the metal binding site in the protein can also be used to determine the secondary structure of the protein. As the binding of metal ion is related to helix stability, a change in helix stability will be reflected in the binding affinity of the metal. Therefore, tmFRET can be used to measure close range distance between two positions as well as secondary structure stability of the protein[16].

2.6 Experimental procedures

2.6.1 Molecular biology

Point mutations are generated using site-directed mutagenesis (QuikChange; Agilent Technologies) with primers of 20-40 bases in length. 1 µl DpnI restriction enzyme is added to digest template DNA. Heat pulse transformation into XL1-Blue supercompetent cells is followed by adding 300 µl of SOC medium. Sample is put to 1 hour incubation with shaking at 250 rpm at 37°C. 200 µl are plated on LB-ampicilin agar plates and incubated overnight at 37 °C. Single colonies are selected and are incubated in 5 ml LB medium and 100 µg/mL ampicillin, with shaking at 250 rpm at 37 °C overnight. A Spin Miniprep Kit (Qiagen) is used to obtain isolated 200 ng/µl DNA in a 50 µl total volume. Sequences are verified in an in-house sequencing facility.

DNA is amplified with a second round of transformation into XL1-Blue supercompetent cells. 10 µl is plated on LB-ampicilin agar plates and incubated overnight at 37 °C. Single colonies are selected and are incubated in 250 ml LB medium and 100 µg/mL ampicillin, with shaking at 250 rpm at 37 °C overnight. A Midiprep Kit (Qiagen) is used to obtain isolated 1.5 ug/µl DNA in

20 µl volume. The DNA is linearized with NotI restriction enzyme and used for RNA in vitro transcription with the mMESSAGE mMACHINE® T7 Ultra Kit (ThermoFisher). RNA is extracted with phenol/chloroform and precipitated with ethanol to obtain a pellet which is resuspended in 20 µl nuclease-free water. Typically, 2 µg/µl of pure RNA is obtained and is ready for injection into oocytes. RNA is stored at -80 °C.

2.6.2 Expression

The pAnap plasmid, a pCDNA3.1+ vector (Addgene #48696), encodes for a mutated E.coli leucyl synthethase and 8 copies of E.coli tRNALeu[17].

4.6-9.2 nl of 0.1 µg/µl of pAnap is injected into the oocyte nucleus, 6-24 hours prior to coinjection of 2-40 ng of mRNA and 23 nl of 1 mM Anap, in a total volume of 46 nl. The 1 mM Anap stock solution is diluted in nuclease-free water with 1% 1N NaOH and is stored at -20℃. The oocytes are then incubated at 18℃ in Barth's solution supplemented with 5% horse serum for 1-3 days after which they are ready for VCF recordings. The amount of DNA and RNA, and the incubation time depends on individual mutant expression efficiency and required expression level.

To ensure high yield and to limit leak expression of channels lacking Anap, tRNA and synthetase expression is allowed before injection of channel mRNA. This way, there will be immediately amber tRNAs amino-acylated with Anap available for insertion when the ribosome encounters the amber stop codon during translation. The success rate for good expression varies within the mutants and within batches of oocytes. When the most efficient mutants express, they show robust currents in 75% of the injected oocytes. The least efficient mutants generally exhibited a success rate of 25%. Regardless of the expression efficiency, it would occasionally happen that a batch of oocytes or injections exhibit no currents at all.

2.6.3 Data analysis

Current and fluorescence are recorded and registered using the GPatch acquisition software and data is analyzed with Analysis software (Department of Anesthesiology, University of California, Los Angeles, CA). Currents and fluorescence changes are elicited by a typical voltage 10 mV step protocol ranging from -120 mV to +50/150 mV from a holding potential of -90 mV.

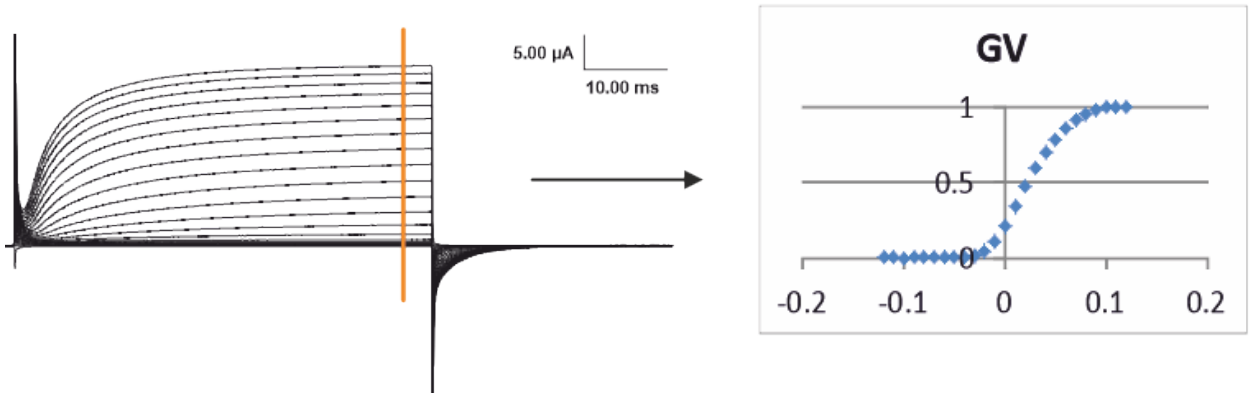

Figure 2.7: Ionic currents and GV

Example of raw data from a Shaker L382Anap expressing oocyte eliciting outward ionic currents in response to a voltage step protocol. The current amplitudes denoted at the orange line are converted to conductance G and plotted as a function of voltage [17]

2.6.4 Ionic currents

Steady state ionic current amplitudes from conducting mutants are analyzed at the end of the voltage step (orange line in Fig 2.7) from which the conductance G, is calculated using

$$G = \frac{I}{V - V_0},$$

where I is the current amplitude, V is the voltage and V_0 is the reversal potential for the conducting ion. The GV curve is obtained by plotting the normalized conductance as a function of voltage (Fig 2.7).

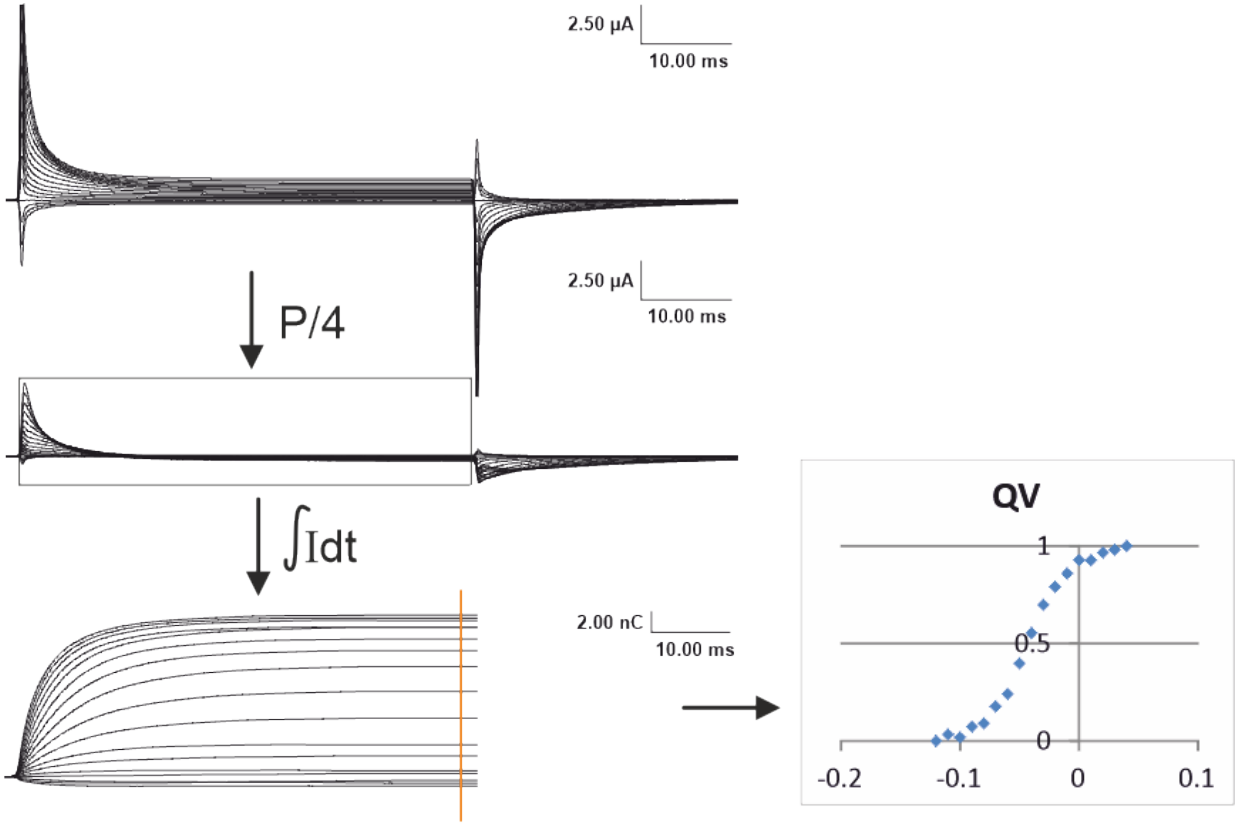

Figure 2.8: Gating currents and QV

Example of a Shaker L382Anap-W434F expressing oocyte eliciting transient gating currents in response to the same voltage step protocol as in Figure 6. Gating currents are isolated from the capacitance current via the P/4 procedure. Next, the gating charge is calculated by integration, and values are plotted at the orange line as a function of voltage (QV).

2.6.5 Gating currents

Gating currents from W434F mutants are obtained by subtracting the capacitive currents using the P/4 procedure [18]. After each voltage step, a pulse in the region of no charge movement and of the same magnitude as the applied voltage step, is added or subtracted online, depending on the direction of the subtraction step (Fig 2.8). To prevent membrane breakdown at large voltage steps, the subtraction step is divided into 4 equal steps. The equivalent gating charge of the elicited gating currents is the integral of the gating current that flows when the ion channel moves within the electric field. The QV curve is then obtained by plotting the calculated charge at the end of the voltage step (orange line in Fig 2.8) as a function of voltage and normalized.

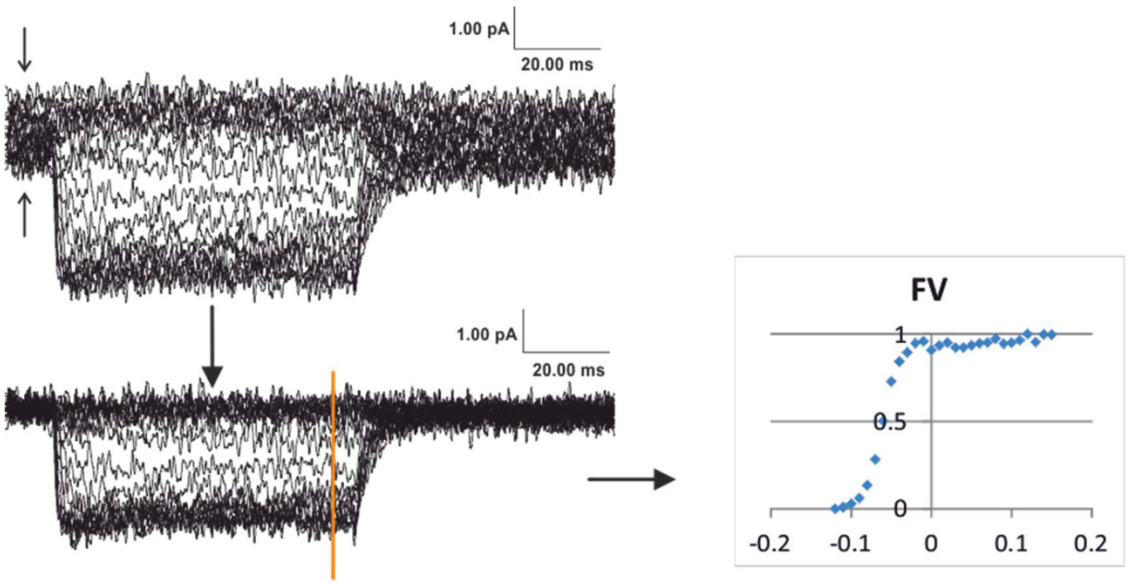

Figure 2.9: Fluorescence intensity and FV

Example of fluorescence data from the same oocyte as in Figure 2.8. Bleaching effects are accounted for by baselining each trace before the voltage step. The fluorescence intensities are then plotted at the orange line as a function of voltage (FV).

2.6.6 Fluorescence changes

The fluorescence intensities are detected simultaneously with the currents. Because of fluorophore bleaching between the voltage steps, the intensity of each trace decreases over time. The bleaching effect is corrected for by baselining each trace to the same value before the voltage step (small arrows in Fig 2.9). The fluorescence intensity amplitudes at the end of the voltage step (orange line in Fig 2.9) are then normalized and plotted as a function of voltage, giving the fluorescence-voltage (FV) characteristics.

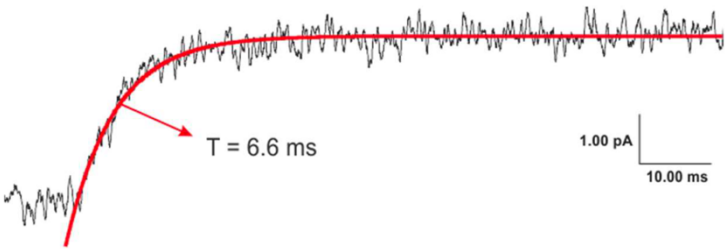

Figure 2.10: Exponential fit of a fluorescence time course

Example of a fluorescence time course fit to one exponential component (red) yielding a time constant of 6.6 ms

2.6.7 Fitting the data

To demonstrate the validity of GV, QV and FV curves, data is obtained from 4-10 oocytes from at least two different batches of oocytes. The normalized average is plotted as a function of voltage with mean standard deviation error bars calculated as,

$$mean\ SD = \sqrt{\frac{\sum(x - \bar{x})^2}{n}}$$

where x is the sample value, $\bar{x}$ is the mean of all the values and n is the sample size. A Boltzmann distribution is fit to the sigmoidal GV, QV and FV curves as we assume that the channel can be in either of two energy levels e.g., open/closed for the pore [17], deactivated/activated for the voltage sensor (QV) and either of two conformational states (FV).

Finally, kinetic information is obtained by fitting the time course traces to an exponential function (Fig 2.10); whenever necessary, a sum of two or three exponentials was used,

$$y = \sum_i A_i \cdot exp(t/\tau_i) + B$$

where A_i are the amplitudes, t is time, τ_i are the time constants, and B is the baseline.

2.7 LRET measurements

For donor only labelling, oocytes were incubated in a depolarizing solution (115 mM K-MeSO3, 2 mM Ca(OH)2, 10 mM HEPES, at pH 7.1) containing Tb3+ complex (5 μM) at room temperature for 20 min. For acceptor labelling, Cy3 tetrazine was injected into the oocytes a day before the experiment. The setup was based on a Zeiss Axiovert 200 microscope (Fig 2.6). Light at 337 nm from a pulsed 3-mW N2-laser (Spectra-Physics) was directed in a wide-field illumination onto the oocytes containing the labeled channels. The light from the oocytes was collected using a 1.25 NA 40× glycerol immersion quartz objective (Partec) and filtered with a bandpass emission filter. Light was detected by a photon counter (Laser Components). Analysis of the lifetime decays was done with an exponential fitting program (MATLAB). Distances were determined using the following equations

$$Energy\ Tranfer\ (E) = 1 - \frac{\tau_{SE}}{\tau_{DO}}$$

where τ_{DO} is the time constant of the donor lifetime decay in absence of acceptor (donor-only), and τ_{SE} is the time constant decay of the sensitized emission of the acceptor (donor excitation with acceptor emission).

The distance between the donor and the acceptor was determined using

$$R = \left(\frac{1 - E}{E}\right)^{1/6} \times R_O$$

where R_0 is the distance at which 50% energy transfer occurs. The R_0 value used for the fluorophore pair of Tb3+ complex and cy3 tetrazine was 61.2Å [19].

2.8 tmFRET measurements

Fluorometry experiments were performed on the VCF setup described above. $CoSO_4$ was injected into the oocytes to a final concentration of 2μM for FRET experiment. Energy transfer efficiency was calculated according to the following equation as mentioned in Dai et al. [20]

$$FRET_{eff} = \frac{F_{noHH} - F_{HH}}{F_{HH} \times F_{noHH} + F_{noHH} - F_{HH}}$$

where F_{HH} is the normalized fluorescence of channels with dihistidines and F_{noHH} is the normalized fluorescence of channels without dihistidines. The distances were then calculated using the Förster equation as follows :

$$R = R_O \left(\frac{1}{FRET_{eff}} - 1 \right)^{1/6}$$

where R_0 is the Förster distance for FRET between L-Anap and Co^{2+}-dihistidine (12 Å).

2.9 References

1. Kaarsholm, N.C., et al., *Engineering Glucose Responsiveness Into Insulin.* Diabetes, 2018. **67**(2): p. 299-308.
2. Liu, C.C. and P.G. Schultz, *Adding new chemistries to the genetic code.* Annu Rev Biochem, 2010. **79**: p. 413-44.
3. Stefani, E. and F. Bezanilla, *Cut-open oocyte voltage-clamp technique.* Methods Enzymol, 1998. **293**: p. 300-18.
4. Gleick, P.H., et al., *Climate change and the integrity of science.* Science, 2010. **328**(5979): p. 689-90.
5. Mannuzzu, L.M., M.M. Moronne, and E.Y. Isacoff, *Direct physical measure of conformational rearrangement underlying potassium channel gating.* Science, 1996. **271**(5246): p. 213-6.
6. Selvin, P.R., *Principles and biophysical applications of lanthanide-based probes.* Annu Rev Biophys Biomol Struct, 2002. **31**: p. 275-302.
7. Heyduk, E. and T. Heyduk, *Thiol-reactive, luminescent Europium chelates: luminescence probes for resonance energy transfer distance measurements in biomolecules.* Anal Biochem, 1997. **248**(2): p. 216-27.
8. Taraska, J.W. and W.N. Zagotta, *Fluorescence applications in molecular neurobiology.* Neuron, 2010. **66**(2): p. 170-89.
9. Best, R.B., et al., *Effect of flexibility and cis residues in single-molecule FRET studies of polyproline.* Proc Natl Acad Sci U S A, 2007. **104**(48): p. 18964-9.
10. Wiczk, W., et al., *Distance distributions recovered from steady-state fluorescence measurements on thirteen donor-acceptor pairs with different Forster distances.* J Fluoresc, 1991. **1**(4): p. 273-86.
11. Horrocks, W.D., Jr., B. Holmquist, and B.L. Vallee, *Energy transfer between terbium (III) and cobalt (II) in thermolysin: a new class of metal--metal distance probes.* Proc Natl Acad Sci U S A, 1975. **72**(12): p. 4764-8.

12. Richmond, T.A., et al., *Engineered metal binding sites on green fluorescence protein.* Biochem Biophys Res Commun, 2000. **268**(2): p. 462-5.
13. Sandtner, W., F. Bezanilla, and A.M. Correa, *In vivo measurement of intramolecular distances using genetically encoded reporters.* Biophys J, 2007. **93**(9): p. L45-7.
14. Taraska, J.W., et al., *Mapping the structure and conformational movements of proteins with transition metal ion FRET.* Nature Methods, 2009. **6**(7): p. 532-U94.
15. Taraska, J.W., M.C. Puljung, and W.N. Zagotta, *Short-distance probes for protein backbone structure based on energy transfer between bimane and transition metal ions.* Proc Natl Acad Sci U S A, 2009. **106**(38): p. 16227-32.
16. Gordon, S.E., et al., *Transition metal ion FRET to measure short-range distances at the intracellular surface of the plasma membrane.* J Gen Physiol, 2016. **147**(2): p. 189-200.
17. Bhatt, D.L., et al., *International prevalence, recognition, and treatment of cardiovascular risk factors in outpatients with atherothrombosis.* Jama-Journal of the American Medical Association, 2006. **295**(2): p. 180-189.
18. Armstrong, C.M. and F. Bezanilla, *Inactivation of the sodium channel. II. Gating current experiments.* J Gen Physiol, 1977. **70**(5): p. 567-90.
19. Zhou, M., et al., *Potassium channel receptor site for the inactivation gate and quaternary amine inhibitors.* Nature, 2001. **411**(6838): p. 657-61.
20. Dai, G. and W.N. Zagotta, *Molecular mechanism of voltage-dependent potentiation of KCNH potassium channels.* Elife, 2017. **6**.

3 Chapter 3

From resting state to inactivation, the journey of inactivation peptide in Shaker Kv channels

Roshan Pandey[1,2], Tanja Kalstrup[1,3] and Rikard Blunck[3,4] *

[2]Department of Biochemistry and Molecular Medicine, [3]Department of Pharmacology and Physiology, [4]Department of Physics, Université de Montréal, Montréal, Québec, Canada

[1] These two authors contributed equally to this work

Author Contribution

R.B. designed research, T.K. performed the VCF experiments. R.P. performed LRET, tmFRET experiments. T.K., R.P., and R.B. did the analysis and wrote the paper.

3.1 Abstract

Shaker Kv channels inactivate rapidly to culminate the action potential and maintain the homeostasis of excitable cells. The so-called N-type inactivation is caused by the first 46 amino acids of the N-terminus of the channel, known as the inactivation peptide (IP). Numerous mutational studies have characterized N-type inactivation functionally, however, the position of the IP in the resting state and its transition during inactivation is still debated. We tracked the movement of IP during inactivation using voltage clamp fluorometry. By inserting an unnatural amino acid, 3-[(6-acetyl-2-naphthalenyl) amino]-L-alanine (Anap), which is sensitive to changes in environment, we identified the movements of ball and chain separately. Our data suggests that N-type inactivation occurs in a biphasic movement by first releasing the IP, which then blocks the pore from the cytoplasmic side. To further narrow down the resting position of the inactivation peptide, we used Lanthanide-based Resonance Energy transfer and transition metal (tm)FRET. We propose that the inactivation peptide is located in the window formed by the channel and the T1 domain, interacting with the acidic residues of the T1 domain.

3.2 Introduction

During an action potential, voltage-gated potassium (Kv) channels open in response to membrane depolarization and allow the passage of K+ ions to repolarize the membrane. Duration and pattern of action potentials in excitable cells is partially regulated by fast inactivation during which the cytosolic N-terminus of Kv channels binds to the open pore and blocks the entry of ions (N-type inactivation) [1-4]. Fast inactivation is observed in Kv 1.4, Kv 3.4, Kv 4.2 and is caused by a peptide at the N-terminus (inactivation peptide IP). Variably, the N-terminus of the auxiliary β-subunit, which co-assembles with the Kv channel α-subunit, is thought to contain an inactivation peptide. Coexpression with β-subunit imparts inactivation to the non-inactivating currents of Kv1.1, 1.2, 1.3 and 1.5 channels [5, 6]. The IPs of N-type inactivating channels have no sequence similarity, but they all contain a hydrophobic tip region of approximately the first 10 amino acids, which in the Shaker Kv channel, have been suggested to inactivate the channel by interacting with hydrophobic pore-lining residues [1, 4]. The downstream hydrophilic region which carries a net positive charge, is responsible for increasing the diffusion rate of the IP towards the pore region via long-range electrostatic interactions [4, 7-9].

Below the transmembrane region of Shaker-related Kv1 channels, the cytoplasmic T1 domain, which is responsible for subunit tetramerization, is located [10-12]. The T1 domain is attached to the first transmembrane helix S1 via the T1-S1 linker in such a way that four windows form between the T1 domain and the transmembrane domain (fig 1A). It has been suggested that the N-terminus enters the window of its own subunit in order to reach the inner pore cavity [13, 14]. The T1-S1 linker contains conserved negative charges important for accommodating the positively charged chain region [7, 13, 15].

Even though the mechanism of N-type inactivation is functionally well characterized, any dynamic information about the pathway by which the IP travels from resting state to inactivation is lacking. By inserting a fluorescent unnatural amino acid (Anap) into the IP, using the amber stop codon suppression technique [16-18], we were able to probe relative movements using voltage clamp fluorometry (VCF). This procedure allowed us to compare tip motion (A3 and Y8) and chain motion (K19 and E35). Anap was also inserted into the T1-S1 linker receptor site (E201) to probe the arrival of the IP through the T1 window.

The current model for N-type inactivation generally implies that the N-terminus diffuses in the cytosol and enters through the side windows upon depolarization. Our results, in contrast, suggest that the N-terminus is already bound near or at the T1 windows. In order to probe the resting state position of IP, we performed lanthanide resonance energy transfer by labelling the alpha subunit of the channel (top of S4 and S5 helix) with a donor and ball (Y8) and chain (E35) with an acceptor fluorophore. To further narrow down the position, we performed transition metal FRET (tmFRET) taking advantage of its sensitivity for shorter distances [19]. To this end, we inserted dishistidine motifs at several positions around the T1-S1 window for binding cobalt. By calculating the energy transfer between cobalt and Anap incorporated at positions Y8 and E35 in the IP, we were able to locate the position of IP in the resting state.

3.3 Results

3.3.1 Anap incorporation does not inhibit N-type inactivation

In order to probe movements of the IP during N-type inactivation, Anap was inserted into selective sites in the Shaker channel via the amber codon suppression technique using the Anap specific tRNA synthetase/tRNA (RS/tRNA) pair [16, 17]. To this end, two positions in the tip

region, A3 and Y8, and two positions in the chain region, K19 and E35, were used as sites for Anap incorporation (fig 3.1A). Since N-terminal insertion of stop codons can lead to translational reinitiation at downstream start codons, nine start codons were silently mutated as previously described [20]. Anap was successfully incorporated into the four positions as determined from the robust expression in presence of Anap and poor expression in the absence of Anap (fig 3.1B-C). All mutants exhibited functional N-type inactivation (fig 1B) with WT-like inactivation voltage dependencies (fig 3.1D).

It has previously been shown that when the IP binds to the pore in the inactivated state, the voltage sensors are unable to return to their resting state, making unbinding of the IP the rate limiting step upon repolarization [21]. In W434F channels, where ionic currents are blocked but the gating machinery remains normal [22], voltage sensor immobilization materializes as a slow off-gating current during repolarization which disappears in the Δ6-46 deletion mutant (fig 3.1E) [21]. We used this feature to verify whether the tip properly reaches the final docking site in the Anap mutants. Indeed, charge immobilization was unaffected in all mutants as shown by the presence of a slow component in the off-gating currents with a time course similar to the one found in WT (fig 3.1F). The finding that the IP reaches the final docking site agrees with the functional current phenotypes seen during N-type inactivation (fig 3.1B). These results show that the presence of Anap in the tip and the chain region did not inhibit the ability of IP to reach the pore and block the ionic currents.

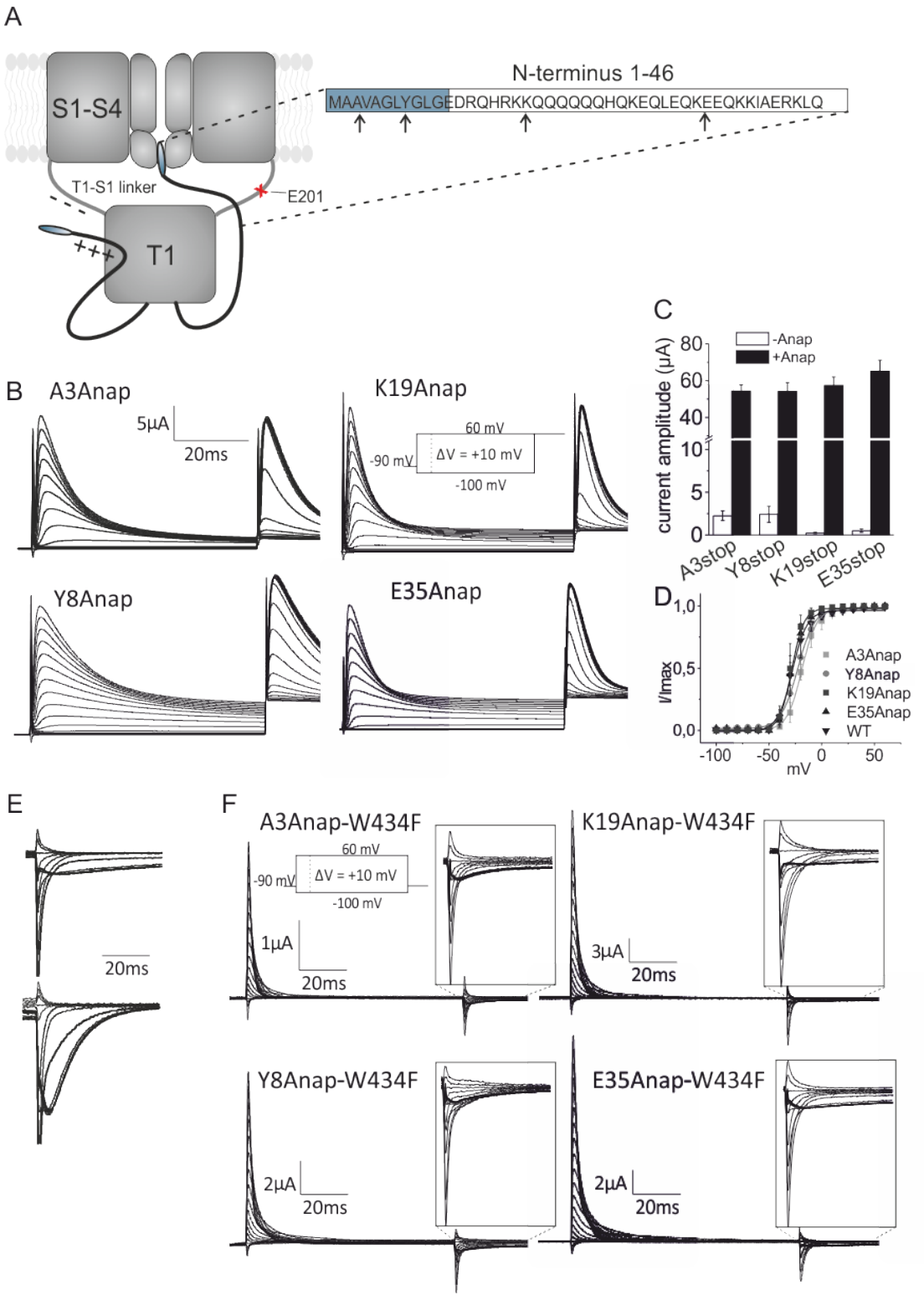

Figure 3.1 Functional expression with Anap in N-terminus

A) Cartoon of the Shaker channel inactivated by the N-terminus. Only two subunits are shown for clarity. Residues used in this study are marked arrows in the N-terminus and a red cross in the T1-S1 lin. **B)** Currents obtained from each N-terminal mutant upon a standard activation step protocol followed by a

second pulse to +60 mV. **C)** Expression levels shown as current peak amplitudes upon depolarizing from -90 mV to +40 mV for each mutant in the absence and presence of Anap. Adapted from Kalstrup and Blunck 2015 [17] **D)** IV curve for inactivation obtained by plotting the peak current during the second pulse in at +60 mV in C). **E)** Off-gating currents obtained with W434F in WT full length (upper) and Δ6-46 channels (lower). **F)** Gating currents obtained during a standard activation step protocol. Insets show the presence of charge immobilization.

3.3.2 Anap in the tip region probes final step in N-type inactivation

A3Anap and Y8Anap exhibited small voltage dependent fluorescence changes at expression levels above 50 μA when depolarizing to 40 mV (supplementary fig S3.1A-B). The slow inactivation kinetics seen in fig S3.1A-B are caused by channel clustering (discussed in following chapter) [23]. The presence of two fluorescence components of opposite direction made the analysis of A3Anap and Y8Anap challenging due to low dF/F values. In order to enhance the fluorescence signal, we therefore decided to use the non-conducting Shaker W434F mutant [24], which allows higher expression levels than the conducting channels. The fluorescence changes in W434F channels were similar to those of the conducting channels and did also exhibit two components of opposite direction (fig S3.1C-D and fig 3.2A-B, upper traces). In order to verify whether the fluorescence changes were caused by binding of the tip region to the pore, we used the Kv channel blocker 4-aminopyridine (4-AP), which inhibits the final transitions during channel activation [25-27]. Since pore opening needs to occur for the IP to reach the final docking site, we were able to identify fluorescence changes sensitive to the ability of the IP in blocking the pore. Indeed, application of 5 mM 4-AP resulted in inhibition of the second fluorescence component, suggesting that the final blocking step is monitored by Anap (fig 3.2A-B, middle traces).

We obtained the slow 4-AP sensitive component by subtraction the signal in presence of 4-AP from the original signal (fig 3.2A-B, lower traces). In Y8Anap, the fluorescence time course upon repolarization followed the slow kinetics of charge immobilization with a time constant τf = 73 ± 4 ms and τg = 74 ± 2 ms obtained from exponential fits (fig 3.2C). This indicates that the slow fluorescence component directly probes conformational changes during the final blocking step in agreement with its 4-AP sensitivity. The 4-AP sensitive component in A3Anap was too small to confidently fit to an exponential curve and was therefore not analyzed kinetically. Plotting the 4-AP insensitive [28] and 4-AP sensitive (slow) component as a function of voltage (FV) for

both mutants, revealed that, for both components, the voltage dependence is similar to that of inactivation (fig 3.2D-E). Taken together, these results strongly suggest that Anap at position A3 and Y8 in the IP probes a movement which causes the docking of the tip into the final receptor site.

The fast fluorescence component seen here also shows that IP starts to move with the activation of the channel. So, the IP is able to detect channel activation and mechanism of inactivation starts simultaneously with the opening of the channel. To further trace the movement of IP, we decided to insert Anap in the chain region.

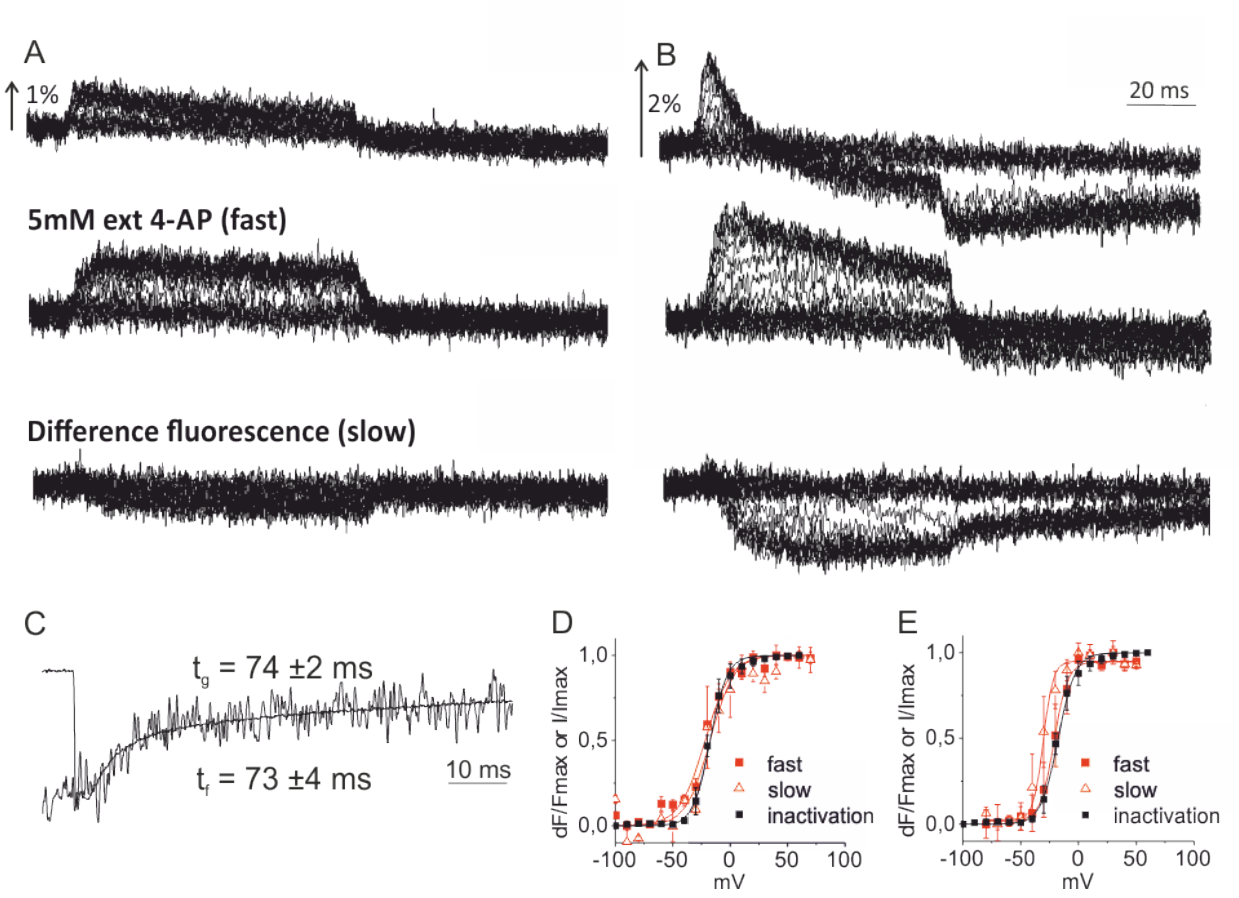

Figure 3.2 VCF results for the tip region mutants A3Anap and Y8Anap

A-B) Voltage-dependent fluorescence changes obtained during recordings of the gating currents in fig 3.1F for A3Anap-W434F A) and Y8Anap-W434F B). Middle traces are obtained in the presence of 5 mM external 4-AP, and the lower traces are the 4-AP sensitive components obtained via subtraction **C)** Overlap of Y8Anap-W434F off-gating current and fluorescence time course during repolarization from 0 mV to -90 mV. **D-E)** A3Anap-W434F (D) and Y8Anap-W434F (E) FV curves of the 4-AP sensitive (slow) and insensitive [28] components plotted together with the IV of inactivation from fig 3.1D.

3.3.3 Anap in the chain region probes movements preceding final block

For the chain mutants K19Anap and E35Anap, we followed the same protocol. In order to optimize the fluorescence changes, we required high expression levels (fig 3.3A-B). In contrast to the tip mutants, they exhibited a single fluorescence component which made the fluorescence signal easier to analyze and thus excluded the need for using W434F. In contrast to the tip mutants, K19Anap and E35Anap produced fluorescence intensity signals insensitive to application of 4-AP (fig 3.3C-D), suggesting that they report movement that occurs prior to the IP entering the pore. The FV of K19Anap correlated with the IV curve for inactivation with midpoint values of -19.3 mV and -14.3 mV respectively, as obtained from Boltzmann fits (fig 3.3F). On the other hand, the FV of E35Anap was more left shifted with respect to inactivation with midpoint values of -24.0 mV and -9.3 mV, respectively (fig 3.3H). The kinetics of inactivation and fluorescence varied from oocyte to oocyte with slower inactivation at increased expression as mentioned earlier (an effect which disappears with W434F, fig 3.3E). We therefore could not directly compare mean time constants. Nevertheless, when comparing inactivation and fluorescence kinetics of single oocytes, the data suggests that fluorescence and inactivation exhibit similar kinetics in K19Anap, whereas, in E35Anap, the time constant of fluorescence is approximately 10 ms faster than the one of inactivation (fig 3.3G and I). Taken together, the results indicate that, in both mutants, Anap is probing a transition which precedes final block, due to their 4-AP insensitivity. However, the two movements are not necessarily the same. The K19Anap movement develops closely with inactivation whereas E35Anap fluorescence signal is both shifted to more polarized potentials and faster than inactivation. A possible mode-of-action which could explain these results could be a sequential transition mechanism. First, the downstream chain region movement (E35) sets in motion, which then is followed by a second movement involving the upstream part of the chain (K19).

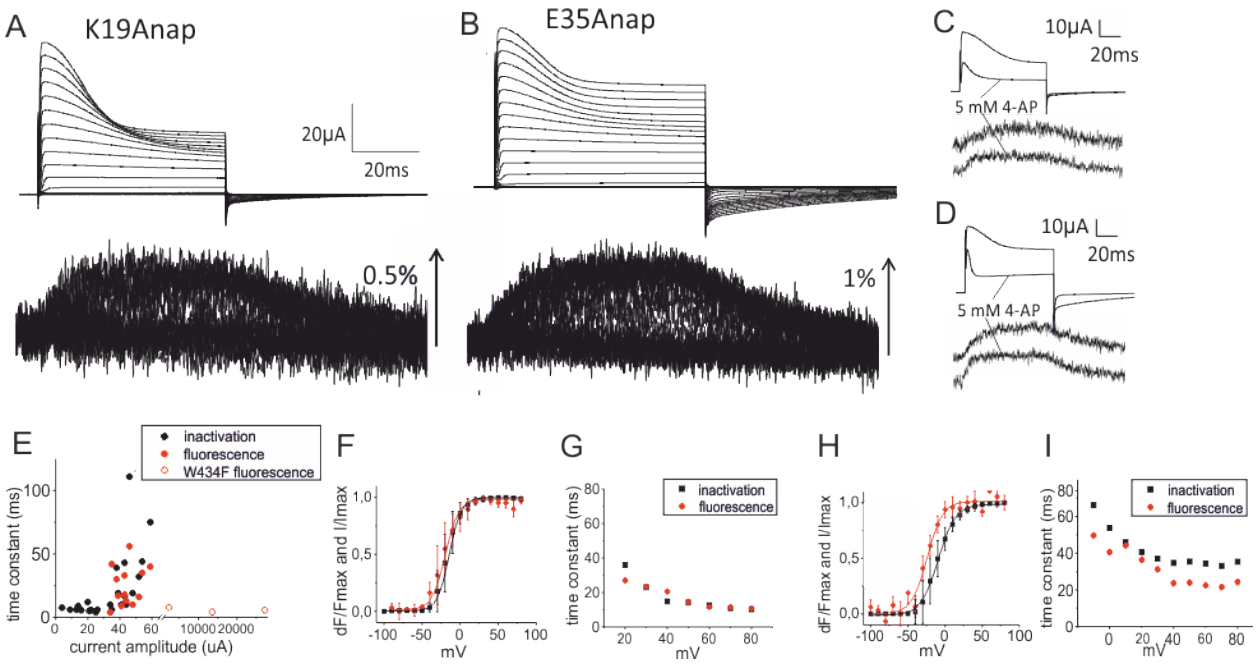

Figure 3.3 VCF results for the chain region mutants K19Anap and E35Anap

Examples of inactivating currents elicited by the chain mutants K19Anap **A)** and E35Anap **B)** and their respective fluorescence changes. **C-D)** Comparison of currents and fluorescence changes before and after application of external 4-AP during depolarization from -90 mV to + 40 mV. **E)** Time constants obtained from exponential fits of E35Anap current inactivation and fluorescence changes during depolarization from -90 mV to +40 mV, are plotted as a function of current amplitude (expression level). The corresponding ionic current of W434F gating currents were calculated using 13 elementary charges per channel [25, 26] with a unitary conductance of 20 pS. **F)** FV (red) and IV (black) curves obtained from K19Anap expressing oocytes. **G)** Time constants obtained from exponential fits of inactivation currents (black) and fluorescence (black) time courses of K19Anap expressing oocytes. H-I) Same as F-G) but for E35Anap expressing oocytes.

3.3.4 Location of the inactivation particle during the resting state of the channel

Our fluorescence data suggested a coordinated movement of ball and chain to cause inactivation of the channel. It senses channel activation and thus has to be in close proximity to the transmembrane domain during the resting state of the channel. This raises the question where the inactivation particle and the transmembrane region interact during the resting state. To identify this position, we probed whether we could detect the movement of the inactivation peptide in the transmembrane domain both during activation and inactivation. To this end, we inserted Anap at

position E201 in the T1-S1 linker (red mark, fig 3.1A). Like the N-terminal mutants, E201Anap exhibited functional N-type inactivation (fig 4A) and displayed fluorescence changes at high expression levels (fig 3.4B). As the T1-S1 linker is situated close to the voltage sensor, it is possible that the fluorescence changes of E201Anap originate from conformational rearrangements in the transmembrane domain during channel activation and not from the inactivation peptide. To verify this, the experiments were carried out in presence and absence of the inactivation peptide (inactivation-removed IR, lacking the N-terminus (Δ6-46)). IR-E201Anap channels exhibited no fluorescence changes (fig 3.4C), demonstrating that the movement, probed by Anap in E201Anap is caused by N-type inactivation. In agreement with this, both the V½ values and the time constants of the fluorescence signal correlated well with the corresponding values of the decay of the ionic current during fast inactivation (-21.6 mV and -15.8 mV, respectively; fig 3.4D-E). Despite this agreement with the kinetics and voltage dependence of fast inactivation, the fluorescence change was not sensitive to application of 4-AP (fig 3.4F), indicating that after release of the inactivation particle from its resting position during activation, it anneals to the window formed by the T1-S1 linker, the TM and T1 domains before the final step of entering and blocking the pore.

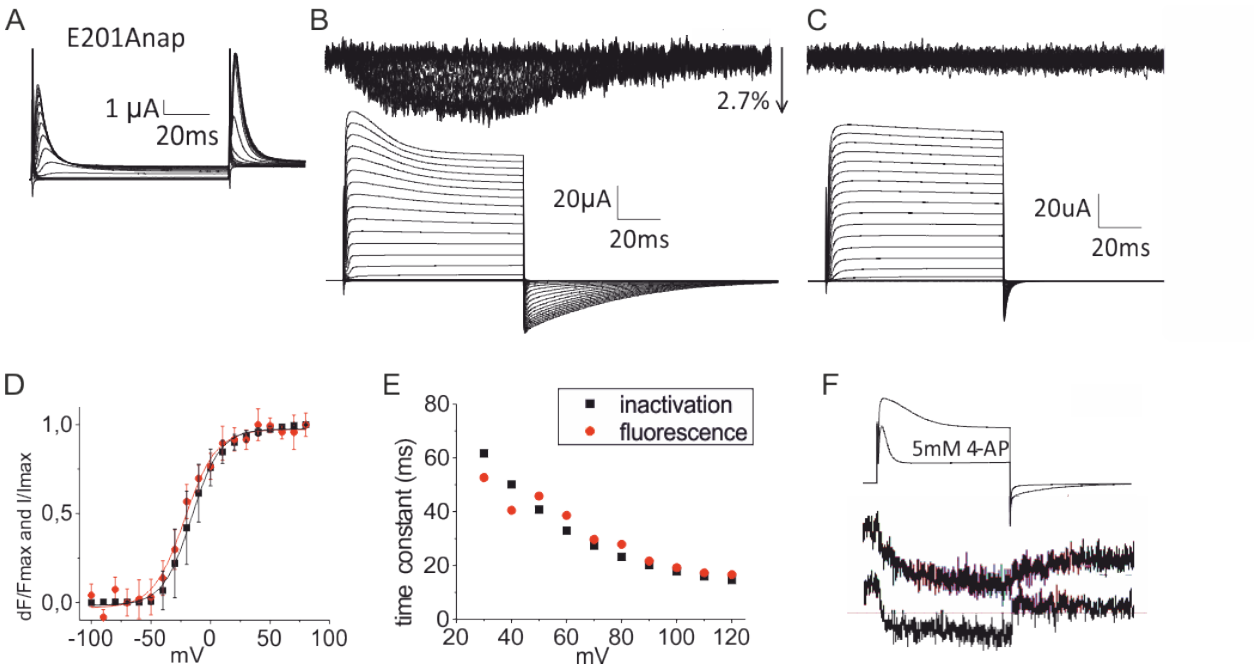

Figure 3.4 VCF results for the receptor site mutant E201Anap in the T1-S1 linker

A) Currents obtained from an E201Anap expressing oocyte from a step protocol as in fig 3.1B. **B)** Example of an oocyte expressing E201Anap showing fluorescence changes upon a standard depolarization protocol.

C) Same protocol as in B except that the oocyte is expressing an E201Anap mutant in which the N-terminus has been removed (Δ6-46). **D)** Comparison of FV (red) and IV for inactivation (black) of E201Anap. **E)** Time constants of exponential fits obtained from the oocyte shown in B. **F)** Currents and fluorescence during a depolarization step from -90 mV to +40 mV before and after application of external 4-AP.

While the results of E201Anap show that the inactivation particle interacts with this position independent of the entry and block of the pore, the correlation of the kinetics and voltage dependence with inactivation suggests that it is not the resting position of the inactivation particle, as the biphasic signal as found in the tip is missing. Scanning of the transmembrane region is challenging because many of the positions give strong fluorescence signals during activation independent of fast inactivation. One way to reconstruct the IP movement is to specifically insert tryptophans along putative binding sites (T1 domain, T1-S1 linker) in the background of a tip mutant and a chain mutant (eg. Y8Anap and E35Anap) to induce quenching (or unquenching) of Anap. Since quenching by tryptophan requires contact formation and depends on van-der-Walls radii [29], the method is useful for determination of short range distances [30, 31]. Such experiments would allow accurate estimates of the position of the IP with respect to the T1 domain, especially during the resting state which is unknown. Moreover, the direction of the fluorescence change would allow us to determine whether the IP moves towards or away from the inserted tryptophans. To this end, we inserted trp residues in the T1 domain at positions G159W, K178W, E192W, I470W and A391W. However, no quenching of anap was observed for these positions. We therefore switched strategy: instead of scanning for the resting position, we employed resonance energy transfer to triangulate the exact position.

To probe the position of IP in the resting state, we performed Lanthanide Resonance Energy Transfer (LRET). LRET is a variant of Förster Resonance Energy Transfer (FRET) that uses as donor a lanthanide, in our case terbium. Since terbium does not have a continuous dipole moment, the emission is fully isotropic. This and its long luminescence lifetime (~1ms) allow a more accurate distance determination compared to FRET [32]. The donor was linked to the channel by labelling at position A359C and F425C with Tb3+- chelate via a maleimide linker (fig 3.5A) as described earlier [33, 34]. The labelling of acceptor positions (Y8 and E35) was challenging as these positions are present on the cytoplasmic side of the channel and therefore, conventional fluorophore labelling using cysteine residues was not possible without avoiding non-specific

binding. Anap, on the other hand, did not overlap sufficiently with the Tb3+ emission spectra to obtain any meaningful transfer. To overcome this problem, we incorporated an unnatural amino acid, trans-cyclooct-4-en-L-Lysine (TCO), using the amber stop codon suppression technique [18, 35]. TCO offers fast, highly specific labelling of fluorophores carrying tetrazine group through strain-promoted inverse electron demand Diels-Alder cycloaddition (SPIEDAC) [36]. For acceptor labelling, we used cy3-tetrazine, which shows good spectral overlap with terbium with a R_0 of 61.2 Å [32]. Oocytes expressing the channels without TCO incorporated were used to correct for background correction (see methods for details).

From the fluorescence decays of donor emission in presence and absence of the acceptor, we calculated the four donor and acceptor distances for the four combinations between two donor and two acceptor positions. By triangulation, we then derived the resting position of the inactivation particle (fig 3.5B): for the donor position A359Tb-Chelate, the resting position was found on a sphere with a radius of 39.5Å and 40.4Å for Y8stop and E35stop respectively. Moving the donor to F425Tb-Chelate resulted in a sphere with slightly longer radius of 41.2Å and 42Å for Y8stop and E35stop, respectively. Since the difference between the two distances (Y8 and E35) for the positions F425 and A359 was very small, an average value was used to plot the sphere. The resting position has to be located on the intersecting part of the two spheres obtained for these positions (fig 3.5C). Most of the circle can be excluded because it is located within the transmembrane region of the channel or the extracellular space. It only remained the region framed by the transmembrane region and the T1 domain close to the pore entry as possible resting state position of the inactivation particle as (fig 3.5C). This result indicates that the IP is prebound to the alpha subunit at that position.

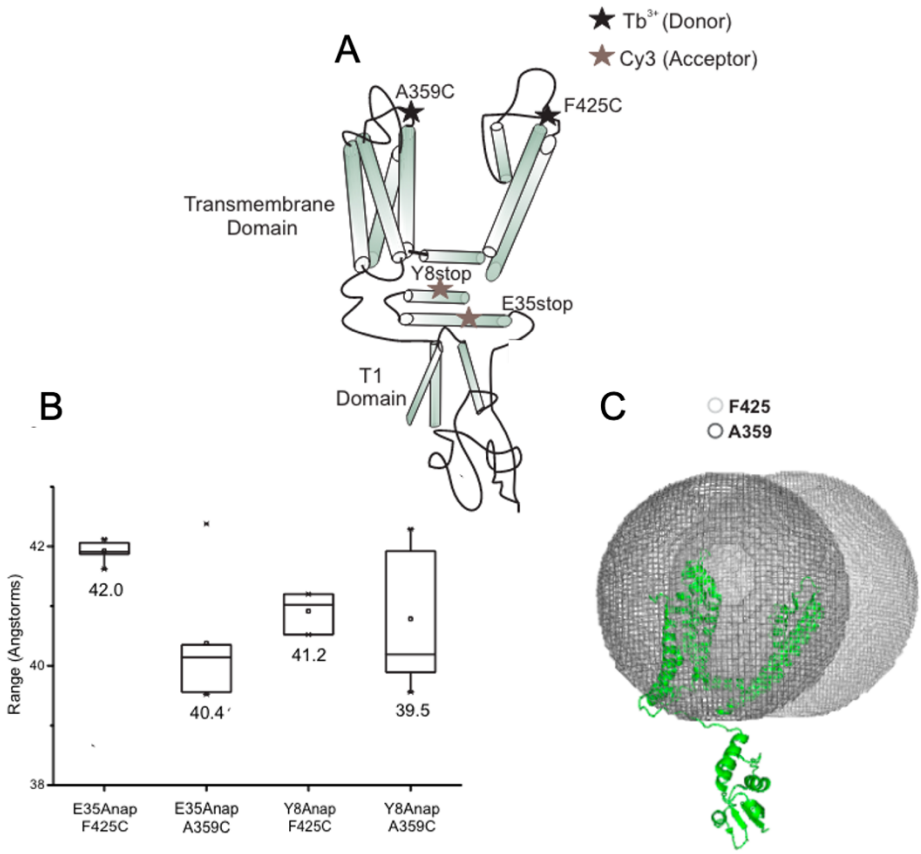

Figure 3.5 LRET measurement to probe the resting state of the channel

A) Labelling positions for the binding of donor (A359C and F425C) and acceptor fluorophores (Y8Anap and E35Anap). B) Box plot showing distances obtained for different labelled positions in the channel. C) Cartoon representation of the channel monomer with the spheres superimposed on it. The overlapping part of the spheres below the pore represents the probable region for the IP in the resting state.

3.3.5 Transition metal FRET shows distinct movements of ball and chain

To further narrow down the position of the inactivation particle, we required smaller R_0 such that the energy transfer becomes more sensitive to short distances. While LRET combinations for short distances exist, labeling at the cytosolic surface of the channel with thiol-reactive chemistry is not specific enough. Therefore, we chose transition metal (tm)FRET experiments [37, 38]. In tmFRET, a fluorescent dye is used as donor, whereas the Tb-ion is replaced with a transition metal ion, but now as an acceptor, with Anap acting as donor. Due to its multivalence, transition metals such as nickel, cadmium or cobalt can be coordinated by dihistidine motifs introduced at the desired position of the protein. Transition metals typically absorb in the visible range, which

gives the characteristic blue and pink colors of Ni- and Co-solutions, respectively. The small spectral overlap between Anap emission and cobalt absorption result in a small R_0 of 12 Å [39] [40] [41]. Due to the much shorter lifetime of Anap in the nanosecond range, we determined energy transfer efficiency from the fluorescence intensities. [19, 42].

In order to confirm the quenching of Anap fluorescence by cobalt ions, we introduced the histidines in the T1-S1 linker (I197H & K198H) and Anap at position E194. As these positions are very close to each other in the crystal structure of Kv channel (PDB ID 2R9R), we expected high energy transfer between these positions. Indeed, we observed significant energy transfer (dF/F = 15%, fig 3.6A, upper trace) and quenching of Anap fluorescence, confirming efficient Anap incorporation at the desired site as well as energy transfer between Anap and cobalt bound to dihistidine motifs.

We next introduced cobalt labeling sites near the region identified in the LRET measurements in the window formed by transmembrane region and T1 domain. We introduced di-histidine motifs (1) in the C-terminus of the S4-S5 linker (positions R387H-A391H), (2) in the T1-S1 linker closer to the N-terminus (I197H-K198H) and (3) in the upper half of the T1 domain (positions Q185H-K189H; fig 3.6C). Anap was introduced, as in the LRET measurements, at positions Y8 in the ball and E35 in the chain region of the IP. FRET efficiencies were calculated after correcting for unspecific effects of cobalt, which were then used to calculate the distances. The distances calculated from the energy transfer for different positions are shown in fig 3.6B. We used the distances from the above mentioned positions to create intersecting spheres as for the LRET results above (fig 3.6D and E). The window identified by the two spheres for the presence of IP was similar to the one observed in LRET measurements. This further confirms our finding that IP resides in the window between the channel and the T1 domain.

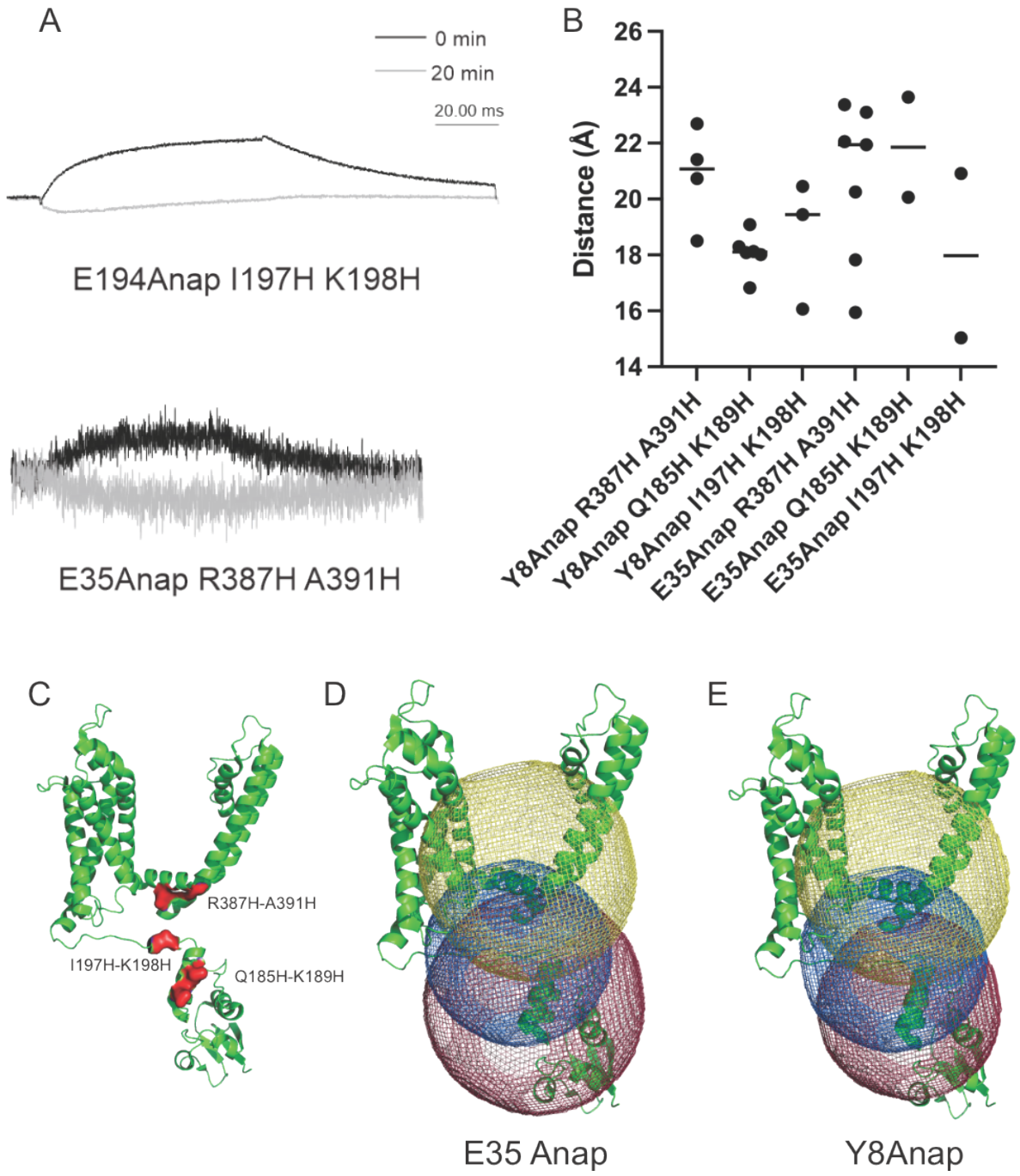

Fig 3.6 tmFRET results

A) Fluorescence traces recorded for the control E194stop (upper trace) and one of the mutant E35stop R387H A391H (lower trace). The black curve represents the recording at 0 min. Grey trace shows fluorescence quenching due to energy transfer between Anap and cobalt after the addition of cobalt. **B)** Calculated distances from tmFRET measurements for the positions mentioned in fig 6C. **C)** Dihistidine mutations introduced at various positions in the channel for the binding of cobalt. **D and E)** Cartoon representation of the channel monomer with the spheres plotted using the distances shown in 6B (Yellow

represents R387H-A391h, blue represents I197H-K198H and red represents Q185H-K189H). The overlapping part of the spheres below the pore represents the probable region for the IP in the resting state.

3.4 Discussion

By genetically incorporating a fluorescent unnatural amino acid on the cytoplasmic side of the Shaker Kv channel, we were able to directly probe conformational changes underlying N-type inactivation. The experiments provide the first structural dynamic information about the IP movement during N-type inactivation. The VCF data suggest a sequential-step model during which the IP undergoes at least two transitions, which is in agreement with previous functional studies that suggest an initial binding of the IP to the T1 domain [13], followed by a second binding to the inner pore [4]. Based on our results, we suggest that, upon depolarization, both tip and chain region initially move (transition 1 in fig 7). Relative to inactivation, the movement of the downstream chain region (E35) preceded the movement of the upstream chain region (K19), suggesting presence of two pre-inactivation steps. A final movement is responsible for docking the IP tip into the pore, and this movement only involves the tip region (A3 and Y8, transition 2 in fig 7).

The finding of two pre-inactivation steps is consistent with previous work on Kv1.4 channels, where a downstream intra-chain electrostatic interaction was identified and suggested to be responsible for initially shortening the distance between the IP and the T1-S1 linker [7, 43]. It is therefore possible that position E35 in Shaker lies within a region that is part of a similar interaction as an initial step upon depolarization.

It is worth mentioning that the E201Anap and K19Anap fluorescence data showed similar inactivation profiles. This suggests that Anap experiences the same transition at both positions (i.e., E201Anap probes the reception of K19, and K19Anap probes the movement of the IP towards E201). This interpretation agrees with findings in two other Shaker-related Kv channels where the three conserved glutamates in the T1-S1 linker (199-EEE-201) have been shown to interact electrostatically with positive charges in the early region of the chain which corresponds to the 17-RKK-19 region in Shaker (R18 in AKv1 and 26-RARERER-32 in Kv1.4) *[7, 15]*. To corroborate this further, we performed resonance energy transfer measurements to triangulate the position of the IP during the resting state of the channel. By measuring the distances from the extracellular surface of the channel (top of helix S4 and S6) as well as from the cytosolic surface of the transmembrane region (S4-S5 linker and T1-S1 linker), our LRET and tmFRET data identified

position E35 and Y8 to be sitting in the window between the T1 domain and the transmembrane domain.

We propose an inactivation model for Shaker Kv channels where the inactivation peptide sits in the window between the channel and the T1 domain (fig 3.7). It interacts with the acidic residues of the T1-S1 linker. Fan and coworkers *[7]* proposed that the acidic residues stablilize the resting state position. During channel activation, the far end of the chain moves first, preceded by the movement of ball towards the pore. The final docking of the hydrophobic ball into the pore blocks the pore to bring the inactivation. Molecular dynamics of a Shaker IP have recently suggested that the IP adopts a helical structure which inserts spontaneously into the intracellular cavity of the pore and subsequently "snakes" deep into the pore when driven by voltage *[44]*. It is possible that the slow fluorescence component of A3Anap and Y8Anap represent this last transition.

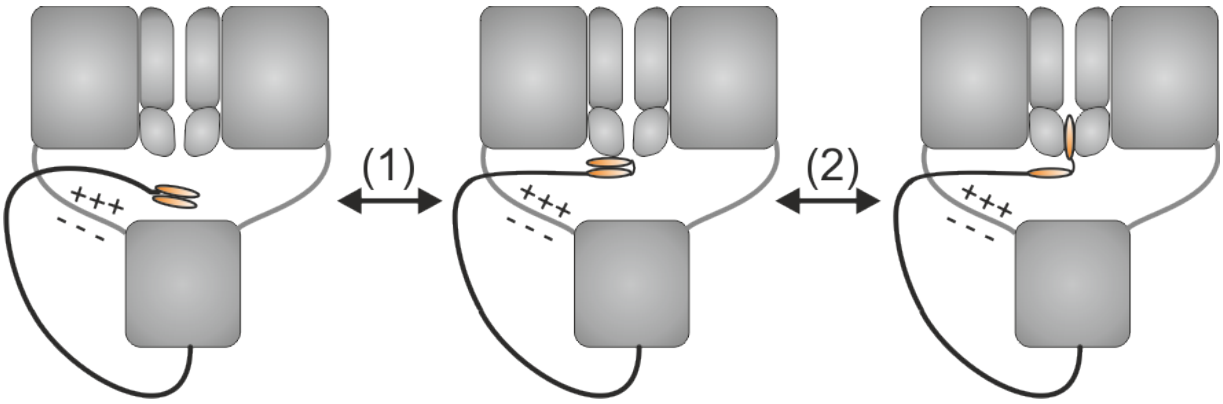

Figure 3.7 Proposed model for N-type inactivation

In the resting state, IP sits between the channel and the T1 domain interacting with the T1-S1 linker. Binding of the IP to the open pore involves at least two conformational changes. The first involves both tip and chain (1), whereas the second only involves the tip (2).

3.5 Materials and Methods

3.5.1 Xenopus oocyte injection

The mutations were introduced into the full-length Drosophila Shaker H4 gene in the pBSTA vector. The N-terminal stop codons (A3, Y8, K19, E35) were inserted into a 9LL background in which 9 noncanonical start codons have been removed via silent mutations as previously described [20, 21]. For Anap and tco incorporation, 9.2 nl of 0.1 ng/nL cDNA encoding the tRNA/RS pair [16, 36] was injected into the nucleus of Xenopus laevis oocytes 6-24 hours prior to coinjection of 23 nL 1 mM Anap (Abzena TCRS, custom synthesis TCRS-170) or Tco (Sichem, SC-8008) and 35 ng in vitro transcribed RNA [17]. All steps during and after Anap injection were performed under red light to avoid bleaching. Oocytes were then incubated for 1-3 days at 18°C in Barth's solution supplemented with 5% horse serum. See Kalstrup & Blunck, 2017 [45] for detailed description and visualization of this procedure.

3.5.2 Electrophysiology

Voltage clamp was performed with a CA-1B amplifier (Dagan). Currents were recorded in the cut open oocyte voltage-clamp configuration [46] and analyzed by using GPatch (Department of Anesthesiology, University of California, Los Angeles). For ionic recordings the external solution contained in mM: 5 KOH, 110 NMDG, 10 Hepes, and 2 Ca(OH)2, and the internal solution contained in mM: 115 KOH, 10 Hepes, and 2 EDTA. For gating recordings, the KOH was replaced by NMDG. All solutions were adjusted to pH 7.1 with MES. For 4-AP blocking experiments, 5mM NMDG (gating) or KOH (ionic) was replaced by 5 mM 4-AP, and the command potential was held at 0 mV for 5 seconds prior to recordings. Conductance (G) was calculated from the steady state currents (I) via G=I/(V-Vrev), where Vrev is the reversal potential. Conductance-, charge- and fluorescence-voltage relationships (GV, QV, FV) were fitted to a Boltzmann relation of the form $y = (1 + \exp(-(V - V1/2)/dV)) - 1$.

3.5.3 Voltage clamp fluorometry

Fluorescence intensities were recorded with a photodiode detection system (Photomax 200, Dagan) using an ex-377/50, dc-409, em-470/40 filter set for Anap fluorescence. Bleaching effects

during step protocols were accounted for by scaling fluorescence traces using the first sweep as reference.

3.5.4 LRET measurements

For donor only labelling, oocytes were incubated in a depolarizing solution (115 mM K-MeSO3, 2 mM Ca(OH)2, 10 mM HEPES, at pH 7.1) containing Tb3+ complex (5μM) at room temperature for 20 min. For acceptor labelling, Cy3 tetrazine was injected into the oocytes a day before the experiment. The setup was based on a Zeiss Axiovert 200 microscope. Picosecond laser pulses of 337 nm from a pulsed 3-milliwatt N2-laser (Spectra-Physics) was directed in a wide-field illumination onto the oocytes containing the labeled channels. The light from the oocytes was collected using a 1.25 NA 40× glycerol immersion quartz objective (Partec) and filtered with a bandpass emission filter. Light was detected by a photon counter (Laser Components). Analysis of the lifetime decays was done with an exponential fitting program (MATLAB). Distances were determined using the following relations

$$Energy\ Tranfer\ (E) = 1 - \frac{\tau_{SE}}{\tau_{DO}}$$

where τ_{DO} is the time constant of the donor lifetime decay in absence of acceptor (donor-only), and τ_{SE} is the time constant decay of the sensitized emission of the acceptor.

The distance R between the donor and the acceptor was determined using

$$R = \left(\frac{1-E}{E}\right)^{1/6} \times R_O$$

where R_O is the distance at which 50% energy transfer occurs. The R_O value used for the fluorophore pair of Tb3+ complex and Cy3 tetrazine was 61.2 Å [32].

3.5.5 tmFRET measurements

Fluorometry experiments were performed on the VCF setup described above. CoSO4 was injected into the oocytes to a final concentration of 2μM for FRET experiment. Energy transfer efficiency was calculated according to the following equations as mentioned in Dai et al[39, 40].

$$FRET_{eff} = \frac{F_{noHH} - F_{HH}}{F_{HH} \times F_{noHH} + F_{noHH} - F_{HH}}$$

where F_{HH} is the normalized fluorescence of channels with dihistidines and F_{noHH} is the normalized fluorescence of channels without dihistidines. The distances were then calculated using the Förster equation as follows :

$$R = R_O \left(\frac{1}{FRET_{eff}} - 1 \right)^{1/6}$$

where R_0 is the Förster distance for FRET between L-Anap and Co^{2+}-dihistidine (12 Å).

3.6 References

1. Demo, S.D. and G. Yellen, *The inactivation gate of the Shaker K+ channel behaves like an open-channel blocker.* Neuron, 1991. **7**(5): p. 743-53.
2. Hoshi, T., W.N. Zagotta, and R.W. Aldrich, *Biophysical and molecular mechanisms of Shaker potassium channel inactivation.* Science, 1990. **250**(4980): p. 533-8.
3. Zagotta, W.N., T. Hoshi, and R.W. Aldrich, *Restoration of inactivation in mutants of Shaker potassium channels by a peptide derived from ShB.* Science, 1990. **250**(4980): p. 568-71.
4. Zhou, M., et al., *Potassium channel receptor site for the inactivation gate and quaternary amine inhibitors.* Nature, 2001. **411**(6838): p. 657-61.
5. Heinemann, S.H., et al., *Functional characterization of Kv channel beta-subunits from rat brain.* J Physiol, 1996. **493 (Pt 3)**: p. 625-33.
6. Rettig, J., et al., *Inactivation properties of voltage-gated K+ channels altered by presence of beta-subunit.* Nature, 1994. **369**(6478): p. 289-94.
7. Fan, Z., et al., *Electrostatic interaction between inactivation ball and T1-S1 linker region of Kv1.4 channel.* Biochim Biophys Acta, 2012. **1818**(1): p. 55-63.
8. Murrell-Lagnado, R.D. and R.W. Aldrich, *Interactions of amino terminal domains of Shaker K channels with a pore blocking site studied with synthetic peptides.* J Gen Physiol, 1993. **102**(6): p. 949-75.
9. Prince, A. and P.J. Pfaffinger, *Conserved N-terminal negative charges support optimally efficient N-type inactivation of Kv1 channels.* PLoS One, 2013. **8**(4): p. e62695.
10. Kreusch, A., et al., *Crystal structure of the tetramerization domain of the Shaker potassium channel.* Nature, 1998. **392**(6679): p. 945-8.
11. Li, M., Y.N. Jan, and L.Y. Jan, *Specification of subunit assembly by the hydrophilic amino-terminal domain of the Shaker potassium channel.* Science, 1992. **257**(5074): p. 1225-30.
12. Shen, N.V., et al., *Deletion analysis of K+ channel assembly.* Neuron, 1993. **11**(1): p. 67-76.

13. Gulbis, J.M., et al., *Structure of the cytoplasmic beta subunit-T1 assembly of voltage-dependent K+ channels.* Science, 2000. **289**(5476): p. 123-7.
14. Venkataraman, G., D. Srikumar, and M. Holmgren, *Quasi-specific access of the potassium channel inactivation gate.* Nat Commun, 2014. **5**: p. 4050.
15. Prince-Carter, A. and P.J. Pfaffinger, *Multiple intermediate states precede pore block during N-type inactivation of a voltage-gated potassium channel.* J Gen Physiol, 2009. **134**(1): p. 15-34.
16. Chatterjee, A., et al., *A genetically encoded fluorescent probe in mammalian cells.* J Am Chem Soc, 2013. **135**(34): p. 12540-3.
17. Kalstrup, T. and R. Blunck, *Dynamics of internal pore opening in K(V) channels probed by a fluorescent unnatural amino acid.* Proc Natl Acad Sci U S A, 2013. **110**(20): p. 8272-7.
18. Lee, H.S., et al., *Genetic incorporation of a small, environmentally sensitive, fluorescent probe into proteins in Saccharomyces cerevisiae.* J Am Chem Soc, 2009. **131**(36): p. 12921-3.
19. Taraska, J.W., et al., *Mapping the structure and conformational movements of proteins with transition metal ion FRET.* Nature Methods, 2009. **6**(7): p. 532-U94.
20. Kalstrup, T. and R. Blunck, *Reinitiation at non-canonical start codons leads to leak expression when incorporating unnatural amino acids.* Sci Rep, 2015. **5**: p. 11866.
21. Bezanilla, F., et al., *Molecular basis of gating charge immobilization in Shaker potassium channels.* Science, 1991. **254**(5032): p. 679-83.
22. Yang, Y., Y. Yan, and F.J. Sigworth, *How does the W434F mutation block current in Shaker potassium channels?* J Gen Physiol, 1997. **109**(6): p. 779-89.
23. Pandey, R.K., T. Blunck, R., *From resting state to inactivation, the journey of inactivation peptide in Shaker Kv channels (in prep).* 2020.
24. Perozo, E., et al., *Gating currents from a nonconducting mutant reveal open-closed conformations in Shaker K+ channels.* Neuron, 1993. **11**(2): p. 353-8.
25. Armstrong, C.M. and A. Loboda, *A model for 4-aminopyridine action on K channels: similarities to tetraethylammonium ion action.* Biophys J, 2001. **81**(2): p. 895-904.
26. Claydon, T.W., et al., *4-aminopyridine prevents the conformational changes associated with p/c-type inactivation in shaker channels.* J Pharmacol Exp Ther, 2007. **320**(1): p. 162-72.
27. Pathak, M., et al., *The cooperative voltage sensor motion that gates a potassium channel.* J Gen Physiol, 2005. **125**(1): p. 57-69.
28. Bhatt, D.L., et al., *International prevalence, recognition, and treatment of cardiovascular risk factors in outpatients with atherothrombosis.* Jama-Journal of the American Medical Association, 2006. **295**(2): p. 180-189.
29. Mansoor, S.E., H.S. McHaourab, and D.L. Farrens, *Mapping proximity within proteins using fluorescence spectroscopy. A study of T4 lysozyme showing that tryptophan residues quench bimane fluorescence.* Biochemistry, 2002. **41**(8): p. 2475-84.

30. Islas, L.D. and W.N. Zagotta, *Short-range molecular rearrangements in ion channels detected by tryptophan quenching of bimane fluorescence.* J Gen Physiol, 2006. **128**(3): p. 337-46.
31. Pantazis, A. and R. Olcese, *Relative transmembrane segment rearrangements during BK channel activation resolved by structurally assigned fluorophore-quencher pairing.* J Gen Physiol, 2012. **140**(2): p. 207-18.
32. Selvin, P.R., *Principles and biophysical applications of lanthanide-based probes.* Annu Rev Biophys Biomol Struct, 2002. **31**: p. 275-302.
33. Faure, E., et al., *A Limited 4 angstrom Radial Displacement of the S4-S5 Linker Is Sufficient for Internal Gate Closing in Kv Channels.* Journal of Biological Chemistry, 2012. **287**(47).
34. Richardson, J., et al., *Distance measurements reveal a common topology of prokaryotic voltage-gated ion channels in the lipid bilayer.* Proceedings of the National Academy of Sciences of the United States of America, 2006. **103**(43): p. 15865-15870.
35. Plass, T., et al., *Genetically encoded copper-free click chemistry.* Angew Chem Int Ed Engl, 2011. **50**(17): p. 3878-81.
36. Nikic, I., et al., *Labeling proteins on live mammalian cells using click chemistry.* Nature Protocols, 2015. **10**(5): p. 780-791.
37. Gordon, S.E., et al., *Transition metal ion FRET to measure short-range distances at the intracellular surface of the plasma membrane.* J Gen Physiol, 2016. **147**(2): p. 189-200.
38. Sandtner, W., F. Bezanilla, and A.M. Correa, *In vivo measurement of intramolecular distances using genetically encoded reporters.* Biophys J, 2007. **93**(9): p. L45-7.
39. Dai, G. and W.N. Zagotta, *Molecular mechanism of voltage-dependent potentiation of KCNH potassium channels.* Elife, 2017. **6**.
40. Dai, G., et al., *The HCN channel voltage sensor undergoes a large downward motion during hyperpolarization.* Nat Struct Mol Biol, 2019. **26**(8): p. 686-694.
41. Zagotta, W.N., et al., *Measuring distances between TRPV1 and the plasma membrane using a noncanonical amino acid and transition metal ion FRET.* J Gen Physiol, 2016. **147**(2): p. 201-16.
42. Taraska, J.W., M.C. Puljung, and W.N. Zagotta, *Short-distance probes for protein backbone structure based on energy transfer between bimane and transition metal ions.* Proc Natl Acad Sci U S A, 2009. **106**(38): p. 16227-32.
43. Fan, Z., et al., *Electrostatic interaction in the NH(2)-terminus accelerates inactivation of the Kv1.4 channel.* Biochim Biophys Acta, 2010. **1798**(11): p. 2076-83.
44. Vergara-Jaque, A., et al., *A Structural Model of the Inactivation Gate of Voltage Activated Potassium Channels.* Biophysical Journal, 2017. **112**(3): p. 247a-247a.
45. Kalstrup, T. and R. Blunck, *Voltage-clamp Fluorometry in Xenopus Oocytes Using Fluorescent Unnatural Amino Acids.* J Vis Exp, 2017(123).
46. Stefani, E. and F. Bezanilla, *Cut-open oocyte voltage-clamp technique.* Methods Enzymol, 1998. **293**: p. 300-18.

3.7 Supplementary Figure

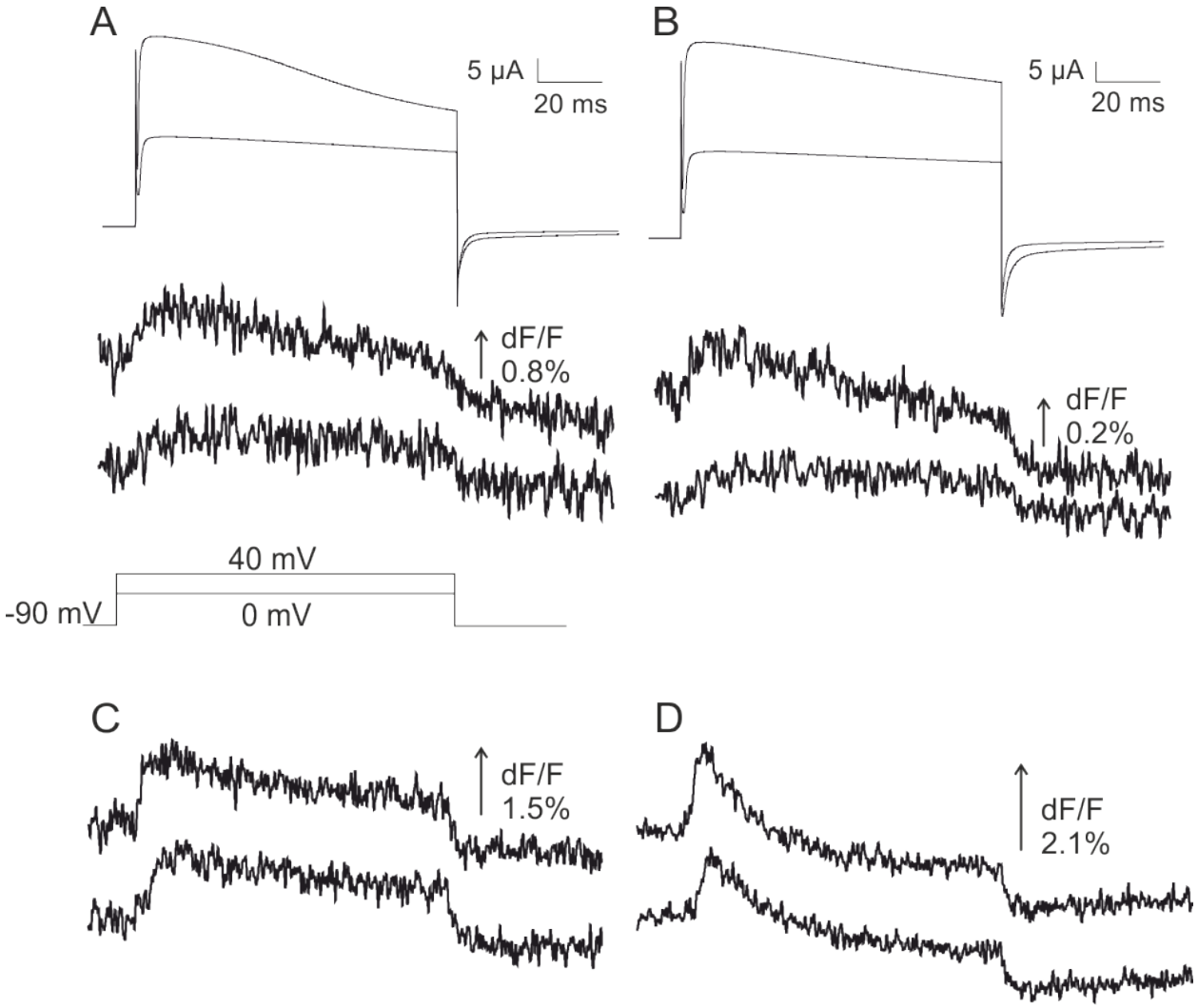

Fig S3.1 Two fluorescence components present in A3Anap and Y8Anap

Currents and fluorescence changes elicited by depolarizations of A) A3Anap and B) Y8Anap channels, obtained at high expression levels. The same protocol was performed with C) A3Anap-W434F and D) Y8Anap-W434F channels

4 Chapter 4

Clustering of Shaker Kv channels prevents fast inactivation

Roshan Pandey[1], Tanja Kalstrup[2] and Rikard Blunck[2,3] *

[1]Department of Biochemistry and Molecular Medicine, [2]Department of Pharmacology and Physiology, [3]Department of Physics, Université de Montréal, Montréal, Québec, Canada

Author Contribution

R.B. designed research, R.P. performed the experiments, T.K. performed the experiments for Fig 5.5, R.P. wrote the manuscript, R.P. and R.B. did the analysis and edited the manuscript.

4.1 Abstract

During an action potential, Kv channels are responsible for membrane repolarization through the efflux of K+ ions. The movement of ions through the pore is regulated by a fast-inactivating mechanism known as N-type inactivation. High expression of Shaker channels results in slow and incomplete N-type inactivation. To elucidate the reason for this impaired inactivation at high expression density, we investigated the relation to known clustering motifs. The C-terminus of the Shaker K+ channel interacts with membrane-associated scaffold proteins for cluster formation. By truncating the last four C-terminal residues involved in cluster formation and thus preventing channel clustering, we were able to recover N-type inactivation even at higher expression levels, except at very high expression levels (>60 μA), when channels are stochastically in close proximity. The slower inactivation kinetics was absent in the nonconducting W434F mutant, suggesting a relation to the local ion concentrations. The altered inactivation kinetics at dense expression emphasize the care that has to be taken when transferring the behaviour of K+ channels from heterologous expression systems to in situ situations.

4.2 Introduction

Voltage-gated K+ channels are involved in the generation and propagation of action potentials in neuronal and muscle cells. During an action potential, depolarization of the membrane opens the K+ channels. They are widely distributed throughout the central nervous system to regulate cellular excitability and repolarize the membrane after excitation. Proper spatial distribution of ion channels is an important aspect to maintain the appropriate transmission of electrical signals. For example, the density of Na+ channels is 25 times more at nodes of Ranvier compared to the internodal region. This so-called clustering of channels is an essential physiological phenomenon to maintain effective saltatory conduction [1]. Kv channels have also been found to be very densely expressed at key regulating sites in the neurons, like nodes of Ranvier (juxtaparanodal region [2], the initial axon segment, and postsynaptic terminals such as dendrites[3-5]. Clustering of K+ channels regulates channel density which, in turn, determines the shape and frequency of transmission of action potential from one neuron to the next [6, 7].

Clustering of the Shaker subfamily has been attributed to the PSD-95 family of membrane-associated proteins. Postsynaptic density 95 (PSD-95) proteins bind to the channel's carboxy

terminals through their PDZ motifs to traffic the channels to the cellular membranes [3, 4, 8-10]. These proteins have been shown to transport both mammalian (PSD-95/SAP97) and Shaker homologs (Drosophila discs large, dlg) of voltage-gated K+ channels [4, 11]. They bind to a conserved XTD/EV motif of four residues at the carboxy-terminal tail, which was found to be conserved in different homologs of the K+ channels.

K+ channels are known to assemble as tetramers. Each monomer contains six membrane-spanning helices. Helices 1 to 4 form the voltage sensor domain, which senses changes in membrane potential to open the channel. Helices 5 and 6 from all four monomers form a single central pore. Within milliseconds after opening, a subgroup of K+ channels, namely Kv 1.4, Kv 3.4, and Kv 4.2, undergo N-type inactivation, rendering the pore non conducting. Inactivation is achieved by blockage of the pore from the cytoplasmic side by one of the four N-termini, known as the inactivation particle, present in each monomer. Fast N-type inactivation is responsible for the early culmination of K+ conduction through the pore, which, in turn, modulates neuronal excitability.

In fluorescence studies of K+ channels, higher expression levels lead to better signal-to-noise ratios. However, when expressing the channels in Xenopus oocytes, we consistently observe partial inactivation of the channel at expression level >50μA (fig 1). Therefore, we decided to explore how expression density influences fast inactivation. The physiological implications are substantial; as, K+ channels are densely expressed in many neuronal regions, one has to be careful when deriving in situ behavior of K+ channels from biophysical studies in a heterologous expression system. In this paper, we have shown that by preventing channel clustering, the fast N-type inactivation can be restored in Shaker channels.

4.3 Results

4.3.1 High expression levels of Shaker channels result in slower N-type inactivation

While working on an alternative project on Shaker Kv channels that required expressing the channels at higher concentrations in Xenopus oocytes, we consistently observed slowing of fast inactivation of the channel. To establish that the slower inactivation kinetics seen at higher

expression is directly correlated with the level of expression of the channel, we compared current profiles of two different oocytes, one with lower expression (~20µA) than the other one (~70 µA). Under the same driving force (-20mV), the low expressing oocytes show much higher inactivation (66%) compared to almost no inactivation seen at the higher expressing oocyte at the same voltage (fig 4.1B). This confirmed that the slower inactivation observed was indeed due to higher expression.

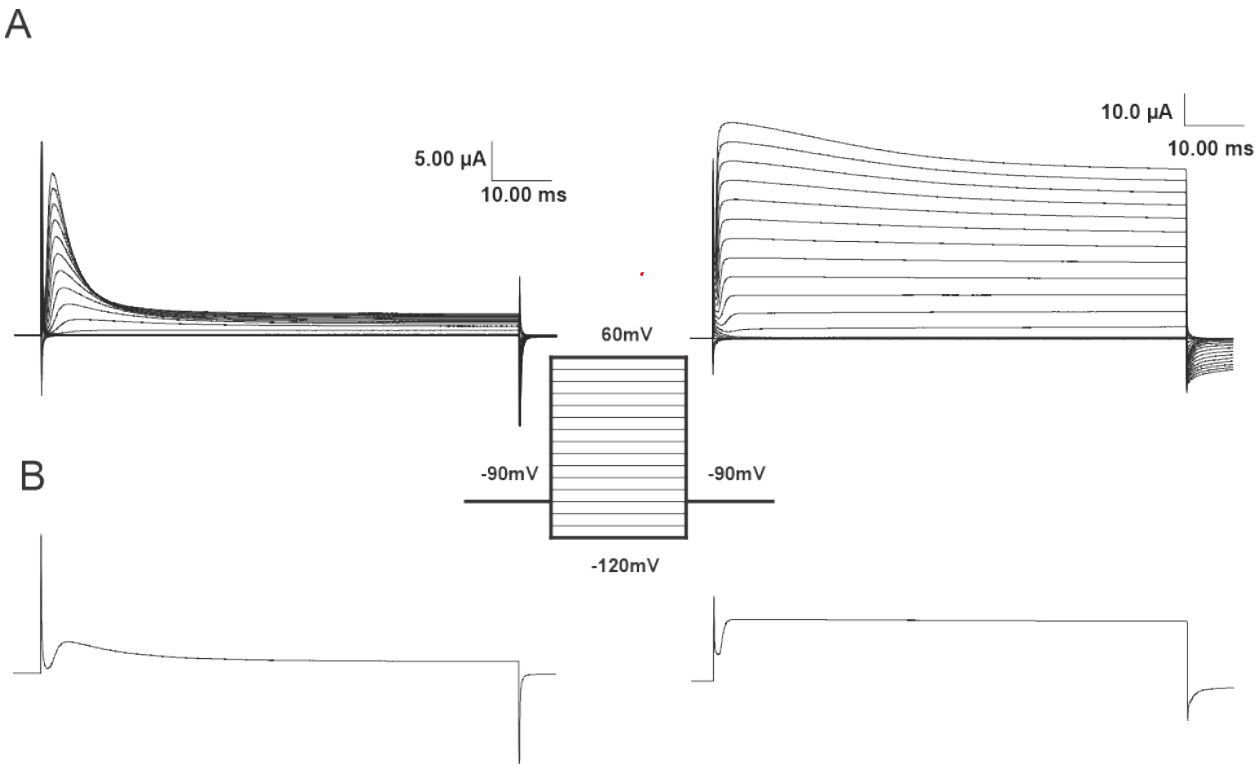

Fig 4.1: Difference in rate of inactivation at low and high expression levels
A) On the left is the current profile of an oocyte showing fast inactivation at a lower expression level. On the right is the current profile of a higher expressing oocyte showing slow inactivation. **B)** Current traces at -20mV from corresponding upper current profiles in 1A.

Since we were injecting high RNA concentration to achieve maximum expression level for our experiments, we first tested whether the accelerated trafficking caused by the high RNA concentration overwhelmed the quality control mechanisms leading to a loss of inactivation. Also, since membrane proteins are synthesized inside the membrane in the ER and Golgi, and is transported via vesicle fusion with the membrane, any horizontal movement of the channels in the plane of the membrane is limited. A faster translation might lead to more channels per vesicle and

thus closer proximity. We assessed the impact of injecting different RNA concentrations on the inactivation of the channel at comparable expression level. The percentage of inactivation was determined by calculating the difference between the steady-state current at the end of the depolarizing pulse and the peak current, normalized to peak current (fig 4.2A). Oocytes were injected with varying amounts of Shaker RNA between 92 and 12 ng, and currents were recorded with the cut-open oocyte voltage clamp technique after 24 hours of injection (see Methods for experimental details). Percentage inactivation was plotted again peak current for different RNA concentrations (fig 4.2 C, D). 92 ng of RNA was injected to achieve maximum expression, and the trend of inactivation was compared to the oocytes with lower RNA concentrations. As expected, injecting lower RNA concentrations resulted in an overall decreased channel expression. However, no significant effect on the inactivation kinetics was observed when the same peak current was achieved with different RNA-concentrations and expression times. Faster inactivation was observed at lower current density, which slows down as the peak current goes higher (fig. 4.2B). Hence, we could conclude that amount of injected RNA does not affect the slow inactivation of channels seen at higher expression levels.

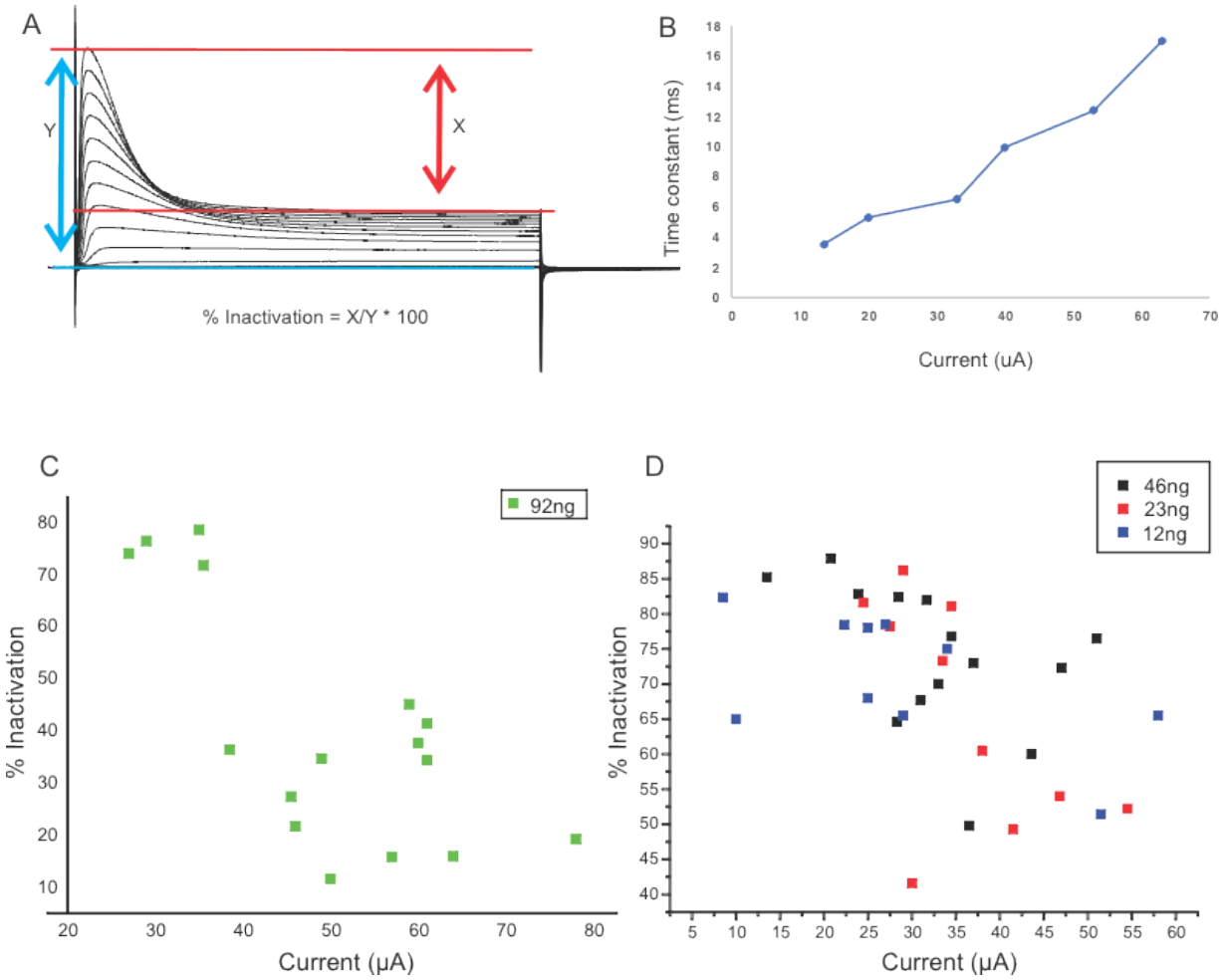

Fig 4.2: Effect of injecting different RNA concentrations on inactivation
A) Calculation of inactivation percentage from the current profile of the channel. **B)** Plot showing increase in time constant of inactivation with increased expression of the channel. **C)** Percentage inactivation vs. RNA concentration (92ng). **D)** Percentage inactivation vs. RNA concentration (46ng, 23ng, 12ng).

4.3.2 Truncating C-terminal residues prevents clustering and restores inactivation

Although we found that the slower rate of inactivation was influenced by total expression, the rate of translation played no role in high channel density and potential cross talk between the channels. For the channels to be expressed in close proximity and any kind of interaction to occur due to high channel density, it has to take place in the cytoplasm during protein synthesis. This idea allowed us to explore the possibility of channel clustering as a phenomenon responsible for cross talk between neighboring subunits and the observed slower inactivation kinetics.

Moran et al. [12] mentioned clustering as a possible mechanism for slow inactivation observed at the higher expression in Shaker channels. Clustering of channels is known to be regulated by a group of scaffold proteins known as membrane-associated guanylate kinases (MAGUKs), including PSD95/SAP90. PSD 95 plays a vital role in the trafficking of K+ channels into the membrane. The PDZ domains of the PSD95 kinases bind to the last four residues of the carboxy-terminal to traffic it to the cell membrane. Therefore, we tested if truncation of the last four residues can inhibit this binding and prevent clustering of the channels, resulting in faster inactivation of the channels. To this end, we introduced a stop mutation at the C- terminal (fig 4.3A) prior to the last four residues to promote premature termination. Truncation of these residues did not visibly affect channel function or their trafficking to the membrane at low expression levels.

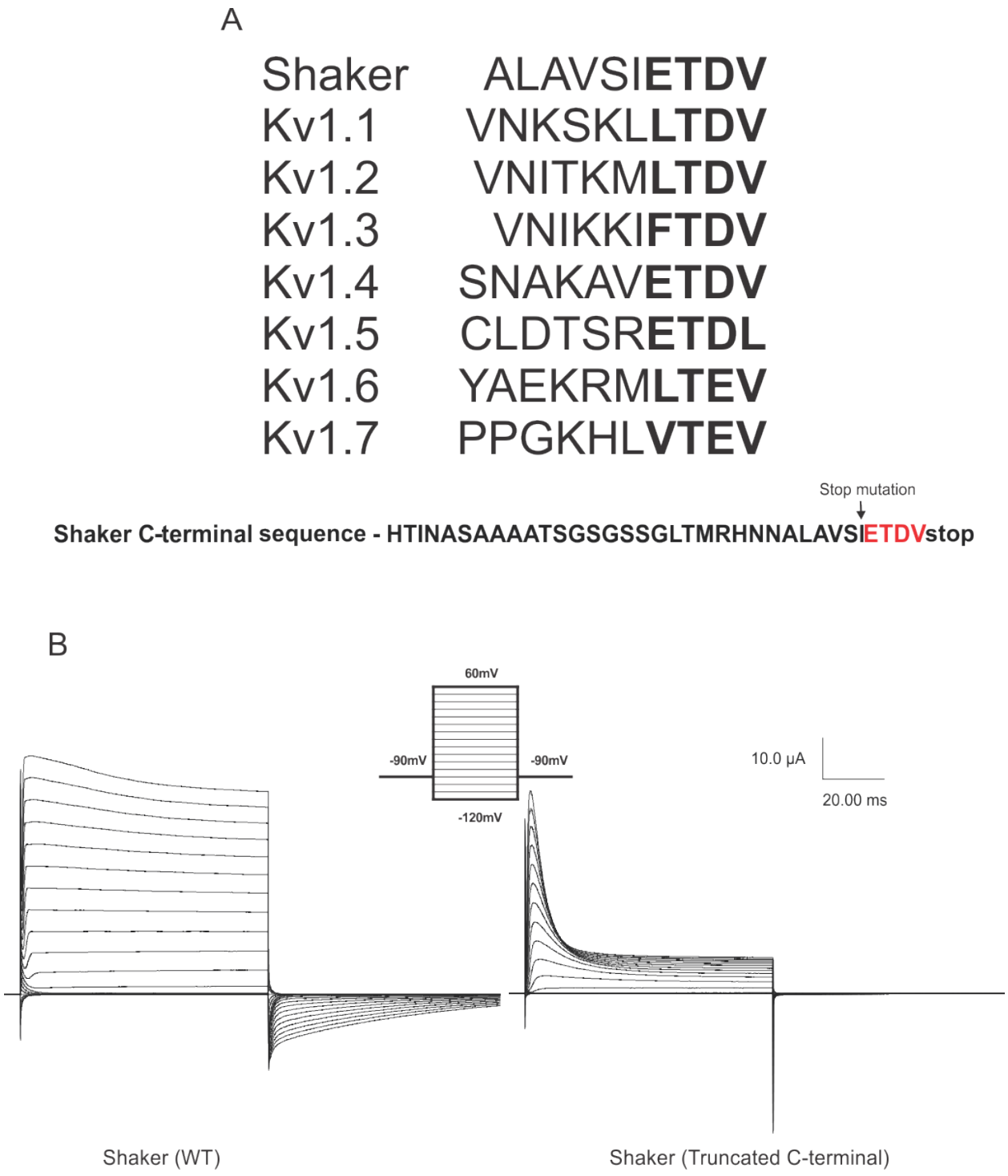

Fig 4.3: Faster inactivation observed with truncation of C-terminal residues
A) Sequence analysis of C-terminal residues of Shaker channel and human Kv1 subfamily. Sequence IDs: Shaker-P08510, Kv1.1-Q09470, Kv1.2-P16389, Kv1.3-P22001, Kv1.4-P22459, Kv1.5-P22460, Kv1.6-P17658, Kv1.7-Q96RP8. **B)** Current profile of wild type and truncated Shaker channel protein showing slow and fast inactivation, respectively.

Current recordings from channels with truncated C-terminal residues at higher expression levels showed in general faster inactivation compared to wildtype (fig 4.3B), but we observed different patterns in the percentage of inactivation resulting from removing the last four residues at the C-terminus. For the oocytes showing less <40µA of current expression, no significant change in inactivation was observed (lower expression group), which was expected from the absence of channel clustering at low expression level (fig 4.4A, B). Inactivation was about 75% in both wildtype and truncated channels. In the medium expression group (40-65 µA), the most significant difference was seen with inactivation of 30% and 70% for wildtype and truncation mutant, respectively. Hence prevention of cluster formation showed a direct effect on the inactivation kinetics. The effect on inactivation was less significant in the high expression group (>65µA) with 30% and 50% for wildtype and truncation mutant, respectively. The lower effect at high expression level is likely due to the stochastic proximity of channels at high density and indicates that it is not the binding to the scaffolding proteins but directly the physical proximity that influences N-type inactivation.

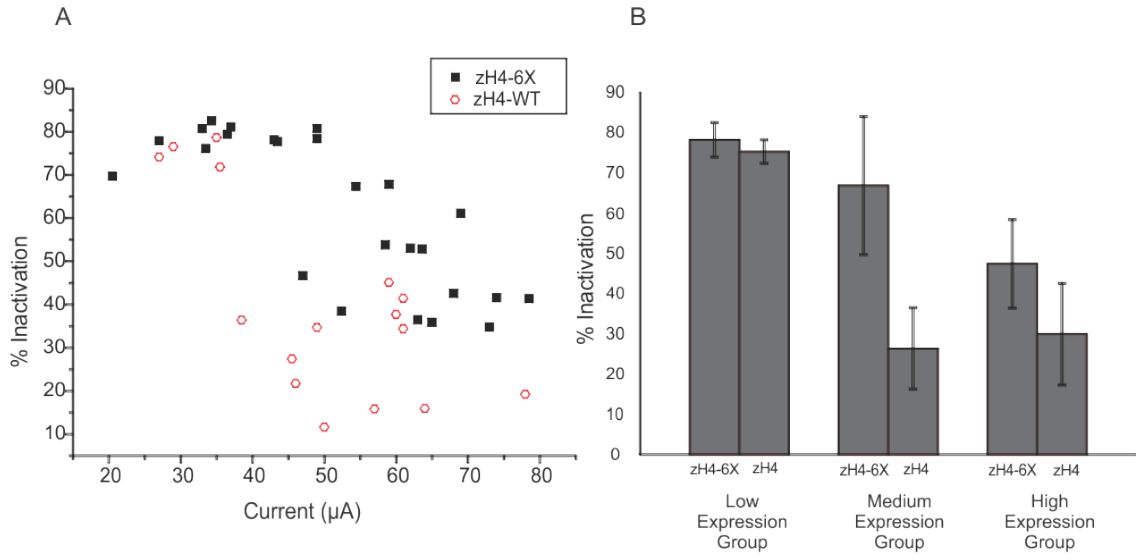

Fig 4.4: Different rate of inactivation in wild type vs. truncated channel
A) Scattering profile of difference inactivation rate in wild type (red circles) vs. truncated (solid black square) Shaker channels. **B)** Bar graph showing three different groups of channel expression and the corresponding difference in inactivation for the wild type and truncated channel.

4.3.3 Slower inactivation is not seen in nonconducting mutant W434F

We observed slower inactivation to some extent at higher expression levels, even in the truncated mutants. This effect could result from direct interaction between the channels at high channel density or an indirect effect of K+ ions accumulation as described by Grigoriev et al. [13] for C-type inactivation. To answer this question, we decided to record the currents in the nonconducting Shaker mutant W434F. The absence of current in this mutant [14] allows us to exclude the effect of K+ accumulation on the extracellular side of the pore. The channels were incorporated with a fluorescent unnatural amino acid Anap {3-[(6-acetyl-2-naphthalenyl) amino]-L-alanine} on the N-terminal position E35, to track the movement of the inactivation particle during N-type inactivation even in the absence of conduction [15]. We did not see any slowing or reduction of N-type inactivation in the W434F mutant at a higher expression level, as shown by the overlapping FV and IV curves for channel inactivation in our fluorescence data (fig 5A, B). This excludes the possibility of any direct interaction of N-termini with the neighboring channels. Therefore, a possible explanation for the slower inactivation observed in truncated channel mutants could be the effect of change in ionic strength on the intracellular side of the pore caused by efflux of K+ ions during channel opening. An alternative explanation is that the interaction sites in the window formed by T1 and transmembrane domain, through which the inactivation particle enters the pore [15], are no longer available after activation. We showed previously, that in W434F, the S4-S5 linker enters its final (C-type inactivated) state immediately after voltage sensor activation and may thus no longer be available for interaction with the inactivation particle [16].

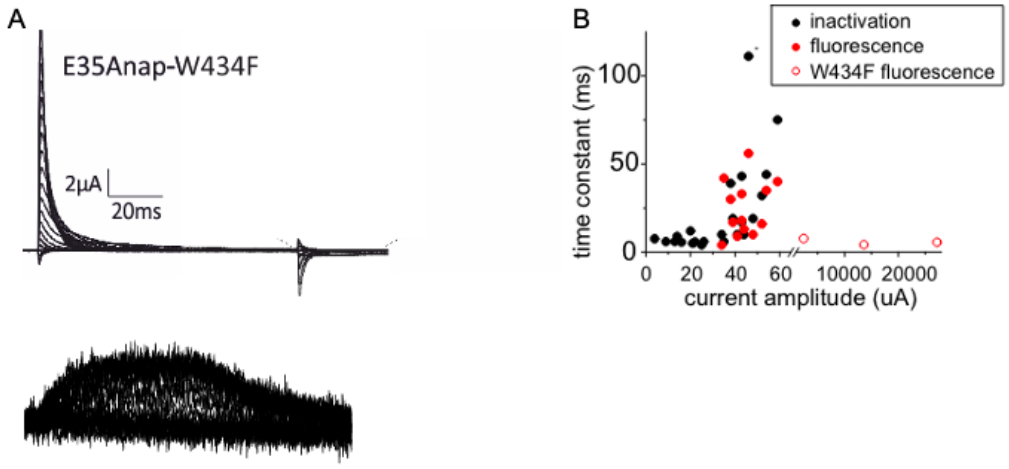

Fig 4.5: Inactivation profile of Shaker mutant W434F
A) Inactivating currents elicited by the mutant E35Anap along with the fluorescence changes. **B)** Time constants obtained from exponential fits of E35Anap current inactivation and fluorescence changes during depolarization from -90 mV to +40 mV, are plotted as a function of current amplitude (expression level). The corresponding ionic current of W434F gating currents were calculated using 13 elementary charges per channel with a unitary conductance of 20 pS [17, 18].

4.4 Discussion

We have gained unprecedented details about the inactivation mechanism in Shaker channels in the last couple of decades. In this paper, we have shown that slower N-type inactivation rates at higher expression levels result from clustering of Shaker channels which can be reversed by truncating the carboxy-terminal residues involved in cluster formation. We also showed that the slower kinetics observed at high channel density did not involve any interaction with the N-termini of the neighboring channels.

Clustering of ion channels is an essential phenomenon in neurons to regulate the generation and transmission of an action potential. Aggregation of various ion channels at postsynaptic junctions determines a robust response generated in relation to the neurotransmitter released at the synapse. Na+ and K+ channels are known to aggregate at the nodes of Ranvier to drive the action potential forward on an axon terminal [7, 19]. Clustering has also been shown to suppress the internalization of ion channels [20].

MAGUKs have been identified as the primary candidate responsible for surface expression and aggregation of ion channels to the membrane. PSD95 and SAP97 are two major scaffold proteins of this class that play a significant role in clustering in mammalian homologs. The transport is mediated by the binding of PDZ domains of these proteins with the carboxy-terminal of the channels. Alternative splicing at the carboxy-terminal is also responsible for the tissue-specific distribution of the Shaker channel, which emphasizes the role of the C-terminus in channel trafficking [21, 22].

Clustering of channels has been suggested in the past to be linked to the slowing of fast inactivation of Shaker channels [12, 23]. Here, we have shown that removing the C-terminal residues involved in cluster formation restores fast inactivation. The presence of channels in close proximity can lead to some crosstalk between neighboring channels, which might affect the kinetics of the channel. Lewin et al.[24] showed previously that N- and C- termini could be substituted to serve each other's function of fast inactivation and interaction with PSD proteins for cluster formation, respectively. Given their similarity in performing each other's functions, close proximity might permit them to interact with neighboring channels to inhibit free diffusion of the N- (or C-) terminus and thus affecting the inactivation kinetics. However, our fluorescence data with the W434F mutant shows that the movement of N-termini remains unaffected by the presence of neighboring channels in the vicinity when present at a higher density. Hence, any interaction between the neighboring channels did not contribute to the slow inactivation kinetics observed in these channels. The effect of local ionic concentration on the interaction between the N-terminal inactivation peptide (IP) and the alpha subunit would explain the effect. We have observed that the IP sits below the channel in the resting state of the channel interacting with the T1-S1 linker[15]. During channel opening, a significant efflux of K+ ions can lower local ionic strength, and the local concentration would be more severely altered in the presence of more channels. Lower ionic strength can further strengthen the electrostatic interaction between the IP and the T1-S1 linker, thus causing delayed movement or even immobilization of the IP, thus resulting in slower N-type inactivation. Further experiments are required to confirm these explanations or to find out other plausible reasons for this behavior.

4.5 Methods

4.5.1 Molecular Biology and oocyte injection

Experiments for this study were obtained using the ShakerIR-H4 channel in the pBSTA vector. Point mutations were introduced using site-directed mutagenesis (QuikChange; Stratagene). Sequences were verified using automated DNA sequencing at the institution's facility. cDNAs were linearized and in vitro transcribed using T7 RNA polymerase (T7 mMessage machine kit; Invitrogen). Oocytes from Xenopus laevis were surgically obtained. The follicular membrane was removed according to a standard collagenase treatment. Amounts between 12 to 92 ng cRNA were injected into each oocyte. After injection, oocytes were incubated in Barth solution at 18°C and the electrophysiological recordings were performed on the next day.

4.5.2 Electrophysiology

Measurements were performed with the cut-open voltage-clamp fluorometry technique for spatial voltage homogeneity and fast temporal resolution [25] Macroscopic currents were recorded and registered using GPatch acquisition software (Department of Anesthesiology, University of California, Los Angeles, Los Angeles, CA). Oocytes were placed in a three-part chamber, top, middle, and bottom containing an external solution (5mM KOH, 110mM NMDG, 10mM Hepes, and 2mM Ca(OH)2) adjusted to pH 7.1 using MES, and then permeabilized by exchanging external solution in the bottom chamber with 0.2% saponin so the current could be injected directly into the oocyte. Saponin was replaced by an internal solution (115mM KOH, 10mM Hepes, and 2mM EDTA) adjusted to pH 7.1 using MES. The voltage electrode was filled with 3 M KCl. Recordings were performed at room temperature.

4.6 Acknowledgements

This work was financially supported by the Canadian Institutes for Health Research (CIHR) Grant PJT-169160 and the Natural Sciences and Engineering Research Council (NSERC) Grant RGPIN-2017-06871.

4.7 References

1. Shrager, P., *Sodium channels in single demyelinated mammalian axons.* Brain Res, 1989. **483**(1): p. 149-54.
2. Rasband, M.N., et al., *Potassium channel distribution, clustering, and function in remyelinating rat axons.* J Neurosci, 1998. **18**(1): p. 36-47.
3. Kim, E., et al., *Clustering of Shaker-type K+ channels by interaction with a family of membrane-associated guanylate kinases.* Nature, 1995. **378**(6552): p. 85-8.
4. Tejedor, F.J., et al., *Essential role for dlg in synaptic clustering of Shaker K+ channels in vivo.* J Neurosci, 1997. **17**(1): p. 152-9.
5. Trimmer, J.S., *Subcellular localization of K+ channels in mammalian brain neurons: remarkable precision in the midst of extraordinary complexity.* Neuron, 2015. **85**(2): p. 238-56.
6. Arhem, P., G. Klement, and C. Blomberg, *Channel density regulation of firing patterns in a cortical neuron model.* Biophys J, 2006. **90**(12): p. 4392-404.
7. Gomperts, S.N., *Clustering membrane proteins: It's all coming together with the PSD-95/SAP90 protein family.* Cell, 1996. **84**(5): p. 659-62.
8. Harris, B.Z. and W.A. Lim, *Mechanism and role of PDZ domains in signaling complex assembly.* J Cell Sci, 2001. **114**(Pt 18): p. 3219-31.
9. Lin, Y., et al., *Postsynaptic density protein-95 regulates NMDA channel gating and surface expression.* J Neurosci, 2004. **24**(45): p. 10138-48.
10. Topinka, J.R. and D.S. Bredt, *N-terminal palmitoylation of PSD-95 regulates association with cell membranes and interaction with K+ channel Kv1.4.* Neuron, 1998. **20**(1): p. 125-34.
11. Ruiz-Canada, C., et al., *DLG differentially localizes Shaker K+-channels in the central nervous system and retina of Drosophila.* J Neurochem, 2002. **82**(6): p. 1490-501.
12. Moran, O., et al., *Level of expression controls modes of gating of a K+ channel.* FEBS Lett, 1992. **302**(1): p. 21-5.
13. Grigoriev, N.G., J.D. Spafford, and A.N. Spencer, *The effects of level of expression of a jellyfish Shaker potassium channel: a positive potassium feedback mechanism.* J Physiol, 1999. **517 (Pt 1)**: p. 25-33.
14. Perozo, E., et al., *Gating currents from a nonconducting mutant reveal open-closed conformations in Shaker K+ channels.* Neuron, 1993. **11**(2): p. 353-8.
15. Pandey, R.K., T. Blunck, R., *From resting state to inactivation, the journey of inactivation peptide in Shaker Kv channels (in prep).* 2020.
16. Kalstrup, T. and R. Blunck, *S4-S5 linker movement during activation and inactivation in voltage-gated K(+) channels.* Proc Natl Acad Sci U S A, 2018. **115**(29): p. E6751-E6759.
17. Armstrong, C.M. and A. Loboda, *A model for 4-aminopyridine action on K channels: similarities to tetraethylammonium ion action.* Biophys J, 2001. **81**(2): p. 895-904.

18. Claydon, T.W., et al., *4-aminopyridine prevents the conformational changes associated with p/c-type inactivation in shaker channels.* J Pharmacol Exp Ther, 2007. **320**(1): p. 162-72.
19. Rasband, M.N. and J.S. Trimmer, *Developmental clustering of ion channels at and near the node of Ranvier.* Dev Biol, 2001. **236**(1): p. 5-16.
20. Jugloff, D.G., et al., *Internalization of the Kv1.4 potassium channel is suppressed by clustering interactions with PSD-95.* J Biol Chem, 2000. **275**(2): p. 1357-64.
21. Mottes, J.R. and L.E. Iverson, *Tissue-specific alternative splicing of hybrid Shaker/lacZ genes correlates with kinetic differences in Shaker K+ currents in vivo.* Neuron, 1995. **14**(3): p. 613-23.
22. Rogero, O., B. Hammerle, and F.J. Tejedor, *Diverse expression and distribution of Shaker potassium channels during the development of the Drosophila nervous system.* J Neurosci, 1997. **17**(13): p. 5108-18.
23. Honore, E., et al., *Different types of K+ channel current are generated by different levels of a single mRNA.* EMBO J, 1992. **11**(7): p. 2465-71.
24. Lewin, L., et al., *Direct Evidence for a Similar Molecular Mechanism Underlying Shaker Kv Channel Fast Inactivation and Clustering.* J Mol Biol, 2019. **431**(3): p. 542-556.
25. Taglialatela, M., L. Toro, and E. Stefani, *Novel voltage clamp to record small, fast currents from ion channels expressed in Xenopus oocytes.* Biophys J, 1992. **61**(1): p. 78-82.

5 Chapter 5

Discussion

In this thesis, we were able to show the resting state position of the inactivation peptide in Shaker Kv channels. We also defined the trajectory followed by the IP to block the pore from the cytoplasmic side. We achieved this by establishing fluorophore labeling of residues that lie on the membrane's intracellular side in Xenopus oocytes. By incorporating unnatural amino acids carrying tetrazine moiety in the channels expressed in oocytes, we labeled the intracellular positions through a click chemistry. Click chemistry labeling allowed the successful implementation LRET in Xenopus oocytes to determine the distances at positions of interest. In the follow-up study, we probed the structural mechanism underlying slow N-type inactivation kinetics, which was consistently observed while carrying out the first project. In this study, we demonstrated that clustering of channels through membrane-associated scaffold proteins causes slow inactivation. By preventing this cluster formation through C-terminal truncation, we were able to restore fast inactivation.

5.1 LRET and tmFRET measurements using intracellular labeling

LRET and tmFRET are powerful tools to measure distances between two labeled positions. These techniques are based on distance-dependent energy transfer between donor and acceptor. Another common feature between the two techniques is using fluorescent properties of a single atom (lanthanides for LRET and cobalt for tmFRET) instead of a big fluorophore molecule. As single atoms, these molecules show isotropic emission (absorption in case of cobalt). During distance calculations by FRET measurements, the formula considers the orientation of the donor fluorophore with respect to the acceptor. Due to the large size of a typical fluorophore, the degree of freedom will be restricted in the timescale of emission lifetimes, leading to anisotropy. The degree of freedom can be determined by measuring the turning of the polarization of donor and acceptor emissions compared to excitation (anisotropy). In the case of LRET, the isotropic emission allows to calculate the orientation factor exactly [1].

LRET and tmFRET differ in the range of distances that can be measured using them. LRET is used to measure distances between 15-100 Å, while tmFRET is used for relatively smaller

distances (8-18 Å). The effective range is determined by the Ro values of different donor-acceptor pairs. These techniques have been used extensively in the past to study conformational changes in proteins. They offer the advantage of accurate dynamic measurements in a native cell environment. LRET was used by Posson et al. to study conformational changes in voltage-gated potassium channels [2, 3], by Richardson et al. to study the structural organization of prokaryotic voltage-gated channels in liposomes[4] and by Faure et al. to investigate the electromechanical coupling between the voltage sensor domain and the pore in Kv channels [5]. tmFRET techniques have been widely used by the Zagotta group (U. Washington, Seattle), who is one of the pioneers of the technique, to study various aspects of potassium channels [6-8].

When we decided to use these techniques to locate the position of the inactivation peptide, we faced the challenge of labeling the channels from the cytoplasmic side. As the channels were expressed in Xenopus oocytes, the desired labeling of fluorophores using conventional labeling through cysteine residues was impossible without nonspecific binding. To overcome this problem, we decided to incorporate unnatural amino acids that can bind to fluorophores linked to a tetrazine group using click chemistry. By genetically incorporating trans-cyclooct-4-en-L-Lysine (TCO) using the amber stop codon suppression technique, we successfully labeled intracellular positions in Shaker channels and measured LRET distances. To narrow down the position of the inactivation peptide (IP) after locating its position by LRET, we still had the problem of intracellular labeling. tmFRET was well suited for this kind of measurement. We were able to achieve cobalt binding to the di-histidine motifs introduced on the cytoplasmic side of the channel.

Intracellular labeling of proteins has always been a challenging area for functional, structural studies. In electrophysiology, accessing the intracellular milieu was previously achieved only in excised patches. Cut open voltage clamp allows access and changing of the internal solution to a certain degree. However, labeling protein with fluorophores intracellularly remains a daunting task. Click chemistry labeling by genetic incorporation of unnatural amino acids has opened new possibilities for such studies [9]. By combining LRET and UAA click chemistry labeling, we were able to label and study the inaccessible parts of the protein expressed in living cells. Although click chemistry provides a fast and accurate way of labeling desired positions in the protein, uncertainty was introduced in the delivery of the fluorophore to the positions expressing UAA intracellularly. We initially attempted to introduce the fluorophore by permeabilizing the oocyte membrane exposed to the lower chamber in a cut-open oocyte setup and adding the fluorophore to the internal

solution. The drawback of this technique was the long wait until fluorophore reached and bound to the desired site. This resulted in strong variability between the oocytes during the time that the fluorophore reached the desired site. To expedite the fluorophore diffusion in the oocyte, we customized the recording chamber to allow us to poke a hole in the bottom of the oocyte. With a bigger entry point, we expected to accelerate diffusion. However, there was a slight improvement in the diffusion time. In the end, we injected the fluorophore using a nanoinjector into the cap of the oocyte from which the fluorescence is being recorded. In this way, we decreased the diffusion time of the fluorophore by approximately 4-fold and resulted in a consistent energy transfer signal between different oocytes.

5.2 From resting state to inactivation, the journey of inactivation peptide in Shaker Kv channels

In the first study, we probed the conformational changes in the Shaker channel through VCF by incorporating a fluorescent unnatural amino acid. Our data shows that the movement of IP during channel inactivation is a two-step process. In response to depolarization, movement of both the tip and chain region takes place. The two movements are independent of each other, where the chain movement precedes the tip movement. This was consistent with the functional studies in the past where the IP binds to the T1 domain followed by blocking the pore [10, 11]. A model for the movement of IP during N-type inactivation was proposed by the Holmgren group previously based on molecular simulations [12]. With our LRET and tmFRET measurement, we provide the experimantal proof that the IP sits between the channel and the T1-S1 linker. This is also consistent with the previous findings in which a conserved stretch of acidic residues in the IP was shown to interact with the basic residues in the T1-S1 linker in Shaker channels [13, 14].

The previous model for N-terminal inactivation implies that the IP diffuses from the cytosolic side through the T1 domain into the channel pore to cause inactivation. However, this was not supported by any structural finding. It also seemed energetically unfavorable to transfer a long stretch of amino acids, some of which are charged and others hydrophobic, to travel that distance in a short time interval. Our VCF measurements show that the movement of IP occurs concomitantly with channel activation, requiring the IP to be located close to the transmembrane domain. For certain Kv1 channels (Kv1.1, 1.2, 1.3, and 1.5), fast inactivation is caused by an IP

linked to an auxiliary ß subunit. It will be interesting to see whether these also bind to the same location during resting.

5.3 Clustering of Shaker Kv channels prevents fast inactivation

During these fluorescence-based studies, maximal channel expression was required to obtain high fluorescence signals. One consistent phenomenon observed at higher expression levels was incomplete inactivation of the channel. Previous studies demonstrated that incomplete inactivation could result from mixed N-type and C-type inactivation or of varying ion concentrations of Na+ and K+ [15-17]. However, our results show that incomplete inactivation is a result of the clustering of ion channels by membrane-associated guanylate kinases (MAGUKs). These proteins interact with the C-terminal of the channel and are responsible for the trafficking of channels to the membrane. To accomplish the repertoire of functions exhibited by Kv channels, mere gene expression control is not sufficient. Protein localization and assembly play an equally important role in exhibiting different functions. Clustering of channels is an essential physiological phenomenon required in various cell types. For example, Kv1.3 channels have been shown to concentrate at the immune synapse in lymphocytes [18] and also in mitochondrial membrane to control apoptosis [19]. Neuronal Kv1 channels are clustered in axons to modulate action potential [20], whereas Kv4 channels assemble in dendrites to integrate incoming excitatory signals [21]. Clustering is not limited to Kv channels only. Na+ have been found to cluster at nodes of Ranvier to drive forward the action potential across the axon. All this site-specific cluster formation is an important aspect for the generation of the excitatory signal along with its propagation and transmission. In this study, we were able to identify that ion channel clustering is responsible for incomplete inactivation.

Since Shaker Kv channels have been shown to interact with MAGUKs through C-terminal, we decided to truncate C-terminal and record its effect on channel inactivation. The truncated channels showed much faster inactivation compared to the wild type. To further explore the effects of any crosstalk between N-and C- termini, as mentioned by Lewin et al. [22], on the slowed inactivation kinetics, we decided to use the Shaker non conducting mutant W434F [23]. Using nonconducting mutant allowed us to express the channel at a much higher level and thus obtain a better fluorescence signal to follow the movement of the N-terminal during inactivation. Our fluorescence data showed that the time constants for fast inactivation were comparable to

inactivation kinetics. This excludes any possible interaction between the two ends of the channels that can slow down inactivation. The normal time constant of inactivation from our fluorescence data with W4343F mutant also excludes any effect of external K+ on fast inactivation.

By bridging the two studies of this thesis together, we have come up with a hypothesis for the slowed inactivation at a higher expression level. Our first study showed that N-terminal inactivation peptide resides between the channel and the T1 domain during the resting state, where it interacts with the T1-S1 linker through electrostatic interaction. When the channel opens following depolarization, the efflux of a large amount of K+ ion results in lower local ionic strength, making the electrostatic bond stronger. The strengthening of electrostatic interactions makes it difficult for the IP to separate from the T1-S1 linker, delaying the inactivation. However, this needs to be confirmed with further experimentation.

Any defect in the inactivation mechanism can have a direct implication on membrane excitability. For example, in episodic ataxia type I, delayed and incomplete inactivation can lead to ataxia [24]. A deep insight into the inactivation mechanism will help understand the diseases associated with the channel malfunction and find a better cure.

5.4 References

1. Selvin, P.R., *Principles and biophysical applications of lanthanide-based probes.* Annu Rev Biophys Biomol Struct, 2002. **31**: p. 275-302.
2. Posson, D.J., et al., *Small vertical movement of a K+ channel voltage sensor measured with luminescence energy transfer.* Nature, 2005. **436**(7052): p. 848-51.
3. Posson, D.J. and P.R. Selvin, *Extent of voltage sensor movement during gating of shaker K+ channels.* Neuron, 2008. **59**(1): p. 98-109.
4. Richardson, J., et al., *Distance measurements reveal a common topology of prokaryotic voltage-gated ion channels in the lipid bilayer.* Proc Natl Acad Sci U S A, 2006. **103**(43): p. 15865-70.
5. Faure, E., et al., *A limited 4 A radial displacement of the S4-S5 linker is sufficient for internal gate closing in Kv channels.* J Biol Chem, 2012. **287**(47): p. 40091-8.
6. Aman, T.K., S.E. Gordon, and W.N. Zagotta, *Regulation of CNGA1 Channel Gating by Interactions with the Membrane.* J Biol Chem, 2016. **291**(19): p. 9939-47.
7. Dai, G., et al., *The HCN channel voltage sensor undergoes a large downward motion during hyperpolarization.* Nat Struct Mol Biol, 2019. **26**(8): p. 686-694.

8. Zagotta, W.N., et al., *Measuring distances between TRPV1 and the plasma membrane using a noncanonical amino acid and transition metal ion FRET.* J Gen Physiol, 2016. **147**(2): p. 201-16.
9. Nikic, I., et al., *Labeling proteins on live mammalian cells using click chemistry.* Nat Protoc, 2015. **10**(5): p. 780-91.
10. Gulbis, J.M., et al., *Structure of the cytoplasmic beta subunit-T1 assembly of voltage-dependent K+ channels.* Science, 2000. **289**(5476): p. 123-7.
11. Zhou, M., et al., *Potassium channel receptor site for the inactivation gate and quaternary amine inhibitors.* Nature, 2001. **411**(6838): p. 657-61.
12. Vergara-Jaque, A., et al., *A Structural Model of the Inactivation Gate of Voltage Activated Potassium Channels.* Biophysical Journal, 2017. **112**(3): p. 247a-247a.
13. Fan, Z., et al., *Electrostatic interaction in the NH(2)-terminus accelerates inactivation of the Kv1.4 channel.* Biochim Biophys Acta, 2010. **1798**(11): p. 2076-83.
14. Fan, Z., et al., *Electrostatic interaction between inactivation ball and T1-S1 linker region of Kv1.4 channel.* Biochim Biophys Acta, 2012. **1818**(1): p. 55-63.
15. Baukrowitz, T. and G. Yellen, *Modulation of K+ current by frequency and external [K+]: a tale of two inactivation mechanisms.* Neuron, 1995. **15**(4): p. 951-60.
16. Starkus, J.G., S.H. Heinemann, and M.D. Rayner, *Voltage dependence of slow inactivation in Shaker potassium channels results from changes in relative K(+) and Na(+) permeabilities.* J Gen Physiol, 2000. **115**(2): p. 107-22.
17. Hoshi, T., W.N. Zagotta, and R.W. Aldrich, *Two types of inactivation in Shaker K+ channels: effects of alterations in the carboxy-terminal region.* Neuron, 1991. **7**(4): p. 547-56.
18. Panyi, G., et al., *Kv1.3 potassium channels are localized in the immunological synapse formed between cytotoxic and target cells.* Proc Natl Acad Sci U S A, 2004. **101**(5): p. 1285-90.
19. Szabo, I., et al., *A novel potassium channel in lymphocyte mitochondria.* J Biol Chem, 2005. **280**(13): p. 12790-8.
20. Bean, B.P., *The action potential in mammalian central neurons.* Nat Rev Neurosci, 2007. **8**(6): p. 451-65.
21. Johnston, D., et al., *Active dendrites, potassium channels and synaptic plasticity.* Philos Trans R Soc Lond B Biol Sci, 2003. **358**(1432): p. 667-74.
22. Lewin, L., et al., *Direct Evidence for a Similar Molecular Mechanism Underlying Shaker Kv Channel Fast Inactivation and Clustering.* J Mol Biol, 2019. **431**(3): p. 542-556.
23. Perozo, E., et al., *Gating currents from a nonconducting mutant reveal open-closed conformations in Shaker K+ channels.* Neuron, 1993. **11**(2): p. 353-8.
24. Zhao, J., et al., *A Common Kinetic Property of Mutations Linked to Episodic Ataxia Type 1 Studied in the Shaker Kv Channel.* Int J Mol Sci, 2020. **21**(20).